Arnold Schwarzenegger
Governor

MODAL ANALYSIS FOR GRID OPERATIONS (MANGO): MODEL AND METHODOLOGY

PIER INTERIM PROJECT REPORT

Prepared For:
California Energy Commission
Public Interest Energy Research Program

Prepared By:
Pacific Northwest National Laboratory

Pacific Northwest
NATIONAL LABORATORY
Proudly Operated by Battelle *Since 1965*

March 2010

PNNL-19246

Prepared By:
Pacific Northwest National Laboratory
Project Manager: Zhenyu Huang

Authors: Ning Zhou, Zhenyu Huang, Frank Tuffner, Yousu Chen, John Hauer, Daniel Trudnowski*, Jason Fuller, Ruisheng Diao, and Jeffery Dagle

Richland, WA 99352
(*Montana Tech of the University of Montana, Butte, MT 59701)

Commission Contract No. 500-07-037
Commission Work Authorization No: TRP-08-08

Prepared For:
Public Interest Energy Research (PIER)
California Energy Commission

Jamie Patterson
Contract Manager

Pedro Gomez
Program Area Lead
Energy Systems Integration

Mike Gravely
Office Manager
Energy Systems Research

Martha Krebs, Ph.D.
PIER Director

Thom Kelly, Ph.D.
Deputy Director
ENERGY RESEARCH & DEVELOPMENT DIVISION

Melissa Jones
Executive Director

Acknowledgement

The preparation of this report was conducted with support from the California Energy Commission's Public Interest Energy Research Program through the California Institute of Energy and Environment, and support from the Transmission Reliability Program of the Department of Energy's Office of Electricity Delivery and Energy Reliability.

Project support provided by Sue Arey and Kim Chamberlin, both with Pacific Northwest National Laboratory, is gratefully acknowledged.

The Technical Advisory Committee for the project entitled "Application of Modal Analysis for Grid Operation (MANGO) on the Western Interconnection", funded by the California Energy Commission's Public Interest Energy Research Program through the California Institute of Energy and Environment, consists of the following academic and industry experts:

- Jeff Dagle, Pacific Northwest National Laboratory
- Soumen Ghosh, California Independent System Operator
- Dmitry Kosterev, Bonneville Power Administration
- Bill Mittelstadt, Retiree, Bonneville Power Administration
- Phil Overholt, Department of Energy
- Manu Parashar, formerly with the Electric Power Group
- John Pierre, University of Wyoming
- Dan Trudnowski, Montana Tech of the University of Montana
- Matthew Varghese, California Independent System Operator

Please cite this report as follows:

Zhou, Ning, Zhenyu Huang, Frank Tuffner, Yousu Chen, John Hauer, Daniel Trudnowski, Jason Fuller, Ruisheng Diao, and Jeffery Dagle. March 2010. *Modal Analysis for Grid Operations (MANGO): Model and Methodology*, California Energy Commission, PIER Program. PNNL-19246.

Preface

The California Energy Commission's Public Interest Energy Research (PIER) Program supports public interest energy research and development that will help improve the quality of life in California by bringing environmentally safe, affordable, and reliable energy services and products to the marketplace.

The PIER Program conducts public interest research, development, and demonstration (RD&D) projects to benefit California.

The PIER Program strives to conduct the most promising public interest energy research by partnering with RD&D entities, including individuals, businesses, utilities, and public or private research institutions.

- PIER funding efforts are focused on the following RD&D program areas:
- Buildings End-Use Energy Efficiency
- Energy Innovations Small Grants
- Energy-Related Environmental Research
- Energy Systems Integration
- Environmentally Preferred Advanced Generation
- Industrial/Agricultural/Water End-Use Energy Efficiency
- Renewable Energy Technologies
- Transportation

Modal Analysis for Grid Operations (MANGO): Model and Methodology is an interim report for the project "Application of Modal Analysis for Grid Operation (MANGO) on the Western Interconnection project" (contract number 500-07-037, work authorization number TRP-08-08) conducted by Pacific Northwest National Laboratory. The information from this project contributes to PIER's Energy Systems Integration Program.

For more information about the PIER Program, please visit the Energy Commission's website at www.energy.ca.gov/research/ or contact the Energy Commission at 916-654-4878.

Table of Contents

Table of Figures

Table of Tables

Executive Summary

Small signal stability problems are one of the major threats to grid stability and reliability in California and the western U.S. power grid. An unstable mode can cause large-amplitude oscillations and may result in system breakup and large-scale blackouts. There have been several incidents of system-wide oscillations. Of those incidents, the most notable is the August 10, 1996 western system breakup as a result of undamped system-wide oscillations.

Significant efforts have been devoted to monitoring system oscillatory behaviors from measurements in the past 20 years. The deployment of phasor measurement units (PMU) provides high-precision time-synchronized data needed for detecting oscillation modes. Modal analysis, also known as ModeMeter, uses real-time phasor measurements to identify system oscillation modes and their damping. Low damping indicates potential system stability issues. Modal analysis has been demonstrated with phasor measurements to have the capability of estimating system modes from both oscillation signals and ambient data. With more and more phasor measurements available and ModeMeter techniques maturing, there is yet a need for methods to bring modal analysis from monitoring to actions. The methods should be able to associate low damping with grid operating parameters, so operators can respond when low damping is observed. A frequently asked question is: what to do with the modal information and how to improve damping when it is low? To address the question, we propose to develop and establish a Modal Analysis for Grid Operation (MANGO) procedure to aid grid operators with decision making to increase inter-area damping. The procedure can provide operation suggestions (such as increasing generation or decreasing loads) for operators to mitigate inter-area oscillations.

Different from power system stabilizers and other modulation control mechanisms, MANGO aims to improve damping through adjustment of operating points. Figure ES-1 illustrates the difference of these two types of damping improvement methods. Modulation control retains the operating point, but improves damping through automatic feedback. Traditional PSS control, represented in blue, has significantly improved system damping, especially for local oscillatory modes. Availability of phasor measurement enables wide-area modulation control for control devices such as PDCI and devices for flexible AC transmission systems (FACTS). MANGO, represented in red, and modulation control, represented in magenta, are complementary towards the same goal.

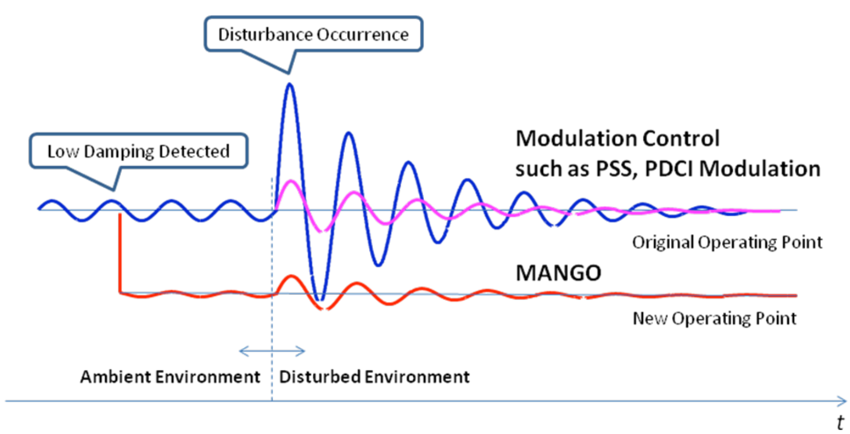

Figure ES-1. MANGO versus modulation control

The developed MANGO procedure is expected to bridge the gap between modal analysis and power grid operations, and enable phasor measurements for real-time grid operations. This application will enable power grid operators of the Western Interconnection to use real-time modal analysis information to damp oscillations, which is not available in today's power grid operation functions. This document reports the progress of MANGO projects supported by the California Energy Commission's Public Interest Energy Research Program through the California Institute of Energy and Environment, and by the Transmission Reliability Program of the Department of Energy's Office of Electricity Delivery and Energy Reliability.

Continued from the previous report, the work reported herein is focused on the following four aspects:

1. Established a MANGO procedure and discussed practical implementation issues;
2. Developed methods for modal sensitivity estimation with case studies to show the effectiveness of using sensitivity information for MANGO control;
3. Studied the impact of topology change on damping; and
4. Conducted WECC simulation studies for further work on developing MANGO control for the full-WECC scale system.

Based on the effect of operating points on modal damping, a MANGO procedure was proposed for improving small signal stability through operating point adjustment. Extensive simulation studies show that damping ratios can be controlled by operators through adjustment of operating parameters such as generation re-dispatch, or load reduction as a last resort. Damping ratios decrease consistently with the increase of overall system stress levels. At the same stress level (total system load), inter-area oscillation modes can be controlled by adjusting generation patterns to reduce flow on the interconnecting tie-line(s). The effectiveness of the MANGO control is dependent on specific locations where the adjustment is applied. The MANGO procedure consists of three major steps:

1. Recognition – operator recognizes the need for operating point adjustment through online ModeMeter monitoring,
2. Implementation – operator implements the adjustment per recommendations by the MANGO approach, and
3. Evaluation – operator evaluates the effectiveness of the adjustment using ModeMeter and repeats the procedure of necessary.

As the first stage, the MANGO procedure is a measurement-based and operator-in-the-loop procedure, as shown in Figure ES-2. Practical implementation is envisioned to be achieved by integrating MANGO recommendations into existing operating procedures per North American Electric Reliability Corporation (NERC) and Western Electricity Coordinating Council (WECC) standards. E-tags can be used an implementation mechanism, which has been addressed in this report. The MANGO model can be updated according to the current measurement and mode estimation results. Operators are included into the loop to bring in expert knowledge. In the future, after the confidence and accuracy of MANGO model is built up, it is expected that the automatic close loop control will be introduced to speed up the implementation and avoid human errors. The automatic process can be integrated into a remedial action scheme (RAS) system or a special protection system (SPS).

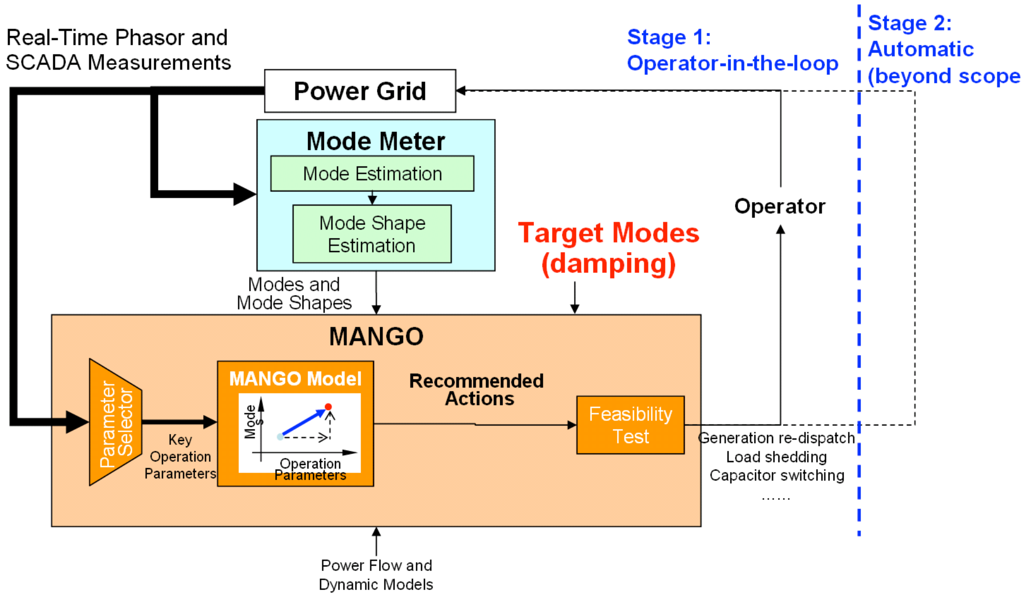

Figure ES-2. MANGO framework

Both Steps 1 and 3 rely on a good ModeMeter to estimate the current modes, while Step 2 builds on modal sensitivity, i.e., the relationship of oscillation modes and operating parameters. The relationship is generally non-linear, and thus it is impractical to derive a closed-form analytical solution for this relationship. Calculating sensitivity from the system model is not applicable, as the model is usually not able to reflect real-time operating conditions. Therefore, our work has been primarily centered on estimating modal sensitivity from real-time measurement. Eigenvalue-theory-based sensitivity has been studied and concluded to be not applicable for real-time estimation. Many items in the eigensensitivity equations cannot be estimated with regular phasor measurement. Several approaches for estimating modal sensitivities are proposed to approximate the relationship. These approaches include artificial neural network (ANN)-based non-linear mapping, relative sensitivity estimation, and relative participation, energy, and mode shapes. ANN-based non-linear mapping has been studied, and it can successfully approximate the modal sensitivity from testing results with medium size systems. The relative sensitivity is formulated using least square principles in the form which can be estimated directly from measurement. The testing has been carried out with a medium size system. The results indicate how strong generation output relates to the damping, giving clear guidance which generator needs to be adjusted in order to improve damping. The same modal sensitivity estimation approach has also been successfully applied to key tie-line flow with a medium size system. The last three ideas will be further developed in future work.

In the modal sensitivity analysis, continuously changing parameters can be well considered. However, it cannot consider discrete changes because the function relationship is not differentiable in mathematical terms. Therefore, extensive topology analysis is conducted to characterize the impact of topology change in oscillation modes. ANN-based non-linear mapping is used in these studies. It was found that for some topology changes, the same ANN can generate reasonable estimate of modal sensitivity, but for some other topology changes, each topology condition would require an ANN, which is not practical in online application. The ANN-based non-linear mapping is improved to consider line status. Test results with a medium size system show the same ANN can then cover multiple topology conditions.

To pave the way to full-WECC MANGO application, we conducted extensive simulation studies of the full-WECC model. A number of problems with WECC models and simulation tools have been solved during this process. More than 1000 cases with randomly adjusted generation outputs have been created using an eigenvalue analysis tool. The data sets from these cases will be used to test the modal sensitivity estimation methods in the full-WECC system application. These data sets will also be further analyzed to derive an empirical relationship between damping and operating parameters. This empirical relationship can be used to validate the modal sensitivity estimation approach, and also as an interim approach for damping control.

In summary, significant progress has been made since last report. A MANGO procedure has been established with practical considerations. The key step in the procedure is the modal sensitivity. Two approaches – ANN-based non-linear mapping and direct modal sensitivity estimation – have been formulated and heavily studied with promising results from a medium-size system. Impact of topology change on damping has been identified using the ANN-based non-linear mapping. The full-WECC simulation studies were conducted, and the resulting data paved the road for full-WECC MANGO application. Further work will continue the development of modal sensitivity estimation and application to the full-WECC system, specifically including work on:

1. Analysis of WECC simulation data to derive empirical relationship between damping and operating parameters.
2. Testing the modal sensitivity estimation method with the full-WECC system;
3. Topology analysis for the full-WECC system.

1.0 Preface

MANGO (Modal Analysis for Grid Operations) is a wide-ranging and ambitious project. This Preface provides background information that lends context to the detailed findings and results in the body of the Report. Special attention is given to the following topics:

- The nature of wide area oscillations, and WECC experience with them
- Integrated use of planning tools for analysis of oscillatory dynamics
- Continuing shortfalls in WECC toolsets and practices for dynamic analysis

The perspective, and much of the material, is directly based upon Dr. John Hauer's (PNNL) contributions to previous reports of WSCC/WECC technical groups. These include the System Oscillation Work Group (SOWG), the Performance Validation Task Force (PVTF), the Disturbance Monitoring Work Group (DMWG), the Modeling and Validation Work Group (M&VWG), and various special groups formed to investigate special events or to coordinate with the U.S. Department of Energy. Partial overviews of the work by these groups can be found in [Hauer et al. 1996; Kosterev et al. 1999; Hauer et al. 2000; Hauer 2000; Hauer et al. 2007; IEEE 2007].

1.1. A Perspective on System Oscillations

It is natural to categorize power system oscillations according to the operational setting in which they occur, and according to the types of equipment involved. Operationally, three kinds of major oscillations have been encountered in the western interconnection:

- **Spontaneous oscillations**, occurring under ambient system conditions. These usually grow slowly, from initially low levels.
- **Transient oscillations**, triggered by loss of a major generation, load, or delivery resource. These tend to be large at the onset, and poorly damped if the post-disturbance network is highly stressed.
- **Forced oscillations**, once a common result of delayed tripping for lines between asynchronous islands. These tended to be large at the onset, and to persist until islanding was completed. This has become rare, and forced oscillations would usually reflect some kind of testing or control problems.

Different oscillation problems require different countermeasures. A controller designed to provide damping under ambient conditions (an *ambient damper*) will usually respond to oscillations of all three types, for lack of contrary information. Its tuning may be quite inappropriate for transient oscillations, or even for step disturbances. A *transient damper* would usually ignore ambient oscillations and use step disturbances as arming information. Local information would probably not permit it to distinguish between transient and forced oscillations, however. The dynamic effects of either an ambient damper or a transient damper during forced oscillations may well be harmful, especially if it is a high performance device with self tuning capabilities.

Reference [CIGRE 1996] is a useful introduction to the extensive literature on this subject. The following general guidelines can be extracted from this and from Western Electricity Coordinating Council (WECC) experience:

- **Some degree of oscillatory activity is normal.** To recognize abnormal behavior, one must know the limits of normal behavior.
- **Abnormal oscillations are usually a symptom of some deeper problems.** Special damping controls may provide a temporary remedy, but ultimately the underlying deficiency must be addressed. In real time operation, this usually involves powerflow adjustments.

- **The ultimate and essential defense against widespread oscillations is to cut the interaction paths.** The necessary actions range from tripping a troublesome generator to controlled separation of the system into stable islands.
- **Major disturbances—and transient oscillations—usually result from a major change in power system topology.** Local control schemes may not be set for this—*Wide area control requires wide area information*.

The general thrust of utility experience with system upsets [Hauer and Dagle 1999; U.S.-Canada Task Force 2004] argues that automated wide area controls are necessary, but not in themselves sufficient to deal with the wide range of challenges that confront emergency management in a large power system. The essential ingredient is *actionable information* at operator level, consisting of:

- **Situational awareness**, *observation* of system conditions related to a knowledge base regarding their implications; and
- **Operational resources**, countermeasure options plus the authority and facilities to execute them.

The arming of special stability controls is a well recognized element among operational resources necessary to the western inter-connection. The major challenge is to develop a knowledge base indicating the conditions under which these and more complex countermeasures are appropriate. This is a major objective of the MANGO project.

1.2. Planning tools for Analysis of Oscillatory Dynamics

Figure 1-1 presents a fundamental paradigm for modeling, analysis, and control of power system dynamics. This graphic was developed in 1999 at the insistence of Mo Beshir, who established the Performance Validation Task Force to resume work by the earlier System Oscillation Work Groups (SOWG). Despite the relatively late date, the tools and processes represented there are precisely those that SOWG utilized and recommended for Western Systems Coordinating Council (WSCC – predecessor to WECC) adoption.

This same paradigm, as well as the same tools, has been applied to all of the following tasks:

- Direct analysis of measured or simulated system behavior
- Model based planning and interpretation of system tests
- Calibration and validation of system models against system measurements
- Compaction of full scale models into reduced equivalents
- Testing and cross-validation of analytical software (including signature recognition)
- Engineering of feedback control systems

The following applications are being developed under MANGO or are implied by future efforts:

- System reconfiguration for modal stability (MANGO)
- Online reduced equivalents for emergency management

All of these are very demanding multi-disciplinary tasks, but most of the key impediments have been mitigated. Measurements are massively improved, the applicable mathematics and software are far more powerful, and well established contractual support has supplemented declining staff among the grid management organizations.

This leaves one formidable problem, which has existed for a very long time. Existing production grade software for large scale simulation and eigenanalysis is, at best, just marginally adequate for the tasks at hand.

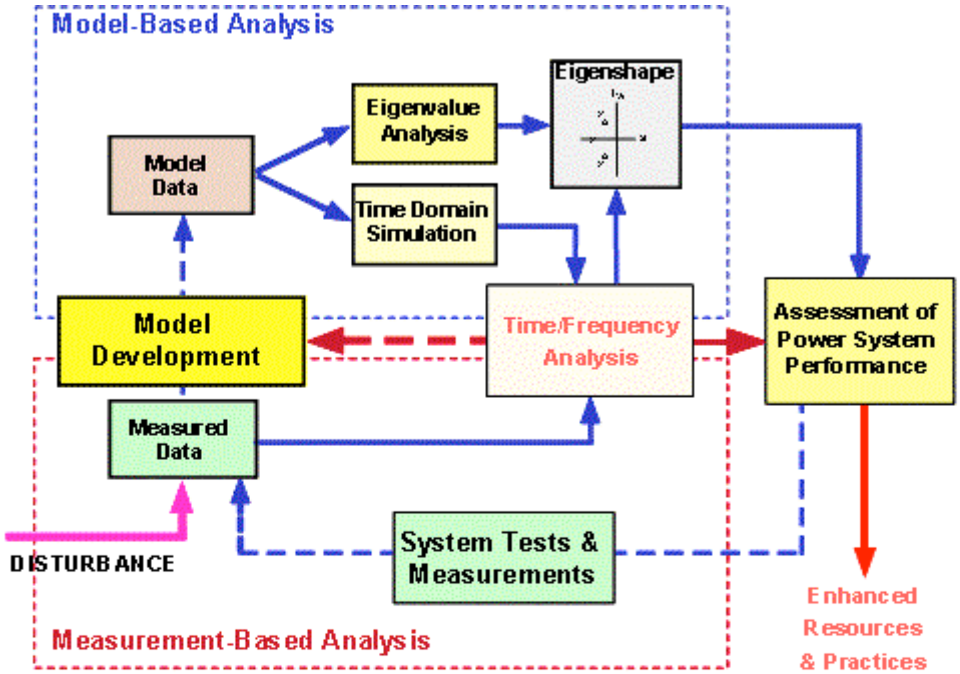

Figure 1-1. Integrated Use of Measurement and Modeling Tools

1.3. Continuing Shortfalls in WECC Toolsets and Practices for Dynamic Analysis

Under ideal circumstances, all software tools for dynamic system analysis would produce equivalent answers from equivalent models. However, there are often discrepancies between different tools and validation methods. These discrepancies are often caused by the following:

- Failure to properly import different model formats completely
- Poor translation of models from one format to another
- Lack of user notification when such import or translation errors occur
- Linear assumptions under clearly non-linear operating regions
- Poorly modeled non-linear devices
- Poor documentation of the actual methods or parameters, leading to improper usage
- No disturbance simulations causing significant transients in a known, stable system
- Inconsistent solver methods within the same "integrated" software
- Improper or a complete lack of validation in simple, widely used system models

Many of these causes can be uncovered through simple validation analysis and closer examination of simulation results. Unfortunately, discrepancies in the analysis of a system model are often overlooked or ignored, resulting in poor trust in the final output. Furthermore, many of these conditions have been apparent in the software for significant periods. Significant project resources are often spent tracking down these issues, or finding workarounds to bypass underlying software issues. Consistent results and better cross-validation are requirements for applications in the real power system. Poorly modeled simulation results can cause unforeseen consequences on a live system implementation, as well as lead to a general distrust of research-oriented results. For projects such as MANGO, the ability to validate and trust the results of a simulation is a key step in progressing towards a true system implementation.

2.0 Introduction and Background

Small signal stability problems are one of the major threats to power grid stability and reliability. An unstable mode can cause large-amplitude oscillations and may result in system breakup and large-scale blackouts [CIGRE 1996]. There have been several incidents of system-wide low-frequency oscillations. Of them, the most notable is the August 10, 1996 western system breakup involving undamped system-wide oscillations [Kosterev et al. 1999]. Figure 2-1 shows the measurement of power transfer from the Pacific Northwest to California during the August 10, 1996 event. The system deteriorated over time after the first line was tripped off at 15:42:03. About six minutes later, undamped oscillations occurred and the system broke up into several islands. Other oscillations events in WECC include the October 9, 2003 Colstrip generation loss, a June 6, 2003 multiple line tripping [Hauer et al. 2003], and the August 4, 2000 Alberta separation [Hauer 2002]. They all exhibited sustained low-frequency oscillations and have led to a great concern about the adverse effect of oscillations on power system operation.

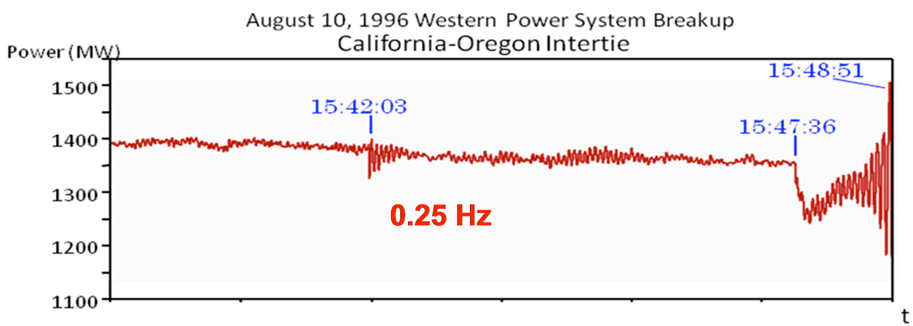

Figure 2-1. Undamped oscillations of the August 10, 1996 western system breakup event

The first step to address this concern is to develop real-time monitoring of low-frequency oscillations. In power systems, low-frequency oscillations are a result of electromechanical coupling between the transmission grid and system generators. Considerable understanding and literature have been developed over the past several decades of the case where these oscillations become very lightly damped, or even unstable. Small-signal oscillation studies have been mainly based on the eigenvalue analysis of its characteristic matrix derived from the linearized model of a power system [Kundur 1994]. Power system stabilizers (PSS) have been used for damping control in common industrial practices. While effective in damping oscillations, especially local-mode oscillations, PSS tuning is a very challenging task for inter-area oscillation modes. In addition, changing system operating conditions also present significant challenges in PSS tuning. The practical feasibility of PSS for inter-area modes is further limited as power system models have been found inadequate in describing real-time operating conditions [Kosterev et al. 1999; Hauer et al. 1996].

Significant efforts have been devoted to monitoring system oscillatory behaviors from measurements in the past 20 years [Hauer et al. 2007; IEEE 2007]. The deployment of advanced sensors, such as phasor measurement units (PMU), provides high-precision time-synchronized data needed for detecting oscillation modes. Many PMUs have been installed in the power systems across the world, such as in the U.S., China, and Brazil. Many gigabytes of phasor data are being collected daily at power company control centers. Phasor data analysis techniques have also been developed, and many are ready for practical use. One notable technique is the measurement-based modal analysis technique, also known as ModeMeter. ModeMeter uses real-time phasor measurements to estimate system oscillation modes and their damping. Low damping indicates potential system stability issues. ModeMeter technology has been demonstrated to have the real-time capability of estimating system modes from both oscillation signals and ambient data [Hauer et al. 1990; Hauer et al. 2006]. The WECC in the U.S. has conducted a number of system tests in the past 10-15 years. The tests include large signal tests through insertion of the 1,400 MW Chief Joseph brake resistance, mid-level signal tests through ±125 MW modulation of Pacific DC Intertie (PDCI) real power set values, and low-level noise probing tests through ±10-20 MW modulation of the PDCI power [Trudnowski et al. 2008]. Recently, the system tests have advanced to be on a regular basis during the summer operating period.

With additional phasor measurements available and ModeMeter techniques maturing, a frequently asked question is what to do with modal information and how to improve system stability when damping is low? There is yet a need for new methods to bring modal information from a monitoring tool to actionable options. The methods should be able to associate low damping with power grid operating conditions in a real-time manner, so that operators can respond by adjusting operating conditions when low damping is observed. The authors propose to develop and establish a procedure using Modal Analysis for Grid Operations (MANGO) to aid grid operators with decision making for improving inter-area damping. The MANGO procedure aims to provide suggestions such as modifying generation levels where it can be done most effectively to mitigate inter-area oscillations.

Different from PSS and other modulation-based methods, MANGO aims to improve damping through adjustment of operating points, whereas the modulation-based methods do not change the system's operating point, but improve damping through automatic feedback control. Figure 2-2 illustrates the difference of these two types of damping improvement methods. Availability of phasor measurements enables wide-area modulation control for control devices such as the Pacific DC Intertie (PDCI) and Flexible AC Transmission Systems (FACTS) devices. MANGO, shown in red, and modulation control, shown in magenta, are complementary towards the same goal. Modulation-based methods are designed to maintain positive damping during expected operating conditions, whereas MANGO-recommended adjustments can be used to move the system to a more stable operating point when low damping conditions are developing that damping would be insufficient in the event of a system disturbance.

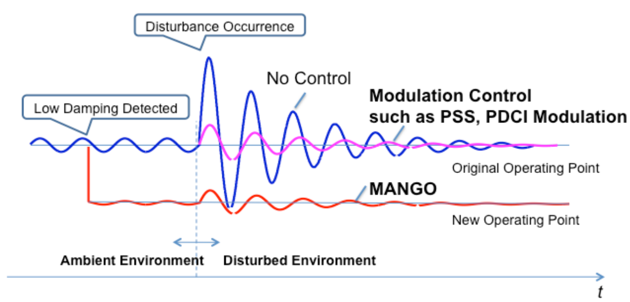

Figure 2-2. MANGO versus modulation control

The developed MANGO procedure is expected to bridge the gap between modal analysis and power grid operations. This application will enable power grid operators to use real-time modal information to respond to oscillation damping issues. This capability is very limited in today's power grid operation functions. Continued from the work summarized in the previous report [Huang et al. 2009], this report reviews ModeMeter work and the MANGO concept, and presents progress in the following aspects:

1. Modal sensitivity analysis
2. Impact of topology change on system oscillations
3. WECC system oscillation studies.

The remainder of the report is organized as follows: Section 3.0 reviews the ModeMeter work, focusing on its relationship to and readiness for MANGO; Section 4.0 investigates the impact of the operating conditions on oscillations, and this the possibility of improving damping through MANGO-recommended operation actions; Section 5.0 proposes the MANGO procedure and discusses practical implementation issues; Section 6.0 addresses modal sensitivity estimation with several proposed methods including Artificial Neural Network (ANN) techniques, relative sensitivity estimation, relative participation factors, oscillation energy, and mode shapes. Relative sensitivity estimation is further formulated and tested with systems of various sizes; Section 7.0 studies the impact of the topology changes on modal damping using the ANN-based MANGO procedure; Section 8.0 links the MANGO studies to the WECC system and summarizes issues encountered in the studies; Section 9.0 defines MANGO prototype testing approaches and specifications; and Section 10.0 concludes the report. Information about test systems used in this report can be found in the Appendix.

3.0 Review of Mode Estimation Using Real-time Measurement

Accurate and timely mode estimation provides vital information about power-system stability. Generally, there are two basic approaches for estimating power system modes: model-based methods and measurement-based methods.

With the model-based method, the nonlinear differential equations governing the system are linearized around an operating point. The power system modes are obtained through eigenvalue analysis [Kundur 1994; Chow and Rogers 2000]. For a large power system, the effort required to build an accurate model using model-based methods is usually not trivial. Even built with great care, a simulation model may not be able to reflect accurately the operational states of the system. A typical example of this comes from the western system breakup event on August 10, 1996. The breakup was caused by a growing oscillation at about 0.25 Hz, as shown in the top of Figure 3-1. Following the event, significant efforts were devoted to build a model with best available information and attempt to duplicate the event in simulation. However, the model simulation showed a stable operating condition, as shown in shown in the bottom of Figure 3-1 [Kosterev et al. 1999]. This study clearly shows how difficult it is to maintain an accurate simulation model using model-based methods.

Power Transfer North-South

Figure 3-1. Observed and Simulated California Oregon Intertie power flow during McNary Generator tripping event [Kosterev et al. 1999; Farmer et al. 2006]

For a measurement-based method, on the other hand, a general linear model structure is first selected, and then model parameters are identified to fit the measurements. Mode estimation methods based on measurement data have been extensively studied. A sample of papers includes [Hauer et al. 1990; Pierre et al. 1997; Kamwa et al. 1996; Zhou et al. 2006; Messina and Vittal 2006; Sanchez-Gasca and Chow 1999; Trudnowski et al. 1999; Trudnowski et al. 2008] and [Wies et al. 2006]. Measurement-based models usually take much less effort to build than those required for a model-based method. Some initial studies were carried out by Drs. John Hauer and John Pierre on the western interconnection blackout in 1996 using measurement-based methods. The results are summarized in Figure 3-2. It can be observed that the 0.25-Hz oscillation, which caused the blackout, is identified. The results also show that the oscillation frequency decreases from 0.27 Hz to 0.25 Hz, and the oscillation damping ratio decreases from 7.0% to 1.2%. These are clear indications of the approaching small signal stability problem. This study shows the great potential of measurement-based methods in monitoring power system oscillation modes.

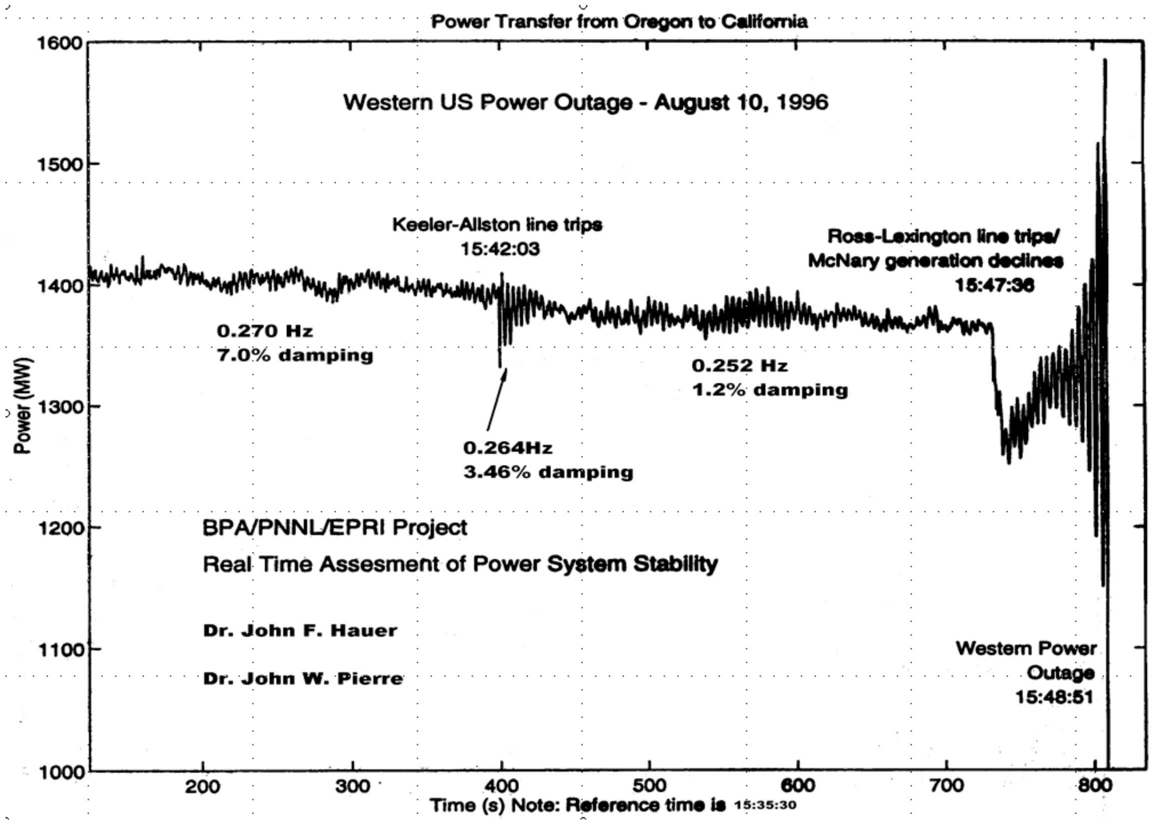

Figure 3-2.Measurement based mode analysis on the blackout data of August 10, 1996.

As discussed by [Hauer General Meeting 2007], any measurement-based approach that automatically estimates modes in near real time has significant potential for system operation and control applications. Such algorithms are termed "ModeMeter" algorithms [Hauer General Meeting 2007]. A "ModeMeter" tool developed by PNNL based on a regularized robust recursive least square (R3LS) algorithm is shown in Figure 3-3 [Zhou et al. 2006; Zhou et al. 2007; Zhou et al. 2008]. The prototype ModeMeter tool has been validated using a 17-machine model and tested with WECC phasor data.

The mode estimation results using 1996 blackout data are summarized in Figure 3-4 [Zhou PSCE 2009]. The blue lines are for the mode estimation without mode initialization. The red lines indicate mode estimation with mode initialization. For comparison, the mode estimation results from Figure 3-2 by Drs. Hauer and Pierre are also shown in the Figure 3-4 as green dots. Figure 3-4 also shows the capability of the ModeMeter tool for on-line continuous monitoring of power system oscillation modes. The online ModeMeter tool has consistent estimation results with the offline expert analysis of Figure 3-2. Such a ModeMeter tool would have recognized the oscillation and issued an earlier warning of the impending outage on August 10, 1996.

To further evaluate the performance of the tool, a 17-machine model [Trudnowski 2008] is used to evaluate the performance of the ModeMeter tool. With the simulation model, 100 simulation data sets are generated, and a Monte Carlo method is used for studying the statistical performance of the ModeMeter tool. One of these simulation data sets is shown in Figure 3-5. It consists of typical data (i.e., ambient, low level probing response, and ringdown signals resulting from disturbances) and non-typical data (i.e., outliers and missing data) to simulate true system responses. With the simulation model, the 'true' modes are available and are used as a reference for evaluating estimation results. The 'true' modes shown in Figure 3-6 are at 0.422 Hz (black dashed line). In the figure, the mean value and standard deviation of the mode estimation are also displayed (blue and gray lines, respectively). It can be observed that the ModeMeter algorithm performs well for a combination of typical and non-typical data sets. The low-level probing and ringdown responses can help improve the mode estimation accuracy. Missing data and outliers do not produce noticeable performance degradation.

The above observations indicate that ModeMeter is becoming mature and ready for real time applications. This lays a great foundation for MANGO studies. As will be shown in Section 5.0, accurately estimated modes are a necessary input to the MANGO procedure.

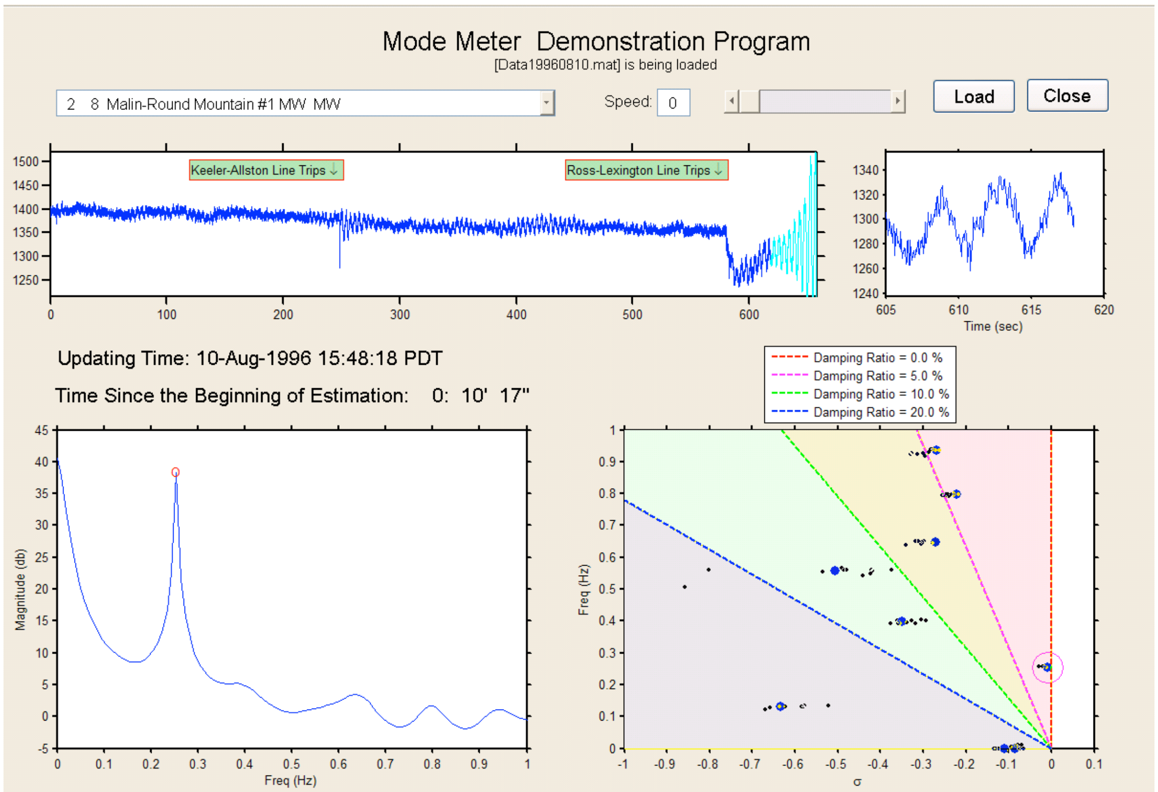

Figure 3-3. PNNL ModeMeter Prototype for 1996 data playback.

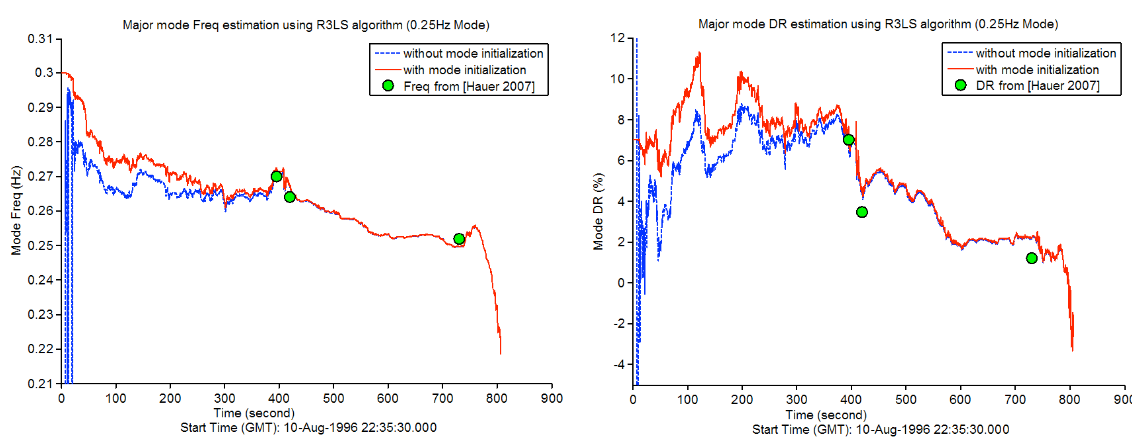

Figure 3-4. Mode frequency and damping ratio estimation using R3LS algorithm.

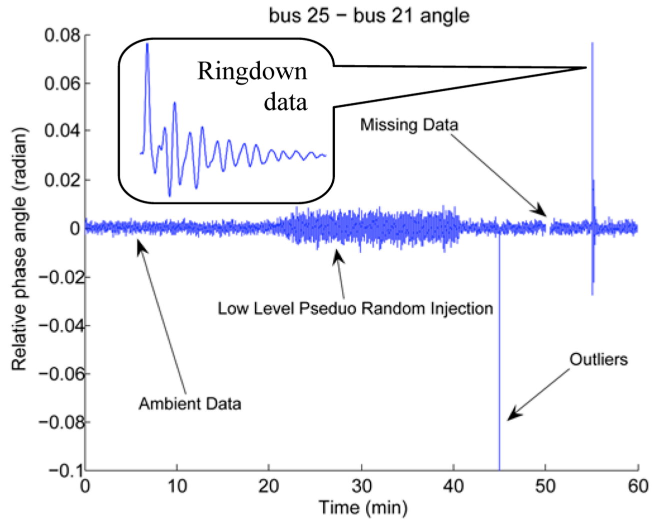

Figure 3-5. Time plot of combined ambient, low-level pseudo-random probing, outlier, missing data, and ringdown from 17-machine model with stationary modes.

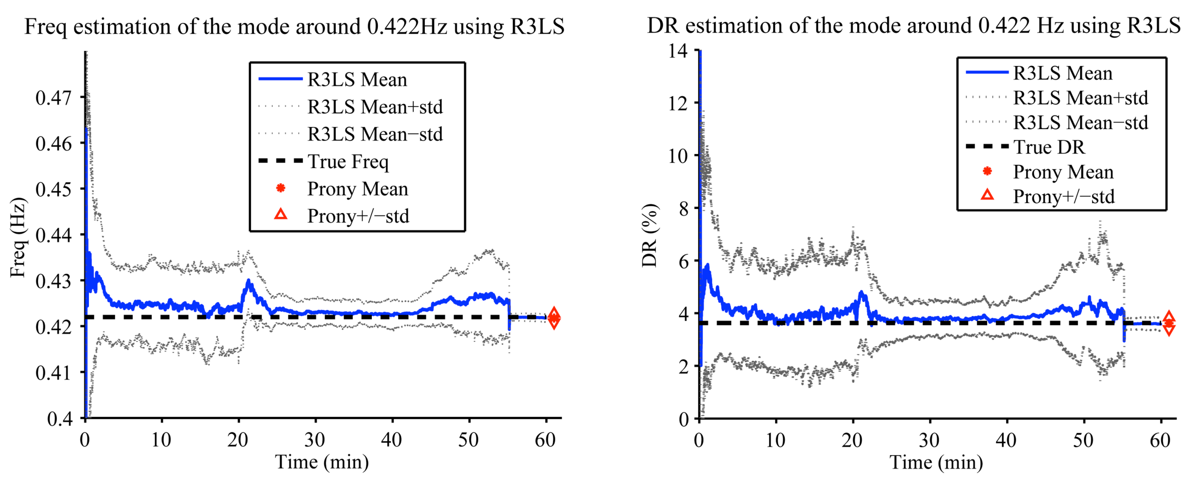

Figure 3-6. Frequency and damping ratio estimation of the major modes around 0.422 Hz of the 17-machine model with stationary modes.

4.0 Effect of Operating Condition on Small Signal Stability

The operation point of a power system determines the eigenvalues, i.e., the oscillation modes, of the system. A power system can be described as a set of non-linear differential algebraic equations:

$$\begin{cases} \dot{x} = f(x, y, u) \\ 0 = g(x, y, u) \end{cases} \tag{4-1}$$

where x is the state vector, y is the algebraic vector, and u is the input vector. The characteristic matrix of the system can be derived by linearizing these non-linear equations at an operation point. The non-real eigenvalues of the characteristic matrix are the oscillation modes of the power system. The characteristic matrix is shown as the **A** matrix in the following equation:

$$\begin{cases} \dot{x} = \mathbf{A}(p)x + \mathbf{B}(p)u \\ y = \mathbf{C}(p)x + \mathbf{D}(p)u \end{cases} \tag{4-2}$$

where p represents operating parameters, such as generator output, load consumption, transformer taps, capacitor MVAr, and DC power settings, which can be adjusted by operators in real-time power system operation. Equation (4-2) indicates that the **A** matrix is related to parameters, p. Thus, the modes can be influenced by adjusting some of the p parameters, i.e., changing the operating point of the power system.

The following sections illustrate the effect of operating parameters on small-signal stability using systems of various sizes.

4.1. The Single-Machine Infinite Bus System

The Single-Machine-Infinite-Bus (SMIB) system (Figure 4-1) provides a unique opportunity to observe the effect of operating conditions on small-signal stability because of its simplicity. The primary operating parameter is the steady-state generation output P, which is same as the power transfer on the tie-lines to the infinite system in this simple case. Another operating parameter is the steady-state terminal voltage V. They can be adjusted through reference settings of the governor and the exciter, respectively.

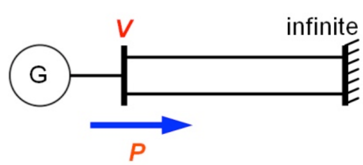

Figure 4-1. The Single-Machine Infinite-Bus (SMIB) system.

To examine the effect of operating points on the small-signal stability of this SMIB system, P and V are randomly varied within their respective operating ranges and the damping ratio for each operating point is calculated. The damping ratio is shown in Figure 4-2 to have a strong correlation with the generator power output P (or the tie-line power). Increasing the power transfer gradually decreases the damping ratio as indicated by the red arrow line. This is consistent with the finding pointed out in [Pai et al. 2004] that one of the main reasons for oscillation problems is "the efforts to transmit bulk power over long distance." The small deviations from the correlation are due to the variations in the voltage setting. It clearly shows the effect of the voltage setting is secondary compared to that of the power setting. Operating point adjustment through generation re-dispatch should be an effective means to increase the damping ratio and thus, the small-signal stability.

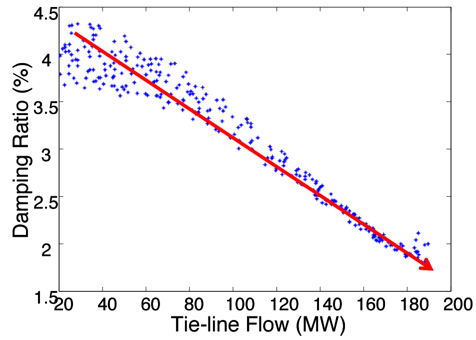

Figure 4-2. Correlation between the damping ratio and the generator power in the SMIB system.

4.2. Two-Area Four-Machine System

A two-area four-machine system is shown in Figure 4-3. The system parameters can be found from the Power System Toolbox (PST) with MATLAB [Chow and Rogers 2000]. The system consists of two areas interconnected by long transmission tie-lines from bus 3 through bus 100 to bus 13. Each area has two generators. The base case has a 400 MW tie-line flow from Area 1 to Area 2. This system has a major inter-area oscillation mode around 0.55 Hz, as identified by its mode shape (right eigenvectors) in Figure 4-4.

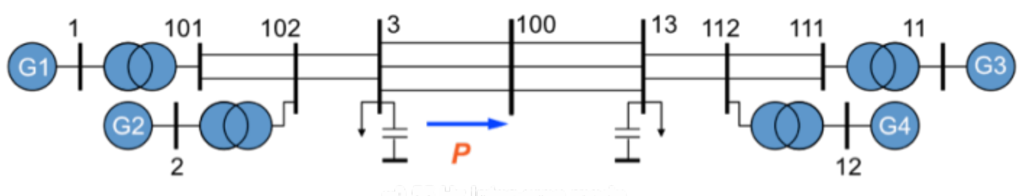

Figure 4-3. A two-area four-machine system.

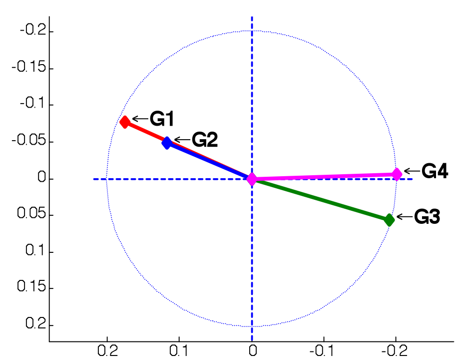

Figure 4-4. Mode shape of the inter-area 0.55 Hz mode.

The correlation of the damping ratio of the 0.55 Hz mode and the tie-line flow is examined first. The tie-line flow is adjusted by changing the system stress level, which is defined as the total load level. In this study, the real and reactive power of the two loads at buses 3 and 13 is changed with the same percentage. To balance the load, the generator real power at buses 1, 2, 11 and 12 is changed accordingly at the same percentage level. This adjustment pattern creates a number of cases with different tie-line flows, and it also minimizes the locational effect of generation and load.

The inter-area mode is calculated for each of the cases. Figure 4-5 shows the correlation between the damping ratio and the tie-line flow. The damping ratio decreases with the increase of the tie-line flow, i.e., the increase of the system stress level. This is consistent with the SMIB system, in which the increase of generator output represents the increase of the stress level. Heavily stressed systems are prone to small signal stability problems. When considering the stability improvement perspective, reducing the stress level or the tie-line flow can effectively improve the damping. The tie-line in this context is the oscillation path identified by the mode shape.

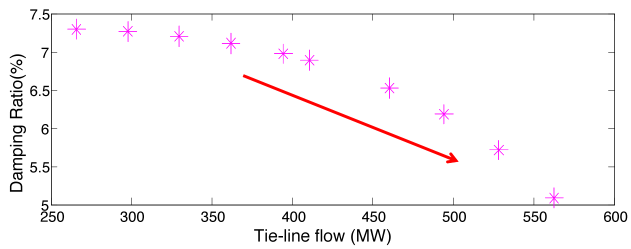

Figure 4-5. Correlation of the damping ratio with the tie-line flow in response to various system stress levels.

The adjustment of tie-line flow, through uniformly adjusting generation in a large system at many locations in real-time operation, would be very difficult. Its practicality is limited by wide-area coordination and load serving obligations. A more practical solution would be to adjust the smallest set of selected generators, with the least disturbance to scheduled transfers, to achieve the desired change in damping. In the two-area four-machine system, all four combinations of generator pairs have been tested. The results are shown in Figure 4-6. For example, "G1 & G4" denotes adjustment of G1 power output balanced by G4. All the combinations result in tie-line flow change, and the damping ratio is consistently correlated with the tie-lie flow level. However, Figure 4-6 also reveals the locational effect of the adjustment, i.e., different pairs of generators have a different effect on the damping ratio, even though they may result in the same tie-line flow level. Cutting tie-line flow may improve damping, but depending on how the decrease was achieved, the quantitative damping ratio increase can be different. For this two-area-four-machine system, the "G1 & G4" pair is the most effective, while the "G2 & G4" pair is the least effective.

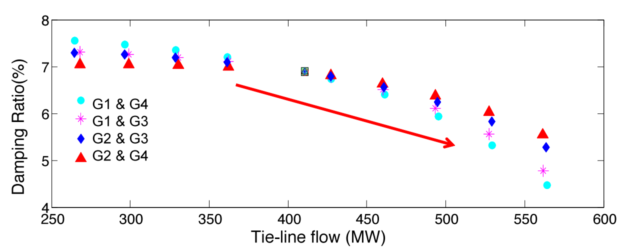

Figure 4-6. Correlation of the damping ratio with the tie-line flow in response to generation re-dispatch of various pairs.

4.3. A 17-Machine System

A 17-machine system is used to further study the effect of power flow effect on small signal stability in an environment with multiple inter-area modes and multiple tie-lines. Eigenvalue analysis shows this system has major inter-area modes around 0.28, 0.40, 0.60 and 0.80 Hz. Tie-lines are indicated as the boxes in Figure 4-7.

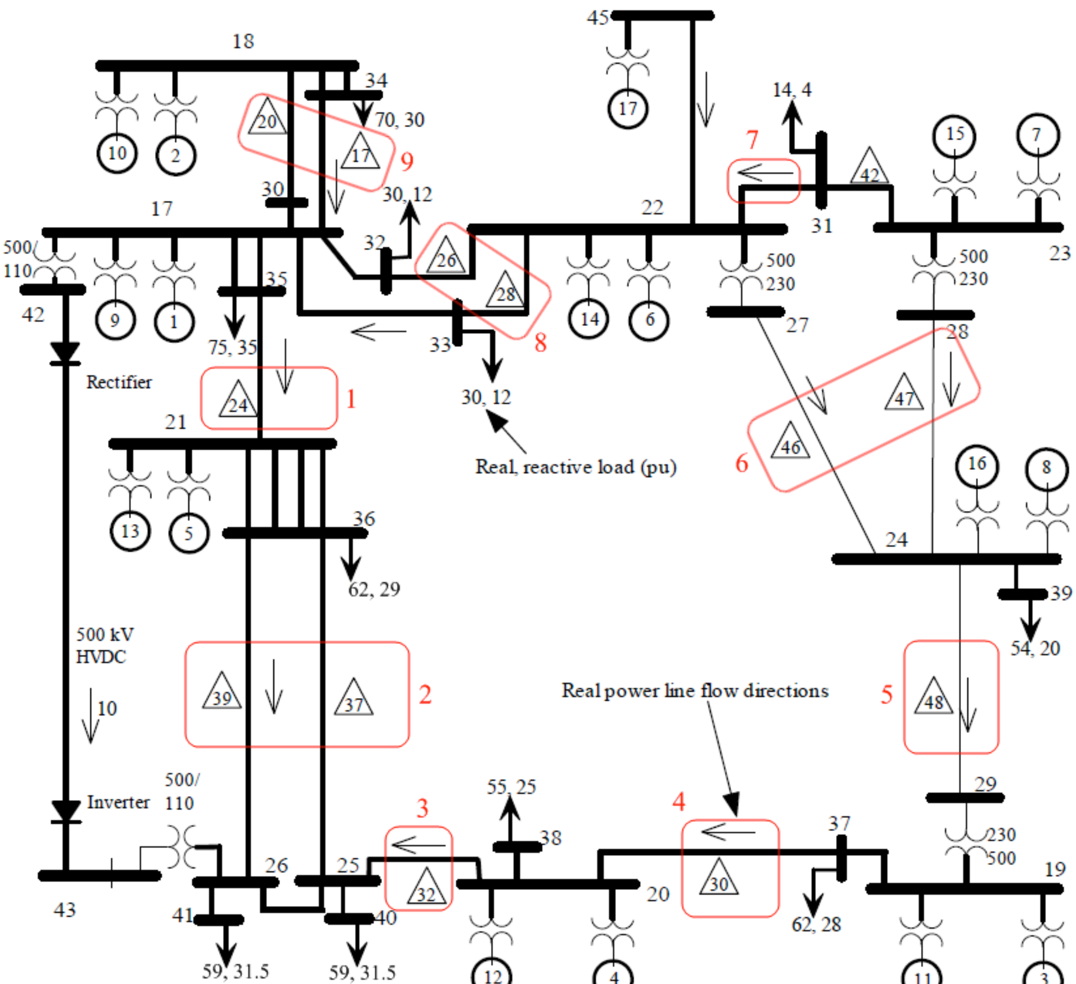

Figure 4-7. Topology of the 17-machine system with tie-lines indicated as the boxes [Trudnowski 2008].

As with the two-area-four-machine system, the stress level test indicates a consistent correlation between the damping ratio of the 0.4 Hz mode with the system stress level (Figure 4-8). Other modes demonstrate a similar correlation, but the results are omitted to conserve space. This also implies that mode damping and tie-line flows have strong correlation as the tie-line flows increase with the increase of the stress level.

The locational effect is confirmed by adjusting different generator pairs in this 17-machine system (Figure 4-9 and Figure 4-10). Most of the modes are not affected by the flow of tie-line #8, as tie-line #8 is not on their major oscillation paths. For the 0.28 Hz mode, generator pair 17 and 11 is not as effective as generator pair 17 and 14 (note the different scale on the *x*-axis between Figure 4-9 and Figure 4-10). However, generator pair 17 and 14 has an adverse effect on the 0.40 Hz mode. It is also interesting to point out that generation re-dispatch for generator pair 17 and 11 could also result in damping reduction if changed past an optimal point

(Figure 4-9). Coordination among modes and adjustment limits are important factors to consider when designing the procedure for damping improvement.

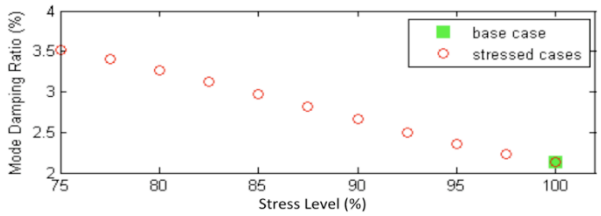

Figure 4-8. Correlation of the damping ratio of the 0.4 Hz mode with the system stress level of the 17-machine system.

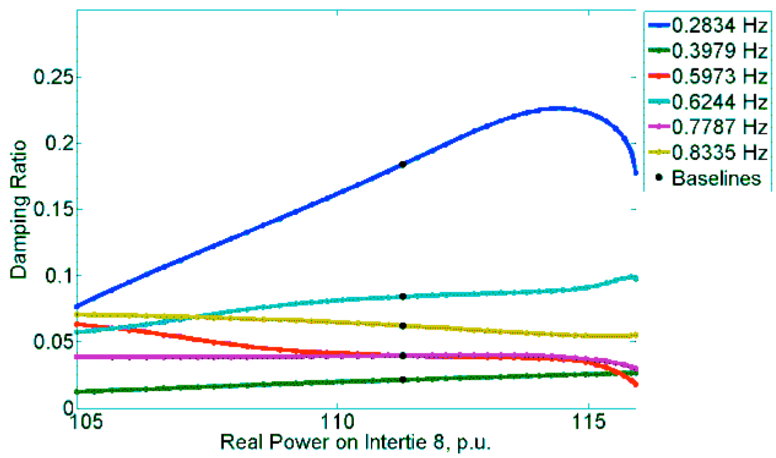

Figure 4-9. Correlation of the damping ratio with the tie-line flow adjusted by generator pair 17 and 11.

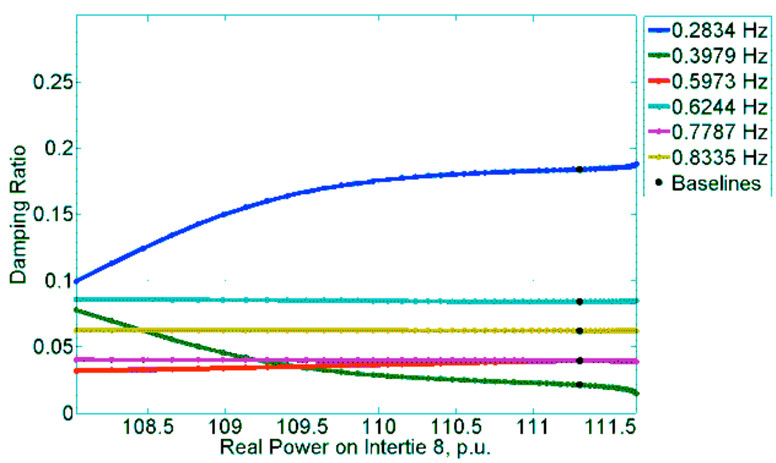

Figure 4-10. Correlation of the damping ratio with the tie-line flow adjusted by generator pair 17 and 14.

Studies of the WECC system show similar characteristics, such as the correlation of its 0.25 Hz mode damping and the tie-line flow of the California-Oregon Intertie (COI), but it also exhibits more non-linear behavior, compared with smaller systems.

5.0 The MANGO Procedure and Its Implementation

Extensive studies shown in the previous section provide strong evidence that small-signal stability can be effectively improved by adjusting the operating point. To enable the adjustment, an operational MANGO procedure needs to be established to guide operators in real-time power system operation. The procedure needs to include three major steps:

1. Recognition – operator recognizes the need for operating point adjustment,
2. Implementation – operator implements the adjustment per recommendations by the MANGO approach, and
3. Evaluation – operator evaluates the effectiveness of the adjustment and repeats the procedure of necessary.

5.1. The MANGO Procedure

Consistent with these three steps, the following MANGO procedure is proposed for improving small-signal stability:

1. Estimate oscillation modes and mode shapes using ModeMeter based on real-time phasor measurements
2. Observe the mode damping and mode energy, as well as its oscillation paths through its mode shape
3. Recognize the need for operating point adjustment when the damping is below a pre-specified threshold and the oscillation energy exceeds a threshold
4. Implement tie-line flow reduction of the oscillation path with a pre-defined amount or percentage. The tie-lines are identified by the mode shapes. This is the preliminary level of implementation. Uncertainties due to locational effect make it difficult to predict the effectiveness and may even cause undesired results
5. Identify the sensitivity relationship between the modes of interest and operating parameters. This is referred to as a MANGO model
6. Generate recommendations for operating point adjustment based on the MANGO model and a damping target. The MANGO recommendations are presented to operators as options to change operating parameters. A sample recommendation would be: "Generator A's output needs to be reduced by 200 MW and Generator B's output increased by 200 MW to improve damping from 1% to 5%."
7. Conduct feasibility test to ensure that the recommended adjustment would result in a solvable power flow, and not violate any generation capacity and other limits
8. Implement the adjustment with consideration of other metrics, such as transient stability and voltage stability. This is the advanced-level implementation as it provides more specific actions and more predictable results
9. Monitor the change in modes and mode shapes from ModeMeter
10. Evaluate the effectiveness by observing whether the damping is adequate and how accurate the MANGO procedure predicts the results. Repeat the MANGO procedure if damping does not achieve the desired level.

Based on the MANGO procedure, Figure 5-1 presents the overall MANGO framework. It shows the relationship to ModeMeter.

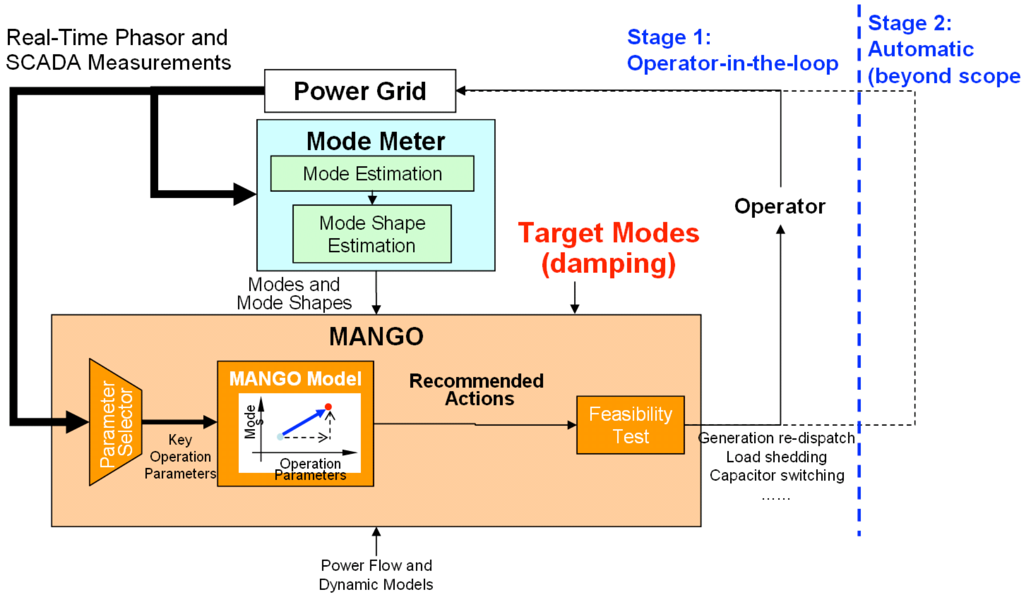

Figure 5-1. The proposed MANGO Framework

5.2. Implementation Considerations

The proposed MANGO procedure can be integrated in current operating procedures, so there would not be new procedures created solely for MANGO. This way, the complexity added to the operational environment is minimized, and it would be easier for grid operators to accept an add-on function rather than a completely new procedure.

Several existing operating procedures can be considered for MANGO integration. Bonneville Power Administration (BPA) currently uses a dispatcher standing order (DSO) 303 for mitigating system oscillation problems. In the general case, when oscillations are observed in SCADA , the DSO calls for reductions in tie-line transfer on the affected path by increments of 10% until the damping is satisfactory. The DSO gives very limited information on adjustment generators, and does not estimate the expected change in damping for a 10% adjustment. The MANGO procedure can be used to enhance the DSO 303 with specifics such as locations and sizes of the adjustment, and expected damping improvement. It can also enhance the DSO 303 with the inclusion of other oscillation modes.

Current North American Electric Reliability Corporation (NERC) operating procedures such as TOP-004 [NERC TOP-004-1 2007; NERC TOP-004-3 2009], TOP-007 [NERC TOP007-0 2005; WECCTOP-007-WECC-1 2008] , TOP-008 [NERC TOP008-0 2005; NERC TOP008-1 2007], and IRO-006 [NERC IRO006-4 2007; WECC IRO-006-4] can also be used to integrate MANGO recommendations. TOP-004 is to ensure interconnection reliability operating limits (IROLs) and system operating limits (SOLs) are satisfied. TOP-007 defines the reporting procedure if IROLs or SOLs are violated. TOP-008 requires the transmission operator experiencing or contributing to an IROL or SOL violation shall take immediate steps to relieve the condition, which may include shedding firm load. Small-signal stability limits are part of the IROLs, and MANGO recommendations align with the requirements in TOP-008. IRO-006 is a tie-line relief (TLR) standard. It defines the procedures for adjusting interchange transactions, network and native load contributions, and market dispatch contributions to relieve overloads on the transmission facilities modeled in the interchange distribution calculator (IDC). MANGO recommendations can be used to relieve transmission overloads per the metric of oscillations.

For the WECC, the selection of generators may consider existing E-Tags when generating and implementing the MANGO recommended actions. E-Tags are used to define transactions with generators grouped for providing energy services [WECC DEC 2006]. Generation re-dispatch according to the E-Tag generator groups enables the use of established channels to influence energy transactions.

At the first stage, the MANGO procedure is a measurement-based and operator-in-the-loop procedure, as shown in Figure 5-1. The MANGO model can be updated according to the current measurement and mode estimation results. Operators are included into the loop to bring in expert knowledge. In the future, after the effectiveness of the MANGO procedure is validated, a greater degree of automation may be possible. For example, the automatic process might be integrated as part of a Remedial Action Scheme (RAS) system or a Special Protection System (SPS).

6.0 Modal Sensitivity Analysis

The most important step in the proposed MANGO procedure is to build a MANGO model, which is highly dependent on modal sensitivity with respect to operating parameters. In some cases, especially for small systems, system experience can provide satisfactory selection of operating parameters for operation actions on the power grid. However, experience-based selection may not identify the most optimal options for large-scale complex systems, such as the U.S. western interconnection. Systematic methods are needed for selecting locations for damping improvement.

6.1. Eigen-theory-based Modal Sensitivity

Eigen-decomposition of the **A** matrix in (4-2) generates

$$\mathbf{A} = \mathbf{\Phi \Lambda \Psi} \tag{6-1}$$

where □ is the diagonal eigenvalue matrix, and □ and □ are the left and right eigenvector matrices. □ is also used to construct the mode shape.

Modal sensitivity with respect to a parameter *p* is given as follows [Kundur 1994]:

$$\frac{\partial \lambda}{\partial p} = \mathbf{\Psi} \frac{\partial \mathbf{A}(p)}{\partial p} \mathbf{\Phi} \tag{6-2}$$

This basic modal sensitivity method has been applied to the 17-machine system. The results of the 0.4 Hz modal sensitivity with respect to generator power output are shown in Figure 6-1. The two largest sensitivities are associated with generator 17 and generator 10; increasing generator 10's power will decrease the damping ratio, while increasing generator 17's power will increase the damping ratio. Generators 17 and 10 would be the most effective pair to use for generation re-dispatch to improve the 0.4 Hz mode damping. The sensitivity information also indicates how much damping changes can be expected by the generator power adjustment.

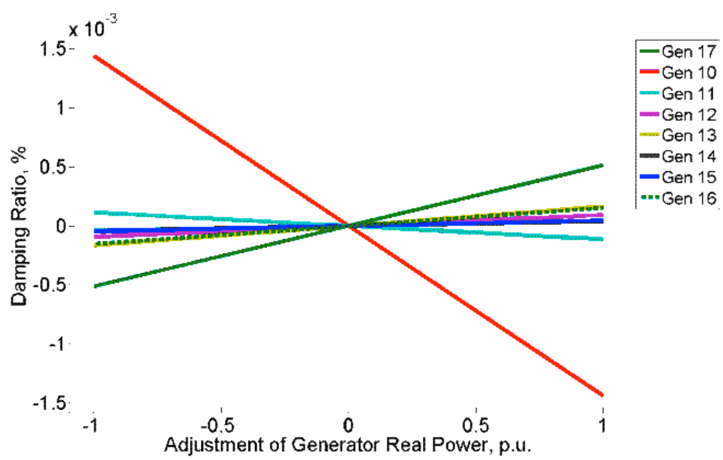

Figure 6-1. Modal sensitivity of the 0.4 Hz mode in the 17-machine system.

In the real-time operation environment, the system model is usually not available, or not accurately reflecting the actual operating conditions. Implementing the eigen-theory-based method would require real-time estimation of the left and right eigenvectors, as well as the eigen-sensitivity matrix $\partial \mathbf{A}(p)/\partial p$ from measurements. Right eigenvectors can be estimated from real-time measurements [Zhou General Meeting 2009]. However, estimating left eigenvectors would require extensive probing signal injections to excite the right state, which is usually not practical for a large system. Estimating the eigen-sensitivity matrix presents an even more challenging problem.

6.2. Artificial Neural Network-based Non-linear Mapping

The non-linear relationship between modal damping and operating parameters such as generator power settings can be described by a non-linear multiple-input-multiple-output (MIMO) function. The inputs are the operating parameters and the outputs are the oscillation modes of interest. Once such a function is identified, it can be used to derive modal sensitivity information. To approximate this non-linear function, an Artificial Neural Network (ANN) approach is proposed for the MANGO procedure. "Neural networks are good at fitting functions and recognizing patterns. In fact, there is proof that a fairly simple neural network can fit any practical function."[Demuth and Hagan 2009]. A three-layer feed-forward ANN network is used, consisting of the input, middle and output layers. The Levenberg-Marquardt method is used to tune the parameters in the ANN network. There are three steps in applying ANN for generating MANGO recommendations:

1. **Collect data for training, validation and testing**. The input variables, i.e., operating parameters, are selected based on eigenvalue analysis results such as mode shapes and participation factors, as well as operating experience. The output variables are the modes of interest. Data can be collected from simulation cases and actual operating cases. Each case is a set of inputs and outputs. It is desirable that the data sets cover the operational region. Interpolation (instead of the extrapolation) can be used to reduce errors.
2. **Train, validate and test the ANN network**. The data sets are divided into three parts to create an ANN network. The training set is used to tune the parameters of ANN. The validation data set is used to check if the training should continue or stop. The training procedure should stop when further training cannot further reduce the mismatches in the validation data set. The test set is used to independently check the accuracy of the trained ANN network. If an ANN network cannot reach a desired level of accuracy, the model order may need to be adjusted and the ANN network needs to be re-trained.
3. **Use the trained ANN to derive modal sensitivity**. Real-time measurement and ModeMeter information are used at this step. The fundamental idea is to iteratively identify the most effective adjustment to reach a targeted damping level. At each iteration step, a small perturbation is introduced to each of the input variables in the ANN network. The deviation of modes is calculated and used as modal sensitivity with respect to the perturbed input variable. An adjustment is applied to the input variables identified by the largest sensitivities. The iterative approach is to ensure the non-linearity is considered in the process. After all the steps, the final adjustment is determined.

This ANN-based approach is applied to a simplified WECC system, which contains 34 generators and 122 buses, while also retaining most of the full WECC system's properties of small signal stability. The 0.4 Hz mode is studied and all the generator power outputs and load consumptions are selected as input variables. Data sets (9000) are generated for training and testing by randomly adjusting the power flow conditions. Excellent training accuracy is indicated in Figure 6-2 by the small mismatch between the ANN-predicted results and the testing data sets.

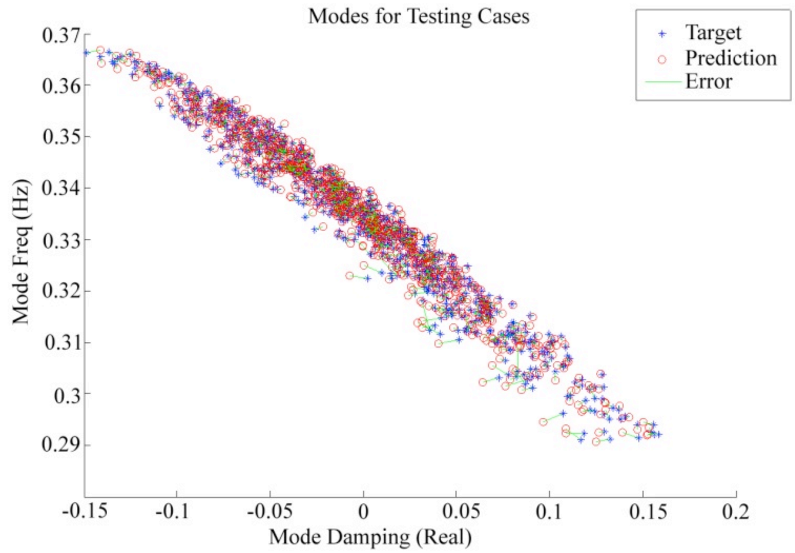

Figure 6-2. Training and testing results of the ANN for the 0.4 Hz mode.

Using this trained ANN network, MANGO recommendations are generated to successfully improve the 0.4 Hz modal damping from 1.26% to 7.36% through adjustment of generation and load at five locations. The effectiveness is confirmed by eigenvalue analysis. Like all other ANN applications, the challenge with this ANN-based approach lies at extrapolating the trained ANN for untrained scenarios such as topology changes. The work is ongoing in studying the impact of topology changes on the ANN-based sensitivity approach. The progress is reported in Section 7.0.

6.3. Relative Participation, Energy, and Mode Shape

The electromechanical oscillations of interest occur between at least two generators, and more generally groups of generators. More relative properties can be explored to derive the correlation of modal damping with operating parameters. Relative participation, energy, and mode shape are currently being investigated. The hypothesis is that when two generators, or two generator groups, oscillate against each other, the relative participation factor would be relatively large and adjusting these two generators would likely to have positive effect on modal damping. It is expected that the relative energy and mode shape have similar properties. Some initial results are shown in Table 6-1 where the relative participation, energy, and mode shape are calculated for the 0.4 Hz mode of the simplified WECC system. Among the selected pairs of generators, the ranking exhibits good consistency with the eigenvalue-based sensitivity results as well as the actual damping changes under the columns "□mode / 100MW" and "□mode / 250MW".

Table 6-1. Initial Results of Relative Participation, Energy, and Mode Shape[1].

ΔP	Δmode / 100MW			Δmode / 250MW			Sensitivity			Relative Participation	Relative Energy	Relative Shape
gen vs gen	Δreal	Δf (Hz)	Δ%D	Δreal	Δf (Hz)	Δ%D	Real	f (Hz)	Abs			
34 vs 7	-0.02323	0.008792	**2.2976**	-0.06067	0.032259	**7.151**	**-0.02233**	0.007395	**0.05155**	**1.0012**	**2.10E-06**	**0.93708**
34 vs 10	-0.02325	0.008824	**2.2999**	-0.06059	0.032312	**7.1472**	**-0.02238**	0.007432	**0.051785**	**1.0035**	**2.31E-06**	**0.98201**
14 vs 7	-0.00028	0.000271	0.031032	-0.00099	0.000771	0.10417	-0.00024	0.000252	0.0016	0.004431	1.42E-09	0.024395
14 vs 10	-0.00034	0.000311	0.036552	-0.00116	0.000878	0.12115	-0.00029	0.00029	0.001842	0.007899	3.87E-09	0.040213
10 vs 18	-1.81E-05	0.000192	0.006376	-8.08E-05	0.000499	0.019471	-9.36E-06	0.000187	0.001175	0.016726	2.49E-08	0.10197
10 vs 21	0.000252	0.000224	-0.01577	0.000583	0.000587	-0.03486	0.000264	0.000218	0.001394	0.032587	5.98E-08	0.15808
7 vs 18	-6.92E-05	0.000231	0.011705	-0.00022	0.000603	0.034091	-5.73E-05	0.000225	0.001414	0.019028	5.15E-08	0.14667
7 vs 21	0.000201	0.000264	-0.01042	0.000441	0.000692	-0.02008	0.000216	0.000256	0.001621	0.033	9.82E-08	0.20261

6.4. Relative Modal Sensitivity Estimation w. r. t. Generators and Loads

It is always desired that modal sensitivity information can be directly estimated from real-time measurement. This avoids the difficulties in estimating the left eigenvectors and eigen-sensitivity matrix, and also alleviates the issue with topology changes. In this subsection, a direct method is formulated for estimating the relative modal sensitivity with respect to load and generation. The estimation process uses a series of ModeMeter results. The algorithm takes advantage of the natural variations in oscillation modes and operating points over a period of time. Preliminary tests have been performed with the two-area-four-machine system [Chow and Cheurg 1992] and the simplified WECC system mentioned in the previous subsection. In these tests, the data sets are simulated using system models.

6.4.1. Algorithm Description

When there is not significant change, the relationship between generation/load changes and mode changes can be approximately linear. Most of time, a power grid is working around an equilibrium operational point. Under such a condition, the major disturbance is random, small-magnitude load variations and small generation variations. Because there is no significant generation and load changes, the relationship between the modes changes and generation/load changes can be described as

$$\Delta\lambda^{(i)} = \frac{\partial\lambda}{\partial P_1}\Delta P_1^{(i)} + \frac{\partial\lambda}{\partial P_2}\Delta P_2^{(i)} + \ldots + \frac{\partial\lambda}{\partial P_{NGen+NLoad}}\Delta P_{NGen+NLoad}^{(i)} + \varepsilon^{(i)} \tag{6-3}$$

where the superscript (i) denotes that it is the ith perturbation, λ represents the eigenvalue of interest, □λ denotes the changes of the eigenvalue from previous instance, □P represent changes in the generator or load real power quantity from previous instance, *NGen* and *NLoad* represents the total number of generators and loads respectively, and □ is for noise. Note that for real-time application, the modal sensitivity $\partial\lambda/\partial P_j$'s are unknown and need to be estimated. On the other hand, the □λ can be estimated from real-time measurement using a ModeMeter algorithm as described in Section 3.0 (Review of Mode Estimation Using Real-time Measurement). □P can be derived from field measurement. To estimate the modal sensitivity $\partial\lambda/\partial P_j$, the following equations can be formed after N time instances.

1 Note: Δreal = change in the real part of the mode, Δf = change in the mode frequency, Δ%D = change in damping ratio.

$$\begin{bmatrix} \Delta\lambda^{(1)} \\ \Delta\lambda^{(2)} \\ \vdots \\ \Delta\lambda^{(N)} \end{bmatrix} = \begin{bmatrix} \Delta P_1^{(1)} & \Delta P_2^{(1)} & \cdots & \Delta P_{NGen+Nload}^{(1)} \\ \Delta P_1^{(2)} & \Delta P_2^{(2)} & \cdots & \Delta P_{NGen+Nload}^{(2)} \\ \vdots & \vdots & \ddots & \vdots \\ \Delta P_1^{(N)} & \Delta P_2^{(N)} & \cdots & \Delta P_{NGen+Nload}^{(N)} \end{bmatrix} \begin{bmatrix} \dfrac{\partial\lambda}{\partial P_1} \\ \dfrac{\partial\lambda}{\partial P_2} \\ \vdots \\ \dfrac{\partial\lambda}{\partial P_{NGen+NLoad}} \end{bmatrix} + \begin{bmatrix} \varepsilon^{(1)} \\ \varepsilon^{(2)} \\ \vdots \\ \varepsilon^{(N)} \end{bmatrix} \quad (6\text{-}4)$$

When $N \geq NGen+NLoad$, equation (6-4) may be used to solve for the modal sensitivity. To simplify notation, the equation (6-4) can be written in matrix format as

$$\Delta\lambda = \Delta P \cdot \frac{\partial\lambda}{\Delta P} + \varepsilon \quad (6\text{-}5)$$

There is a special constraint for solving above equation, i.e., the load and generation should be balanced. Ignoring transmission line loss, this constraint can be expressed as

$$\Delta P_1^{(i)} + \Delta P_2^{(i)} + \cdots + \Delta P_{NGen+NLoad}^{(i)} = 0\,. \quad (6\text{-}6)$$

This means that loads and generations cannot change independently. There has to be one swing bus to pick up the slack. This constraint indicates that the columns of ΔP matrix in equation (6-5) are linearly dependent. The conditional number of ΔP approaches infinity, which leads to an ill-conditioned problem. If the equation (6-4) is directly used to solve for modal sensitivity, the solutions are going to be very sensitive to noise, and thus have large estimation errors [Stoica and Moses 1997].

To resolve this ill-conditioned problem, the constraints of equation (6-6) can be used as follows. Assuming that ΔP_1 be the slack variable, the equation (6-6) can be rewritten as

$$\Delta P_1^{(i)} = -\Delta P_2^{(i)} - \Delta P_3^{(i)} \cdots - \Delta P_{NGen+NLoadNG}^{(i)} \quad (6\text{-}7)$$

Substituting (6-7) into (6-4),

$$\begin{bmatrix} \Delta\lambda^{(1)} \\ \Delta\lambda^{(2)} \\ \vdots \\ \Delta\lambda^{(N)} \end{bmatrix} = \begin{bmatrix} \Delta P_2^{(1)} & \Delta P_3^{(1)} & \cdots & \Delta P_{NGen+Nload}^{(1)} \\ \Delta P_2^{(2)} & \Delta P_3^{(2)} & \cdots & \Delta P_{NGen+Nload}^{(2)} \\ \vdots & \vdots & \ddots & \vdots \\ \Delta P_2^{(N)} & \Delta P_3^{(N)} & \cdots & \Delta P_{NGen+Nload}^{(N)} \end{bmatrix} \begin{bmatrix} \dfrac{\partial\lambda}{\partial P_2} \\ \dfrac{\partial\lambda}{\partial P_3} \\ \vdots \\ \dfrac{\partial\lambda}{\partial P_{NGen+NLoad}} \end{bmatrix} + \begin{bmatrix} \Delta P_1^{(1)} \\ \Delta P_1^{(2)} \\ \vdots \\ \Delta P_1^{(N)} \end{bmatrix} \frac{\partial\lambda}{\partial P_1} + \begin{bmatrix} \varepsilon^{(1)} \\ \varepsilon^{(2)} \\ \vdots \\ \varepsilon^{(N)} \end{bmatrix}$$

$$= \begin{bmatrix} \Delta P_2^{(1)} & \Delta P_3^{(1)} & \cdots & \Delta P_{NGen+Nload}^{(1)} \\ \Delta P_2^{(2)} & \Delta P_3^{(2)} & \cdots & \Delta P_{NGen+Nload}^{(2)} \\ \vdots & \vdots & \ddots & \vdots \\ \Delta P_2^{(N)} & \Delta P_3^{(N)} & \cdots & \Delta P_{NGen+Nload}^{(N)} \end{bmatrix} \begin{bmatrix} \dfrac{\partial\lambda}{\partial P_2} \\ \dfrac{\partial\lambda}{\partial P_3} \\ \vdots \\ \dfrac{\partial\lambda}{\partial P_{NGen+NLoad}} \end{bmatrix} - \begin{bmatrix} \Delta P_2^{(1)} + \cdots + \Delta P_{NGen+Nload}^{(1)} \\ \Delta P_2^{(2)} + \cdots + \Delta P_{NGen+Nload}^{(2)} \\ \vdots \\ \Delta P_2^{(N)} + \cdots + \Delta P_{NGen+Nload}^{(N)} \end{bmatrix} \frac{\partial\lambda}{\partial P_1} + \begin{bmatrix} \varepsilon^{(1)} \\ \varepsilon^{(2)} \\ \vdots \\ \varepsilon^{(N)} \end{bmatrix}$$

$$= \begin{bmatrix} \Delta P_2^{(1)} & \Delta P_3^{(1)} & \cdots & \Delta P_{NGen+Nload}^{(1)} \\ \Delta P_2^{(2)} & \Delta P_3^{(2)} & \cdots & \Delta P_{NGen+Nload}^{(2)} \\ \vdots & \vdots & \ddots & \vdots \\ \Delta P_2^{(N)} & \Delta P_3^{(N)} & \cdots & \Delta P_{NGen+Nload}^{(N)} \end{bmatrix} \begin{bmatrix} \frac{\partial \lambda}{\partial P_2} \\ \frac{\partial \lambda}{\partial P_3} \\ \vdots \\ \frac{\partial \lambda}{\partial P_{NGen+NLoad}} \end{bmatrix} - \begin{bmatrix} \Delta P_2^{(1)} & \Delta P_3^{(1)} & \cdots & \Delta P_{NGen+Nload}^{(1)} \\ \Delta P_2^{(2)} & \Delta P_3^{(2)} & \cdots & \Delta P_{NGen+Nload}^{(2)} \\ \vdots & \vdots & \ddots & \vdots \\ \Delta P_2^{(N)} & \Delta P_3^{(N)} & \cdots & \Delta P_{NGen+Nload}^{(N)} \end{bmatrix} \begin{bmatrix} \frac{\partial \lambda}{\partial P_1} \\ \frac{\partial \lambda}{\partial P_1} \\ \vdots \\ \frac{\partial \lambda}{\partial P_1} \end{bmatrix} + \begin{bmatrix} \varepsilon^{(1)} \\ \varepsilon^{(2)} \\ \vdots \\ \varepsilon^{(N)} \end{bmatrix}$$

$$= \begin{bmatrix} \Delta P_2^{(1)} & \Delta P_3^{(1)} & \cdots & \Delta P_{NGen+Nload}^{(1)} \\ \Delta P_2^{(2)} & \Delta P_3^{(2)} & \cdots & \Delta P_{NGen+Nload}^{(2)} \\ \vdots & \vdots & \ddots & \vdots \\ \Delta P_2^{(N)} & \Delta P_3^{(N)} & \cdots & \Delta P_{NGen+Nload}^{(N)} \end{bmatrix} \left\{ \begin{bmatrix} \frac{\partial \lambda}{\partial P_2} \\ \frac{\partial \lambda}{\partial P_3} \\ \vdots \\ \frac{\partial \lambda}{\partial P_{NGen+NLoad}} \end{bmatrix} - \begin{bmatrix} \frac{\partial \lambda}{\partial P_1} \\ \frac{\partial \lambda}{\partial P_1} \\ \vdots \\ \frac{\partial \lambda}{\partial P_1} \end{bmatrix} \right\} + \begin{bmatrix} \varepsilon^{(1)} \\ \varepsilon^{(2)} \\ \vdots \\ \varepsilon^{(N)} \end{bmatrix} \qquad (6\text{-}8)$$

Note that during this procedure, the linear dependency of the columns in matrix ΔP is removed. The ill-conditioned problem is removed. After resolving the correlated column issue, the equation (6-8) can be solved for the modal sensitivity in least square sense [Stoica and Moses 1997]. Note that the solution is relative modal sensitivity. It means that any modal sensitivity is with respect to the swing bus. For example, the first component of the solution, $\frac{\partial \lambda}{\partial P_2} - \frac{\partial \lambda}{\partial P_1}$, is the modal change when P_2 is increased by one unit and P_1 is decreased by one unit.

When using other components as reference, the relative modal sensitivity can be derived directly from the solution. For example, $\frac{\partial \lambda}{\partial P_2} - \frac{\partial \lambda}{\partial P_3} = \left(\frac{\partial \lambda}{\partial P_2} - \frac{\partial \lambda}{\partial P_1} \right) - \left(\frac{\partial \lambda}{\partial P_3} - \frac{\partial \lambda}{\partial P_1} \right)$. Minor numerical errors may be introduced as a result of noise. Note that for application in real time on field measurement data, a sliding window may be used to obtain continuous solutions. To further improve implementation efficiency, a recursive method may be used.

6.4.2. Case Studies Using a Two-Area Four-Machine System

To verify the performance of the proposed algorithm in estimating modal sensitivities, the two-area-four-machine system shown in Figure 4-3 is used to generate simulation data sets. The following study was carried out with the Power System Toolbox (PST) version 3.0 [Chow and Rogers 2000; Chow and Cheurg 1992]. The base case of the two-area-four-machine system is originally from the Power System Toolbox, and stored in "`data2a.m`". For the base case, the system has an inter-area mode at Freq=0.60Hz Hz and DR=6.89%, which is chosen as the mode of interest. To simulate the random load and generation variation, random perturbations are added to the generators and loads to generate 300 cases. G1 is chosen as the reference for calculating relative modal sensitivity. Two groups of data are generated with different levels of perturbation. The first group has 1% of load and generation perturbations, while the 2nd group has 10% of load and generation perturbations. The PST is used for calculating eigenvalues. For simulation, the mode sensitivity can be calculated directly from the model and is used as the reference for evaluating the performance of the model sensitivity estimation algorithm. To unify the sign notation of load and generation, the loads are denoted as negative generation. The study results for damping ratio sensitivity analysis are summarized in Figure 6-3. The sensitivity is relative to the reference generator G1. It can be observed that the estimation results are consistent with direct computation. This consistency verifies the validity of the proposed algorithm. It is also observed that the estimation error increases with the level of perturbation. The damping ratio sensitivity estimation from 1% perturbation carries slightly less error than the sensitivity estimation from 10% changes, which indicates the non-linear behavior introduced by the larger perturbation and not modeled in the linearized method.

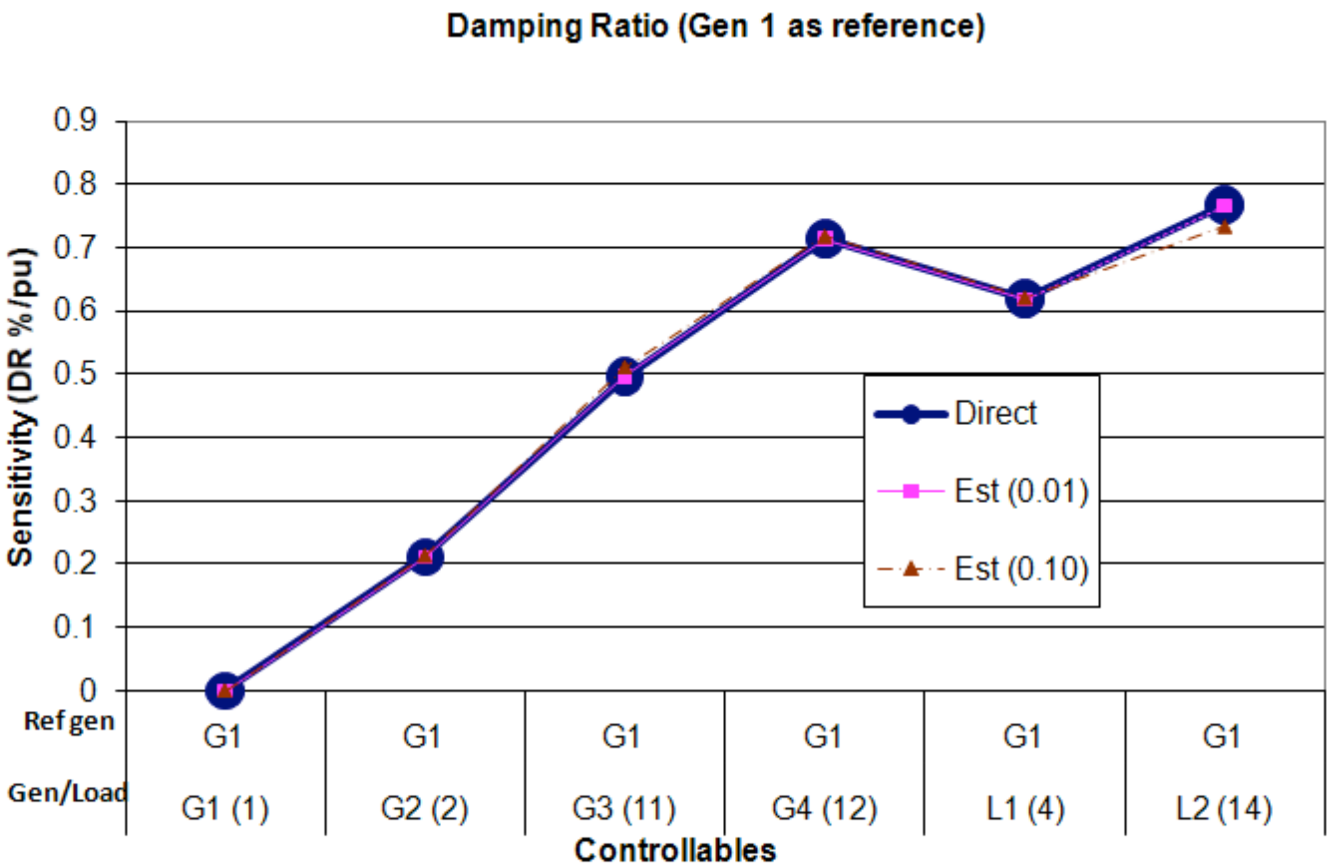

Figure 6-3. Estimated modal sensitivity of the two-area-four-machine system.

To apply the analysis results shown in Figure 6-3 for generating a MANGO recommendation, the largest sensitivity difference should be examined when identifying the most effective generator pair. Figure 6-3 indicates that the most effective pair is G4 and G1, with the largest sensitivity difference being 0.7% per p.u. power. The corresponding MANGO recommendation is "increase the G4 power output by 3 p.u. and decrease G1 by 3 p.u., and the damping ratio is expected to increase by about 2.1% (3 p.u. * 0.7 % per p.u.)".

To further verify this MANGO recommendation, a time domain dynamic response is generated by simulating three phase fault at bus 3 on the line from bus 3 to bus 101. The fault starts at 0.1 seconds and clears at 0.15 seconds. The dynamic response for the case before and after MANGO adjustment is shown in Figure 6-4. The blue line shows that responses from the original base case. The red dashed line shows the response of system after implementing MANGO recommendation. It can be observed that the oscillation response damped out more quickly with the system after MANGO adjustment. The figure clearly shows the damping improvement after the implementation of the MANGO recommendation. Prony analysis on the simulated ringdown signal confirms the damping improvement.

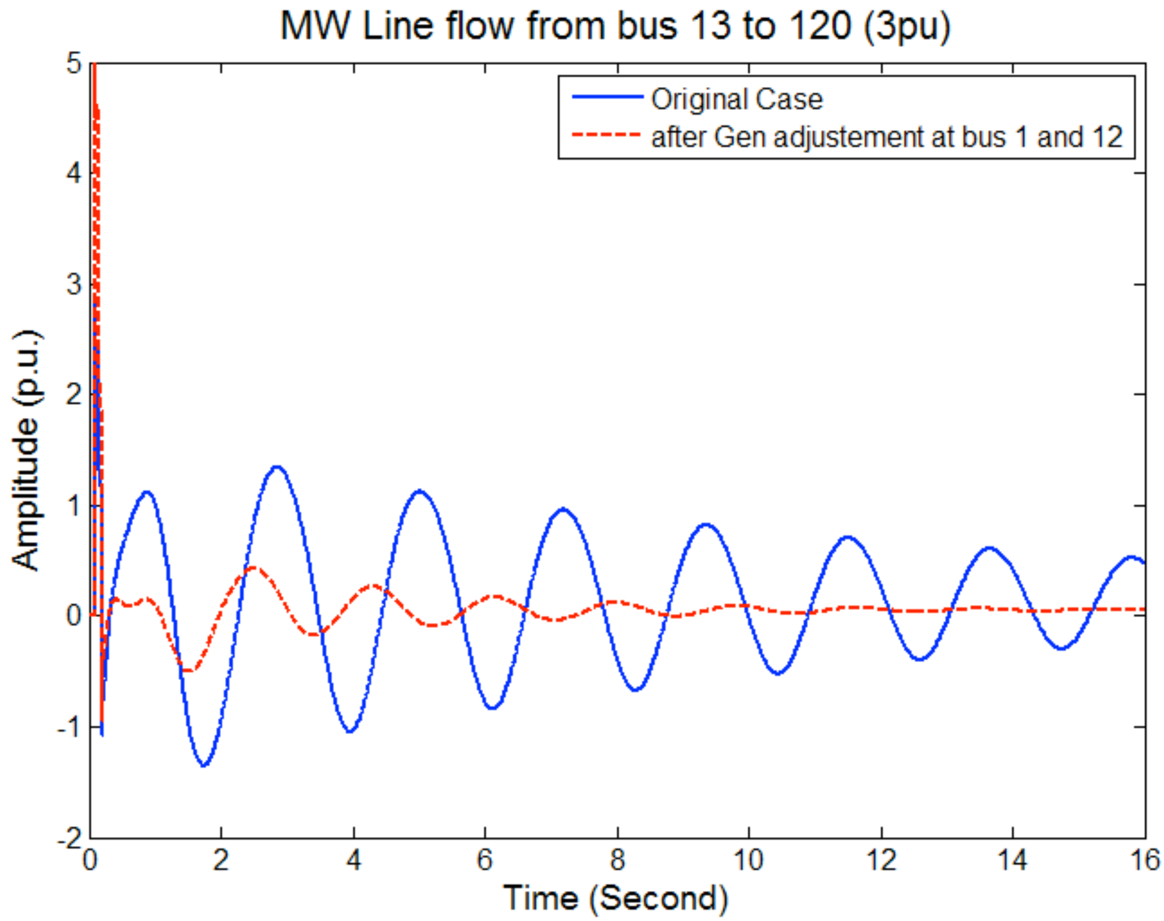

Figure 6-4. Effectiveness of MANGO recommended adjustments for the two-area-four-machine system.

6.4.3. Case studies using the minniWECC System

To evaluate the performance of the proposed algorithm for a mid-size system, the minniWECC system [Trudnowski and Undrill 2008], shown in Figure A-11, is used to generate simulation data. For the base case, the system has an Alberta mode at Freq=0.339Hz Hz and DR=1.26%, which is chosen as the mode of interest. To simulate the random load and generation variation, random perturbations are added to each generator and load to generate 1000 cases. Similar to the previous subsection, two levels (i.e., 1% and 10%) of perturbation are simulated. The Power System Toolbox is again used for simulating and calculating the eigenvalues for the two perturbation levels. The modal sensitivities calculated directly from the model are used as reference for evaluating the performance of the proposed algorithm. To unify the signs of loads and generations, the loads are again denoted as negative generation. The study results for damping ratio sensitivity analysis are summarized in Figure 6-5. The sensitivity is relative to the reference generator Gen1. It can be observed that the estimation results are consistent with direct computation. This consistency verifies the validity of the proposed algorithm.

To apply the analysis results shown in Figure 6-5 for generating MANGO recommendation, the largest sensitivity difference is examined when identifying the most effective generator pair. Figure 6-5 shows that the most effective pair is generators at buses 118 and 76 with a relative sensitivity of about 0.8 %/p.u. The corresponding MANGO recommendation is “increase the generator power output at bus 76 (Gen 32) by 3 p.u. and decrease generator at bus 118 (Gen 34) by 3 p.u., and the damping ratio is expected to increase by about

2.4% (3 p.u. * 0.8 % / p.u.)”. The damping improvement is confirmed by the eigenvalue analysis shown in Figure 6-6, where the two estimates (shown in black and green) are very close to the reference sensitivity (shown in red).

To further verify this MANGO recommendation, a time domain dynamic response is generated by simulating three phase fault at bus 86 on the line from bus 86 to bus 87. The fault starts at 5 seconds and clears at 5.095 seconds. The dynamic response for cases before and after MANGO adjustment is shown in Figure 6-7. The blue line shows that responses from the original base case. The red dashed line shows the response of system after implementing MANGO recommendation. It can be observed that the oscillation response damped out more quickly with the system after MANGO adjustment. The figure clearly shows the damping improvement after the implementation of the MANGO recommendation.

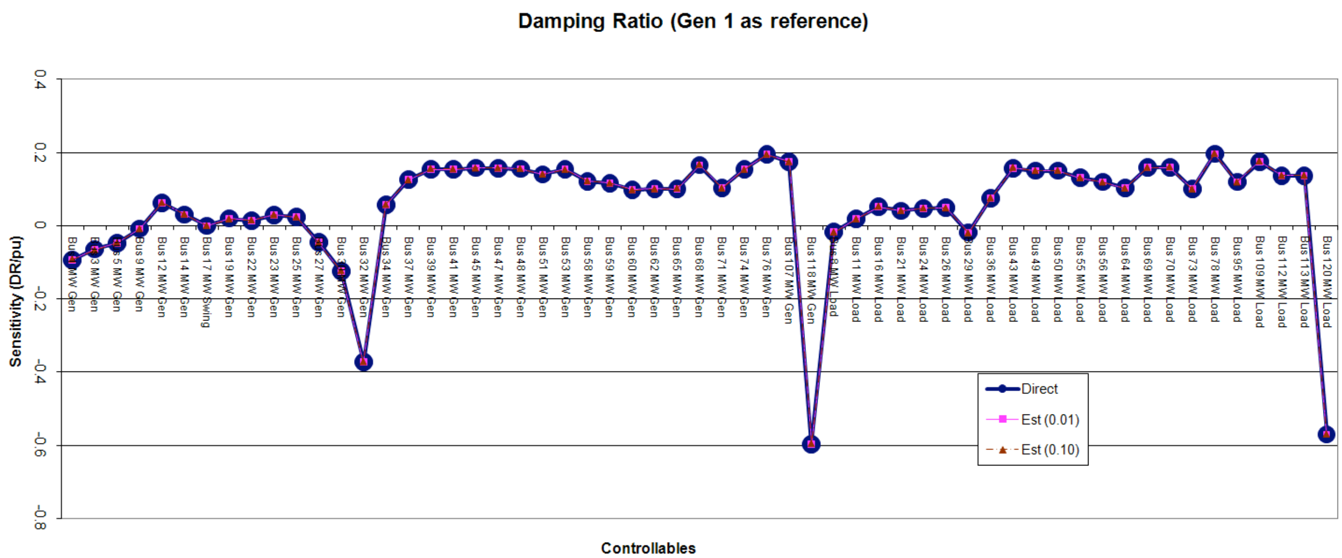

Figure 6-5. Estimated modal sensitivity of the minniWECC system.

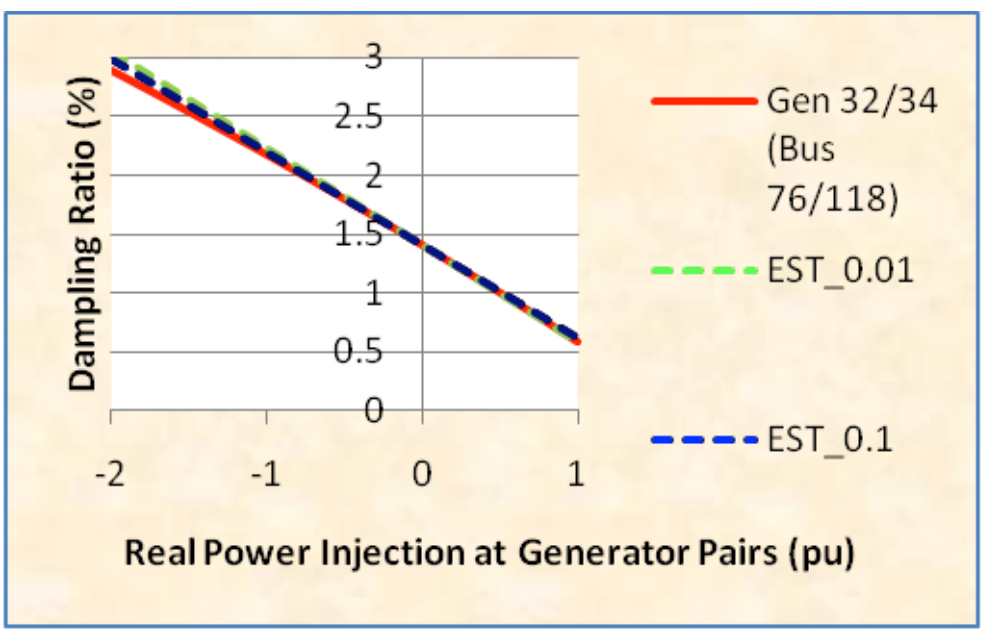

Figure 6-6. Effectiveness of MANGO recommended adjustment for the minniWECC system.

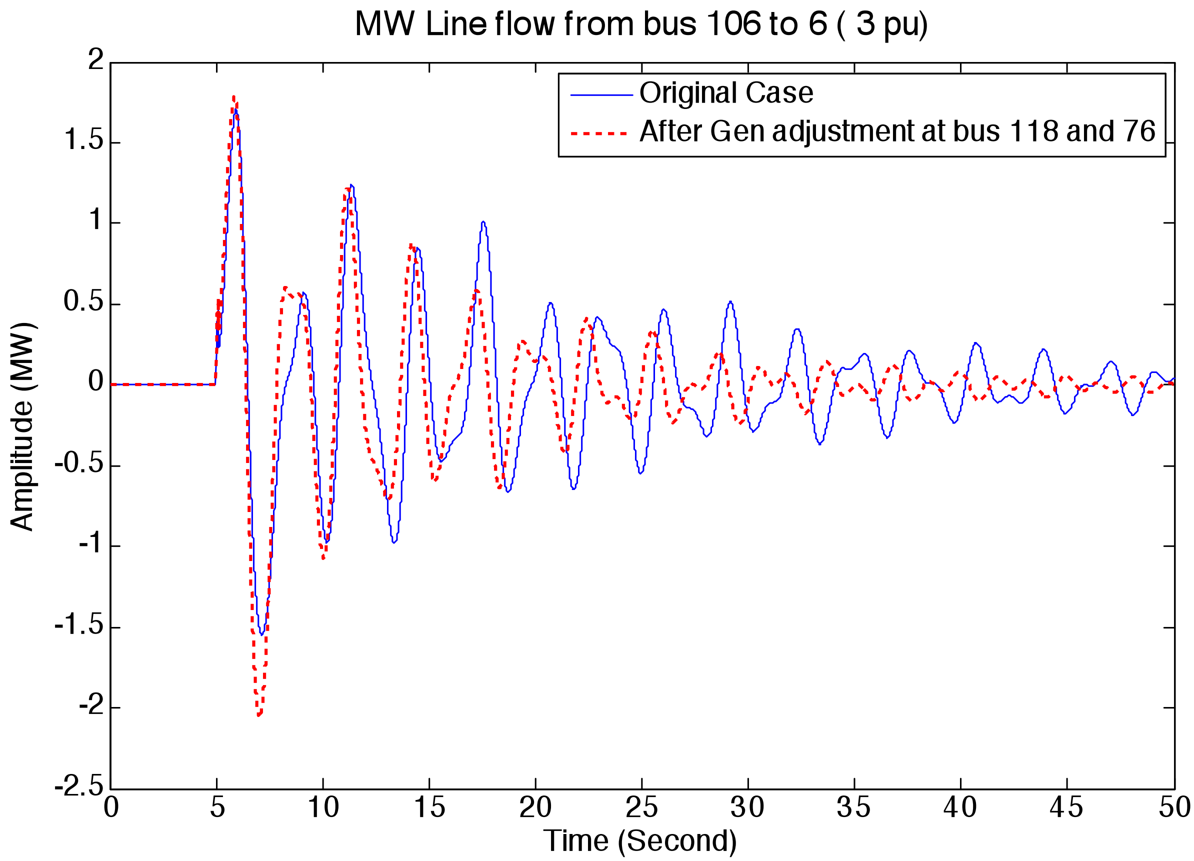

Figure 6-7. Effectiveness of MANGO recommended adjustment for the minniWECC system

6.5. Relative Modal Sensitivity Estimation w. r. t. Power flow on Transmission Lines

The appearance of lightly damped modes has been associated with "transmitting bulk power over long distances" [Pai et al. 2004]. The small signal stability problem puts an upper limit on how much power can be transferred over some tie lines. BPA DSO 303 provides guidelines to reduce tie-line flows when light damping modes are observed. It is desirable for grid operation to find the modal sensitivity with respect to the power flow of key transmission lines. In this subsection, an iterative method is formulated for estimating the modal sensitivity with respect to power flow on major transmission lines. The estimation process uses a series of ModeMeter results. The algorithm takes advantage of the natural variations in oscillation modes and operating points over a period of time. Preliminary tests have been performed with the two-area-four-machine system and the minniWECC system mentioned in the previous subsection. The performance of the proposed algorithms is evaluated based on simulation data from the tests.

6.5.1. Algorithm Description

Similar to the modal sensitivity with respect to generation and load, when the operational points of power grid do not change significantly, the relationship between the modes changes and line flow changes can be described as

$$\Delta\lambda^{(i)} = \frac{\partial\lambda}{\partial p_1}\Delta p_1^{(i)} + \frac{\partial\lambda}{\partial p_2}\Delta p_2^{(i)} + \ldots + \frac{\partial\lambda}{\partial p_{NLine}}\Delta p_{NLine}^{(i)} + \varepsilon^{(i)} \quad (6\text{-}9)$$

where the Δp represents real power changes in the transmission line from previous instance, *NLine* represents the total number of transmission lines, the superscript (i) denotes that it is the ith perturbation, λ represents the eigenvalue of interest, and $\Delta\lambda$ denotes the changes of the eigenvalue from previous instance. Note that for real-time application, the modal sensitivity $\partial\lambda / \partial p_j$'s are unknown and need to be estimated. The $\Delta\lambda$ can again be estimated from real-time measurement using a ModeMeter algorithm. Δp can be derived from field measurement. To estimate the modal sensitivity with respect to line flows, the following equations can be formed after N time instances.

$$\begin{bmatrix} \Delta\lambda^{(1)} \\ \Delta\lambda^{(2)} \\ \vdots \\ \Delta\lambda^{(N)} \end{bmatrix} = \begin{bmatrix} \Delta p_1^{(1)} & \Delta p_2^{(1)} & \cdots & \Delta p_{NLine}^{(1)} \\ \Delta p_1^{(2)} & \Delta p_2^{(2)} & \cdots & \Delta p_{NLine}^{(2)} \\ \vdots & \vdots & \ddots & \vdots \\ \Delta p_1^{(N)} & \Delta p_2^{(N)} & \cdots & \Delta p_{NLine}^{(N)} \end{bmatrix} \begin{bmatrix} \dfrac{\partial\lambda}{\partial p_1} \\ \dfrac{\partial\lambda}{\partial p_2} \\ \vdots \\ \dfrac{\partial\lambda}{\partial p_{NLine}} \end{bmatrix} + \begin{bmatrix} \varepsilon^{(1)} \\ \varepsilon^{(2)} \\ \vdots \\ \varepsilon^{(N)} \end{bmatrix} \tag{6-10}$$

When $N \geq NLine$, equation (6-10) may be solved for the modal sensitivity using least squares optimization. To simplify notation, the equation (6-4) can be written in matrix format as

$$\Delta\lambda = \Delta p \cdot \frac{\partial\lambda}{\Delta p} + \varepsilon \tag{6-11}$$

However, because of correlations among the real power flows on transmission lines, the columns in Δp matrix of equation (6-11) can be linearly dependent. In this case, the Δp matrix is ill-conditioned. Standard least square solvers usually fail to provide a good solution for ill-conditioned problems.

The linear dependency of columns in the Δp matrix of equation (6-11) is much more complex than that of the ΔP matrix in equation (6-5). For example, in ΔP the only constraint is equation (6-6). There can be *NGen+NLoad*-1 columns of data in ΔP that are linearly independent. In comparison, the linear dependency of Δp matrix can take many forms. For example, in Figure 4-3 of the two-area-four-machine model, there are two transmission lines between bus 3 and bus 101. Due to the symmetric structure, the power flows in those two transmission lines are highly correlated. Another example is that the sum of real power flow into a bus equals the sum of the real power flow out of the bus. In Figure 4-3, the sum of real power flows into bus 3 equals to 0. These relationships determine that the columns of Δp matrix in equation (6-11) are highly correlated. Consequently, the equation (6-11) is an ill-conditioned problem. Due to the complexity of the linear dependency, it is not possible to resolve the ill-conditioned problem analytically as was done for the case of generation and load sensitivities in Section 6.4. Therefore, a new numerical method is proposed in this study.

Several commonly used algorithms for solving ill-conditioned regression problem are explored. Some initial tests were performed and revealed that these algorithms cannot be applied directly to solve the problem defined by equation (6-11). A brief discussion and summary of these algorithms is as follows:

1. **Standard regression method**: In MATLAB®, the standard linear regression is provided by function [`regress`]. To deal with linearly dependent columns, [`regress`] generates a 0 solution for the linearly dependent column. Applying the function [`regress`] directly on the simulation data generated from the two-area-four-machine model, big errors in sensitivity estimation are observed. Instead of perfectly linearly dependant, most of columns of the □*p* matrix are very close to be linearly dependent. This causes the ill-conditioned problem and results in significant errors in the solution. Therefore, the standard regression method is not suitable for solving the modal sensitivity problem.
2. **Partial least-square regression**: In MATLAB®, the partial linear regression is provided by function [`plsregress`]. To find the fundamental relationship between the line flow and the mode, latent variables are introduced by the partial least square regression. The latent variables are independent variables, which serve as a transform to connect transmission line flows and oscillatory modes. The ill-conditioned problem is well taken care of by this method. Yet, the latent variables are purely from mathematical computation. It lost the physical meaning and, in turn, cannot provide the guidance needed for MANGO recommendations. The modal sensitivity cannot be readily obtained from the solution of partial least square regression.
3. **Stepwise regression method**: In MATLAB®, the stepwise regression is provided by function [`stepwisefit`]. "Stepwise regression is a systematic method for adding and removing terms from a multilinear model based on their statistical significance in a regression" [MathWorks 2010]. It uses statistical methods to remove the redundant variables. This method appears to be a good fit for the modal sensitivity problem. However, a detailed review shows that the stepwise regression method checks the null hypothesis (i.e., whether a coefficient should be set to 0) to determine whether a variable should be included. According to initial tests on the two-area-four-machine system model, this results in some lines with little changes being mistakenly included with top priority, and the inclusion of these variables results in large errors in sensitivity estimation.

The proposed algorithm for the modal sensitivity analysis adopts a similar estimation procedure as the stepwise regression algorithms. The major change is that instead of focusing on the null hypothesis tests, the proposed method is focused on the percentage of the contribution from the explaining variables. In the line flow case, the explaining variables are transmission line flows. The proposed algorithm is referred to as a modified stepwise regression (MSR). The essence of the MSR is to select a subset of independent columns from matrix □*p*. This subset of independent columns should be able to reflect most of the variations of the modes. The modified stepwise regression is carried out using the following procedure:

1. Set [*nStep*]=1; Initialize the subset of selected independent columns to be empty ; Initialize the subset of processed columns to be empty; Initialize the remaining columns as all the columns from matrix □*p*.
2. Add one column from the remaining columns to the selected independent columns one at a time to form a group of [*nStep*] column subsets. Fit the formed subset to the mode changes using standard linear regression function [`regress`].
3. Identify one new formed subset, which can best explain the mode changes. The corresponding column added in step (2) from remaining columns is moved permanently to the subset of selected independent columns.
4. Fit each of the remaining columns with the selected independent columns to identify the linear dependency. If a column is identified to be linearly dependent on the selected independent columns, it is moved to the subset of processed columns. The correlation between the processed columns and selected independent column are recorded.
5. Set [*nStep*]= [*nStep*]+1.

6. If the subset of remaining columns become empty or adding an additional column in the selected independent columns does not help improve the mode change significantly, end the procedure, otherwise go to step 2.

With the MSR algorithm, a subset of independent columns in matrix □p can be identified. This subset of the independent columns can be used to fit the mode changes without causing an ill-conditioned problem. Also, the line flows can be sorted according to their contribution to explaining the mode changes. In addition, correlation between the processed column and selected independent columns can be used to group the transmission line together to reveal their dependency.

6.5.2. Case Studies Using a Two-Area Four-Machine System

To verify the performance of the proposed MSR method, the two-area four-machine system shown in Figure 6-9 is used to generate simulation data for studying the modified algorithm in estimating modal sensitivities. The study was again conducted with the Power System Toolbox, version 3.0. For the base case, the system has an inter-area mode at Freq=0.65 Hz and DR=5.37%, which is chosen as the mode of interest. To simulate the random generation variation, 10% random perturbations are added to the generators to create 300 cases. To simplify the study, loads are kept unchanged. The study results for damping ratio sensitivity using the MSR algorithm are summarized in Figure 6-8 an Table 6-2.

In Table 6-2, columns of □p are arranged in 5 groups. The first transmission line in each group consists of the selected independent columns of □p. The other transmission lines in the same group are highly correlated to the first line. It can be observed from Figure 6-8 that about 94% of mode DR changes can be explained by the power flow on the transmission lines in group #1. This means that the mode DR is most sensitive to the power flow in group #1. The transmission lines in group #1 are marked in magenta lines in Figure 6-9. It can be observed that these are inter-area tie lines and lines highly correlated to tie lines. The mode sensitivity with respect to the tie line, defined by bus 3 to 101, is -2.38. This means that to increase the DR of the inter-area mode by 2.38%, the real power flow in the tie line (from 3 to 101) should decrease by 100 MW.

It is also observed that the sensitivity with respect to lines #3 and #4 is extremely large, while the percentages of contribution are small. Further examination of the data reveals that those lines do not have significant power flow changes. The sensitivity solution for these lines should be considered invalid.

With the sensitivity derived, it can be observed that the tie line plays a dominant role in the inter-area mode.

The DR changes of the inter-area mode are related to the line flow as follows:

$$\Delta DR = -2.38\Delta p_{3->101} - 0.22\Delta p_{1->10} + \varepsilon \qquad (6\text{-}12)$$

To verify the results, some additional independent validation cases are generated. The DR changes predicted from equation (6-11) are compared against the true mode changes from PST simulation. The results are summarized in the Table 6-3. It can be observed from the Table 6-3 that the estimation results are consistent with the true sensitivities, with only minor estimation errors.

Table 6-2. Mode Sensitivity w.r.t. Line Flow in the Two-Area-Four-Machine System[2].

Group Index	Line Index	From Bus	To Bus	Mode Sensitivity of DR changes.	Percentage Contribution to mode DR
1	5	3	101	-2.38	94.2%
	4	3	20	-	-
	6	3	101	-	-
	11	13	101	-	-
	12	13	101	-	-
	13	13	120	-	-
2	1	1	10	-0.22	3.5%
	2	2	20	-	-
	7	10	20	-	-
3	3	3	4	5.6e8	1.7%
4	4	13	14	-3.8e5	0.2%
5	9	12	120	-0.12	0.0%
	8	11	110	-	-
	14	110	120	-	-

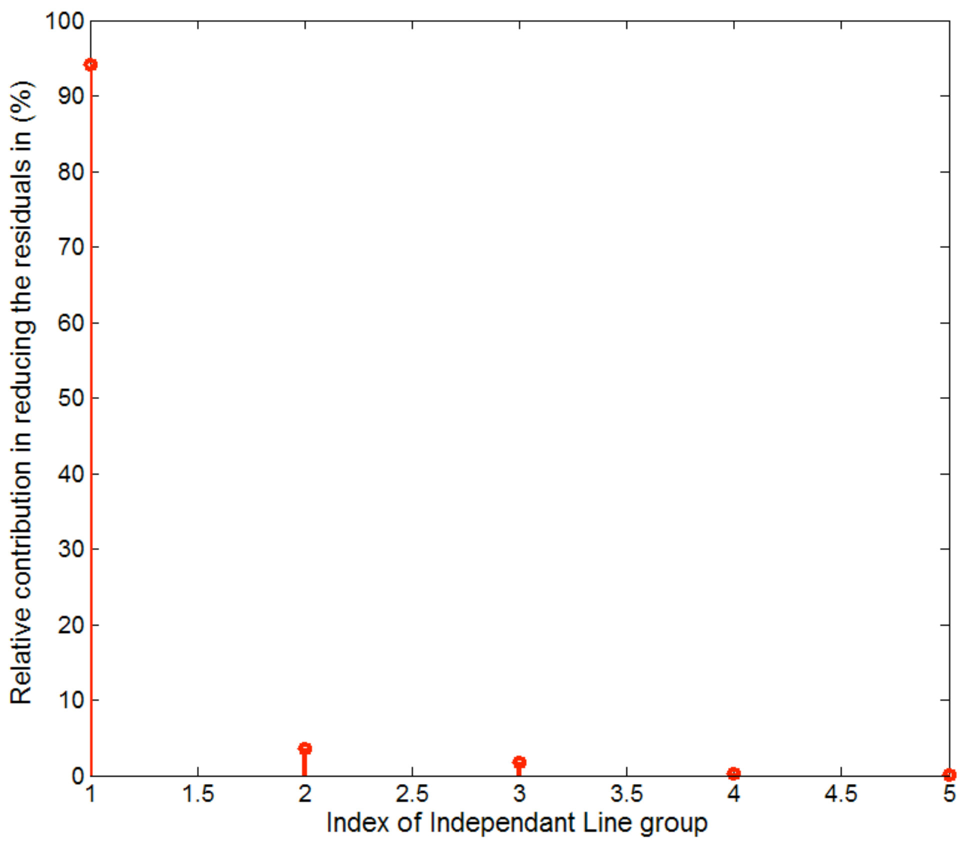

Figure 6-8. Percentage of Contributions from Line Flow to the Damping Ratio in the Two-Area-Four-Machine System

2 Note: "-" indicates that this line is not selected in the dependence analysis using the MSR algorithm

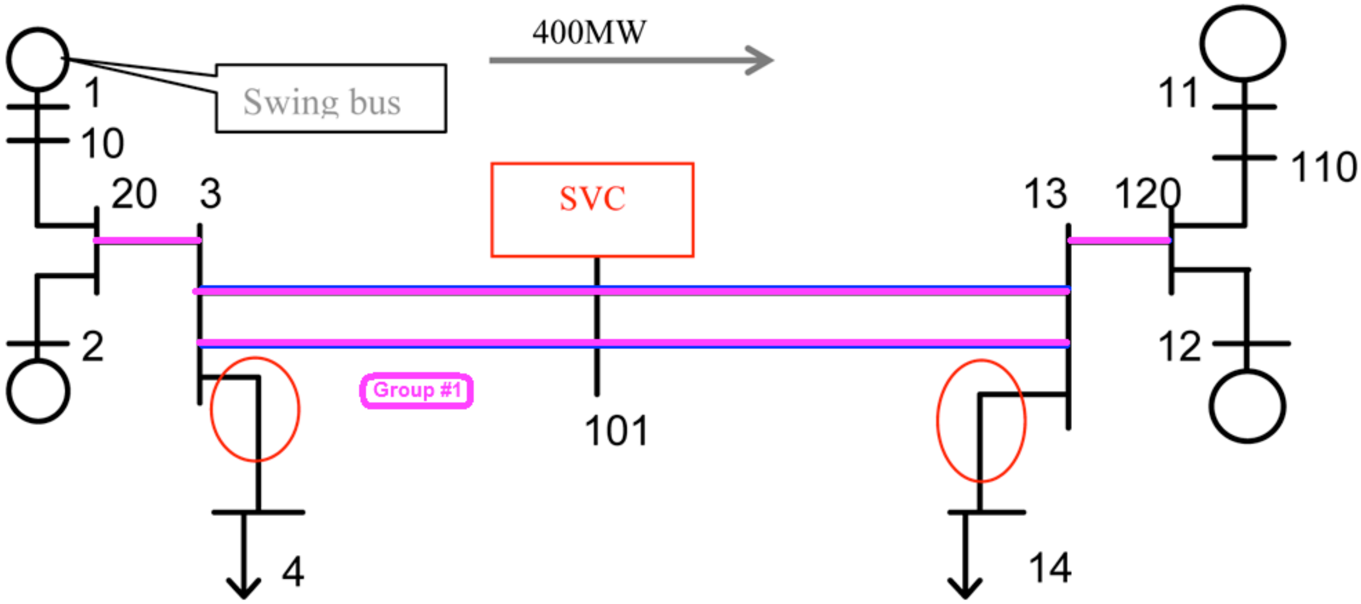

Figure 6-9. Transmission Line with Major Modal Sensitivities in the Two-Area-Four-Machine System (Figure adapted from [Chow and Rogers 2000].

Table 6-3. Validation of Mode Sensitivity w.r.t. Line Flow in the Two-Area-Four-Machine System.

Ref bus	Adjust Gen	Adjustment (PU)	$\Delta p_{3\to 101}$	$\Delta p_{1\to 10}$	Estimated DR changes (%)	True DR changes (%)	Relative Err
1	Gen3 (on bus 11)	0.5	-0.254	-0.546	0.724%	0.790%	-8.4%
1	Gen3 (on bus 11)	1.0	-0.502	-1.076	1.432%	1.475%	-2.9%
1	Gen4 (on bus 12)	0.5	-0.265	-0.569	0.756%	0.763%	-1.0%
1	Gen 4 (on bus 12)	1.0	-0.525	-1.125	1.498%	1.440%	4.0%

6.5.3. Case Studies Using a minniWECC Model

A mid-size system, the minniWECC system [Trudnowski and Undrill 2008], shown in Figure A-11, is used to further evaluate the performance of the proposed algorithm. For the base case, the system has an Alberta mode at Freq=0.339Hz and DR=1.26%, which is chosen as the mode of interest. To simulate the random generation variation, 10% random perturbations are added to each generator to generate 1000 cases. To simplify the study, loads are again kept unchanged. The study results for damping ratio sensitivity using the MSR algorithm are summarized in Table 6-4 and Figure 6-10. For clarity, only the lines with a contribution higher than 0.5% are presented.

In Table 6-4, major columns of □*p* are arranged in 14 groups. The first transmission line in each group consists of the selected independent columns of □*p*. The other transmission lines in the same group are highly correlated to the first line. It can be observed from Figure 6-10 that two groups of transmission lines contribute significantly to the variation of the Alberta mode. The first group contributes about 39.4% of the DR changes. The geographic location of the first line group is marked in blue in Figure 6-11. Also overlaid on this geographic map are the mode shapes of the Alberta mode. It can be observed that the 1st line group is a group of tie lines between two oscillation areas defined by the mode shape. The sensitivity of first line is -0.53, which means that the DR of the Alberta mode can be increased by about 0.53% if the line flow from bus 83 to bus 103 is reduced by 100 MW. The second group of tie lines is located at the border of British Columbia and Alberta. They are marked in magenta in Figure 6-11. Its contribution to the DR variation of Alberta mode is about 35.4%. According to the mode shape, these are also tie lines between the two areas which oscillate against each other. The sensitivity is 1.08, which means that the DR of the Alberta mode can be increased by 1.08% if the tie line flow from bus 119 to bus 117 is reduced by 100 MW.

Table 6-4. Modal Sensitivity w.r.t. Line Flow for the minniWECC System[3].

Group Index	Line Index	From Bus	To Bus	Mode Sensitivity of DR changes.	Percentage Contribution to mode DR
1	97	83	103	-0.53	39.4%
	98	103	102	-	-
2	166	117	119	1.08	35.4%
	163	6	106	-	-
	164	106	119	-	-
	165	106	117	-	-
3	79	84	20	-0.22	4.8%
4	133	49	113	0.05	2.3%
5	73	33	83	-0.50	3.8%
	14	32	33	-	-
	74	33	85	-	-
	75	83	85	-	-
	76	83	84	-	-
	77	83	84	-	-
6	65	7	10	-0.03	2.8%
7	142	57	66	0.13	1.4%
	143	57	98	-	-
	144	98	66	-	-
8	69	10	13	-0.06	0.71%
9	161	72	69	-0.06	0.73%
10	89	86	88	-0.32	1.07%
11	58	80	7	-0.28	1.02%
	56	80	81	-	-
	57	81	7	-	-
12	124	114	46	0.08	0.80%
13	138	113	57	0.09	0.68%
	136	113	57	-	-
	137	113	57	-	-
	138	113	57	-	-
	139	113	116	-	-
	140	116	57	-	-
14	40	29	28	0.03	0.51%

3 Note: "-" indicates that this line is not selected in the dependence analysis using the MSR algorithm.

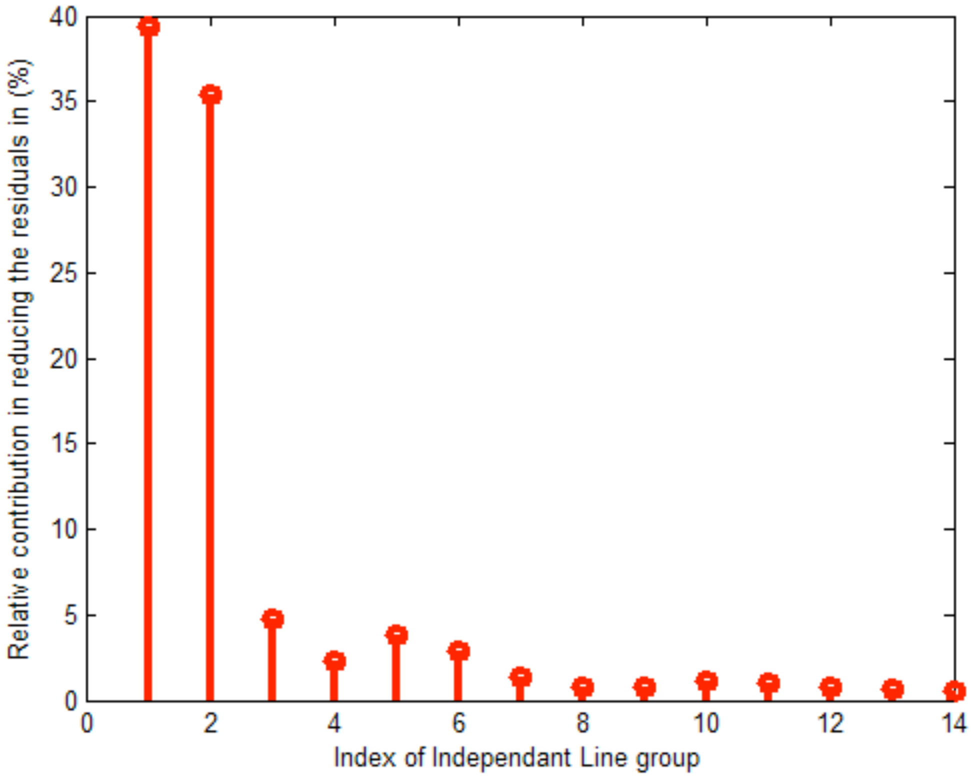

Figure 6-10. Percentage of Contributions from Line Flow to the Damping Ratio in the minniWECC System

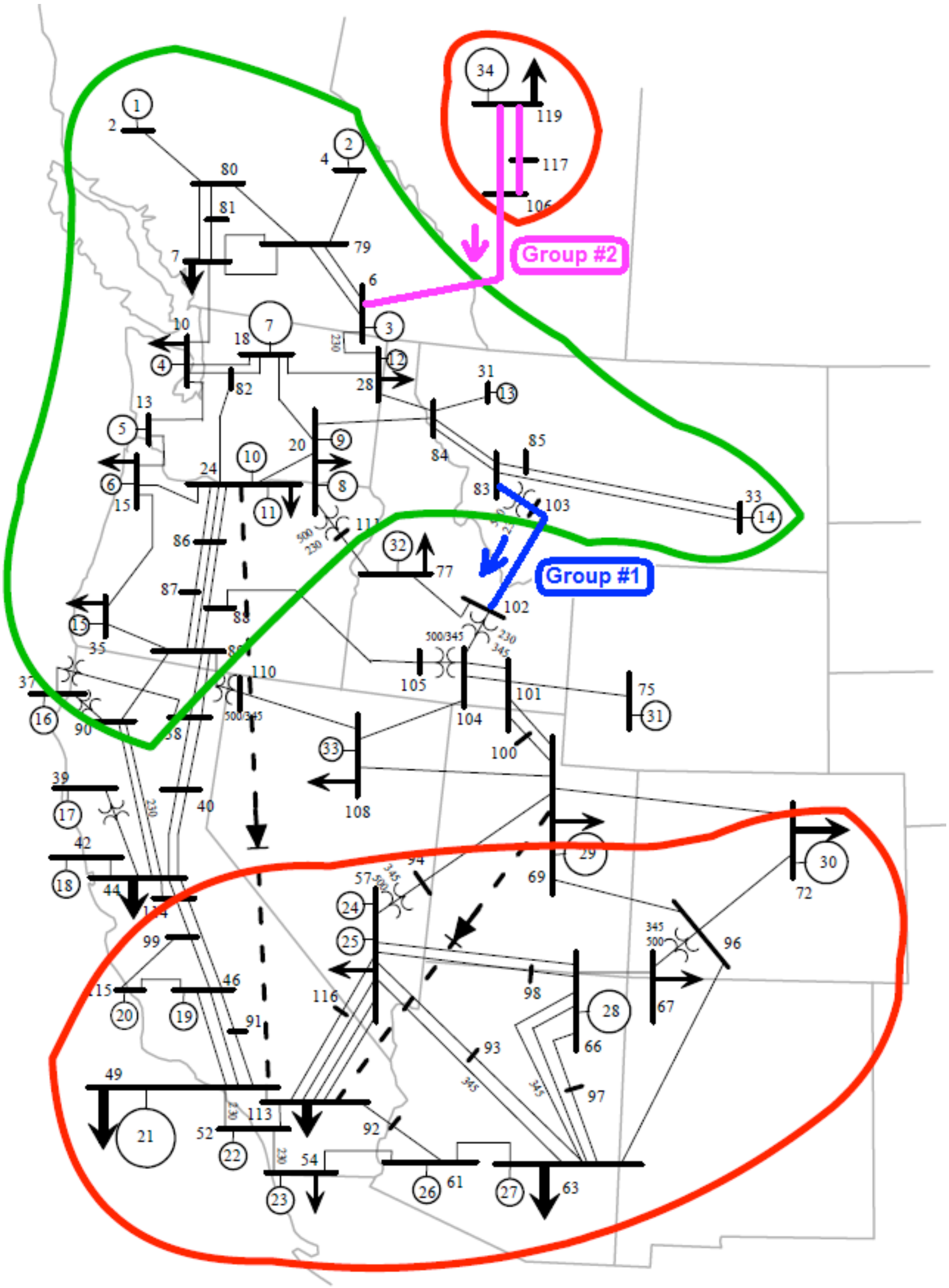

Figure 6-11. Transmission Lines with Major Modal Sensitivities in the minniWECC System (Figure adapted from [Trudnowski and Undrill 2008]).

7.0 Topology Impact Analysis

7.1. Problem Formulation

In previous studies, it was shown that the sensitivity relationship between operator actionable variables and modal damping ratios exhibits highly non-linear phenomena and varies with system stress levels and generation patterns. Prior work applied Artificial Neural Network (ANN) techniques to the MANGO framework as a means to represent the non-linear relationship. Extensive studies using a large number of operation conditions showed the ANN model was sufficient in determining MANGO recommendations with the minniWECC system for a certain power grid topology [Huang et al. 2009].

Power grid topology is of great importance in power grid analysis. Different power grid topologies can change grid characteristics, power flow patterns, and even the robustness of a power system. Power grid topology changes are a common behavior due to maintenance, faults, economics, or other reasons. Therefore, there is a need to investigate the performance of the previously reported MANGO approach for different network topologies; it should be studied whether MANGO recommendations with one certain topology is applicable to power systems with different topologies. In the following discussion, it will be shown how topology changes affect MANGO recommendations, and how to accommodate the changes in the MANGO framework. The objective is to evaluate and improve the effectiveness of a MANGO framework with different topologies.

7.2. Technical Approach

As described in the August 2009 MANGO CEC report [Huang et al. 2009], an Artificial Neural Network approach is used as an approximate fit to the non-linear relationship between operating paratmeters and inter-area modes. This is a three-step approach: (1) Prepare the data for training, validation and testing; (2) Train, validate, and test the ANN; (3) Use the ANN output to implement the MANGO Control. The minniWECC system (Figure 6-11) is used as a base model for our topology change study. The minniWECC model is a simplified dynamic model for the western interconnection which consists of 34 generators, 120 buses, 115 lines and high-voltage transformers, 54 generator and load transformers, 23 load buses, and 2 HVDC lines. It intends to represent the overall inter-area modal properties, which are geographically consistent with the WECC system. Both training and validation test sets were generated using the minniWECC model. The validation set is used to determine the performance of the ANN model created with the training set. If the ANN model does not reach a desired level of accuracy, the model is adjusted and the ANN re-trained until specifications are met. The ANN model is then used to generate MANGO recommendations to control inter-area modes.

In order to study the effects of different topologies, a large amount of simulations were performed for different combinations of topology changes through the entire ANN and MANGO procedure. Additionally, line status vectors were explored for inclusion in the data set to determine if the ANN could be applied to differing topologies. The effects on the MANGO control were then studied. Since the minniWECC base case is a low damping system, removing one or more lines from the topology of the system tended to create a system close to instability. Therefore, to present a less drastic change in topology, all transmission lines within the minniWECC were replaced with equivalent sets of two lines and only one was removed in the studies.

7.3. ANN Method Procedure

To implement the entire MANGO framework based on ANN, three steps are needed. First, test data must be prepared for training, validation, and testing. Second, an ANN model must be trained, validated, and tested using this data. Finally, the MANGO controller uses the ANN model to determine control steps. These steps are outlined below.

7.3.1. Preparing Data Set

Data sets were generated using the minniWECC model. Eleven cases were created for the ANN training by varying the stress level on the system. Incremental adjustments of -2.5% (load and generation) on the system were made from the COI_P=10 minniWECC case (i.e. 100%, 97.5%, 95%, etc.). Additionally, for each of the eleven cases, the individual load demands (real and reactive power consumption) and generator outputs (real power generation) were randomly perturbed +/- 2.5% around the base case values, giving a continuous spectrum of generator and load combinations. The eigenvalue and damping ratio of the Alberta inter-area mode at 0.339 Hz was then determined using the Power System Toolbox in MATLAB. Three thousand (3000) cases were generated per topology, of which two-thirds (2000) were used for training, and one-third (1000) were used for validation of the MANGO recommended adjustment.

Six lines were chosen to test the effects of topology changes. These were loosely classified as more important and less important lines, mainly due to the magnitude of their effects on the British Columbia to Alberta tie-line. The lines chosen and their classifications are shown in Table 7-1. The status of each of the lines, in-service or out-of-service, was recorded as a binary value (1 or 0) and used in varying configurations as inputs to the ANN, and the effects on the ANN solution observed.

Table 7-1. Transmission Lines for Topology Change Studies.

From bus	To bus	Equivalent Name	Classification
24	86	John Day to Grizzly 1	Less important
46	49	Midway to Vincent 1	Less important
79	7	Nicola to Meridian	Less important
89	38	Malin to Round Mt. 2	More important
113	57	Adelanto to Marketplace (LV-LA)	More important
83	84	Garrison to Taft 1 (Colstrip)	More Important

During the first attempt, the original minniWECC model with a high COI flow was used. It was found that removing one or more lines from the topology of the system frequently resulted in an unsolvable power flow cases when varying the stress levels and generator and load magnitudes. This limited the number of allowable cases that could be generated and hampered the ANN training process, due to the limited range of damping ratios that could be solved within the marginally stable system. To compensate, all transmission lines within the minniWECC model were modified by splitting them into two parallel lines with equivalent impedances. Instead of dropping the entirety of the line, only one of the two parallel lines was removed. This had the effect of doubling the impedance of that particular line, changing the load flow and damping ratio, without causing the system to move too close to voltage instability. The cases that follow use this double-line method. Since the minniWECC model was created as an equivalent model, where each line represents multiple lines within the complete WECC system, this representation is more analogous to the actual WECC and should be a valid assumption.

7.3.2. Training, Validation and Testing of the ANN

The sets of data generated previously were incorporated into the ANN model and used to tune the parameters of the ANN. A two layer Levenberg-Marquardt method is used for creation and training of the ANN. The set of 2000 out of 3000 data points generated were randomly divided into 70% for training of the ANN, 15% for validation of the ANN, and 15% for initial testing. The validation data set is used to determine whether training should continue or stop, while the test set is used to check the model accuracy. If the model accuracy is insufficient, then the ANN model order may need to be re-adjusted. Inputs to the ANN model included some or all of the generator power outputs, real and reactive power demands, and the binary line status configurations.

7.3.3. Using the ANN to implement the MANGO Control

The output of the ANN solution is the system damping at a specified frequency of interest. After an ANN is trained, it can be used in the MANGO controller to generate recommendations using the following pseudo-code:

1. [*ΔDamping*]= [*Target Damping*] -[*System Damping*]
2. [*ΔStepDamping*]=[*ΔDamping*]/[*MANGO Step*]
3. Find $\frac{\partial[Damping]}{\partial[Input_i]}$ for all the input channels in the ANN model.
4. Find $I = \max_i \left\{ \frac{\partial[Damping]}{\partial[Input_i]} \right\}$. *I* is the most sensitive input channel.
5. Move the ANN operational point to $[Input_I] = [Input_I] + \frac{[\Delta StepDamping]}{\partial[Damping]_i / \partial[Input_I]}$.
6. [*MANGO predicted Damping*]=ANN output at the new operational point.
7. Check to see if abs([*Target Damping*] -[*MANGO predicted Damping*]) < [*Pre-selected limit*].
8. If the inequality in step (7) does not hold, go to step (3)
9. If the inequality in step (7) holds, summarize the results from step (5) and provide MANGO recommendation.

The MANGO controller is designed to generate the smallest total power flow change to the system while still meeting the desired damping target. During each of the iterations, the most sensitive input (step 4) is selected and used to first modify the system, while successive iterations adjust less sensitive inputs at a lesser amount. These recommendations are then implemented by the MANGO controller and tested against the validation data reserved earlier.

7.4. Case Studies

Four different topology changes were considered to study the effect of topology changes:

1. Base case with all lines in-service:
2. A "less important" line status change (John Day to Grizzly 1 removed).
3. A "more important" line status change (Malin-to-Round Mt. 2 removed).
4. Multiple line status change.

The base case served as a reference for comparing the effectiveness of MANGO approaches with different topologies.

7.4.1. Base case

As a basis for comparison, the MANGO procedure was implemented with the previously discussed double-line minniWECC base case topology (all lines in-service). In Figure 7-1, the error associated with the ANN training and the resultant validation of the ANN model is shown. It can be see the error is minimal for both the dot position plots and the histograms. Figure 7-2 shows the MANGO display of the initial system state, followed by the final state. This sample shows the complete graphical interface of the ANN-based MANGO prototype tool, with all of the information that is available to the user. The block on the right of the MANGO display is a graphical representation of the target damping (the green line), of the MANGO predicted damping value (blue solid circle), and the actual system damping after application of the MANGO recommendations (red open circle). Numerical values for actual system damping, MANGO predicted damping, and target damping can be seen on the bottom left. The added red graphics indicate changes between the two states, shown in Figure 7-2 (a) and (b), respectively. Additionally, in Figure 7-3, the amount of generation and load change implemented by the MANGO solution is shown. The system initially starts with a damping value of -0.024, and through a single implementation of MANGO recommendations, damping is moved to -0.150 through the adjustment of 23 of 56 available loads and generators.

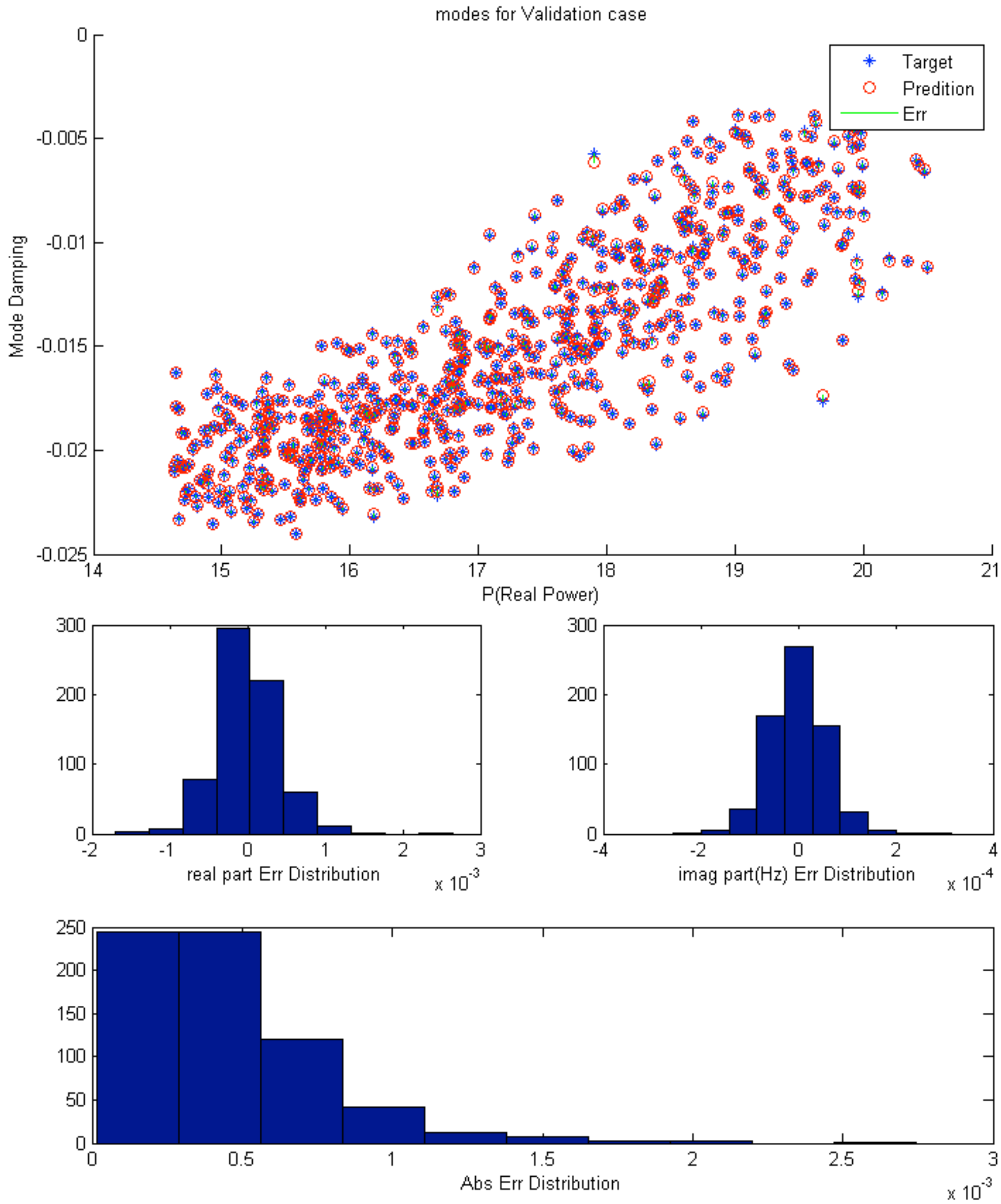

Figure 7-1. ANN training error for the base case shown as dot position errors and histograms of the real, imaginary, and absolute value of the modes.

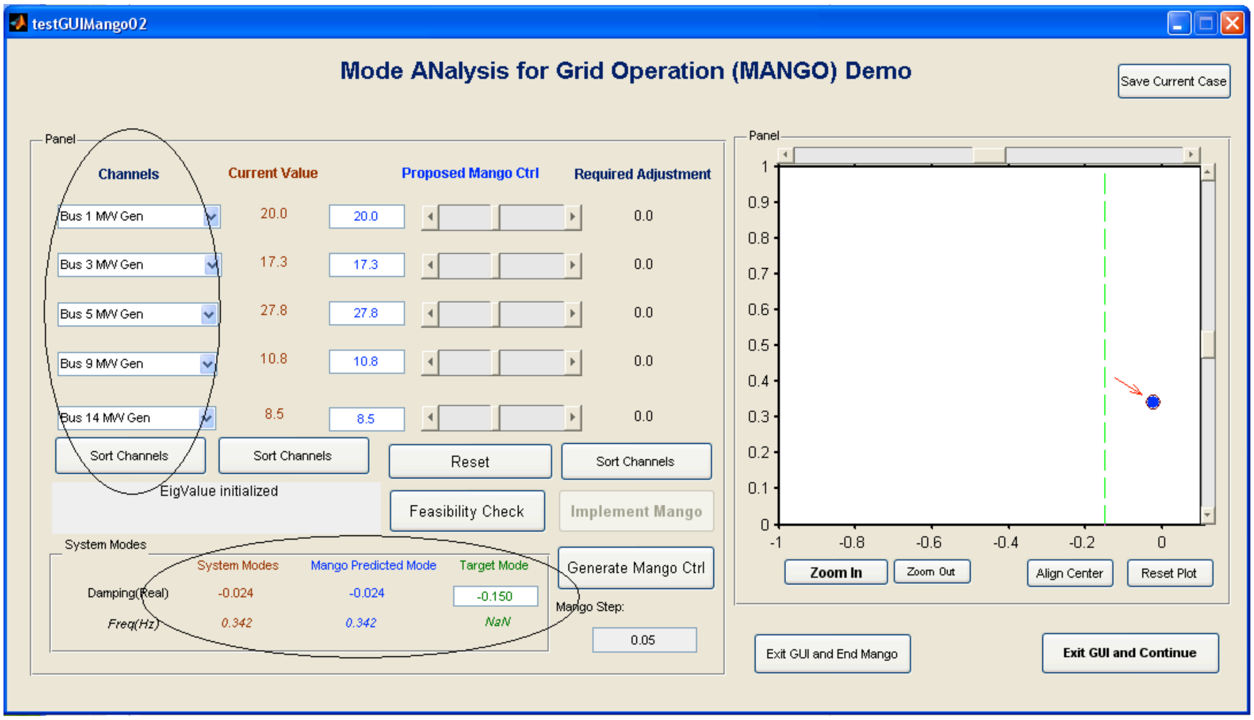

(a)

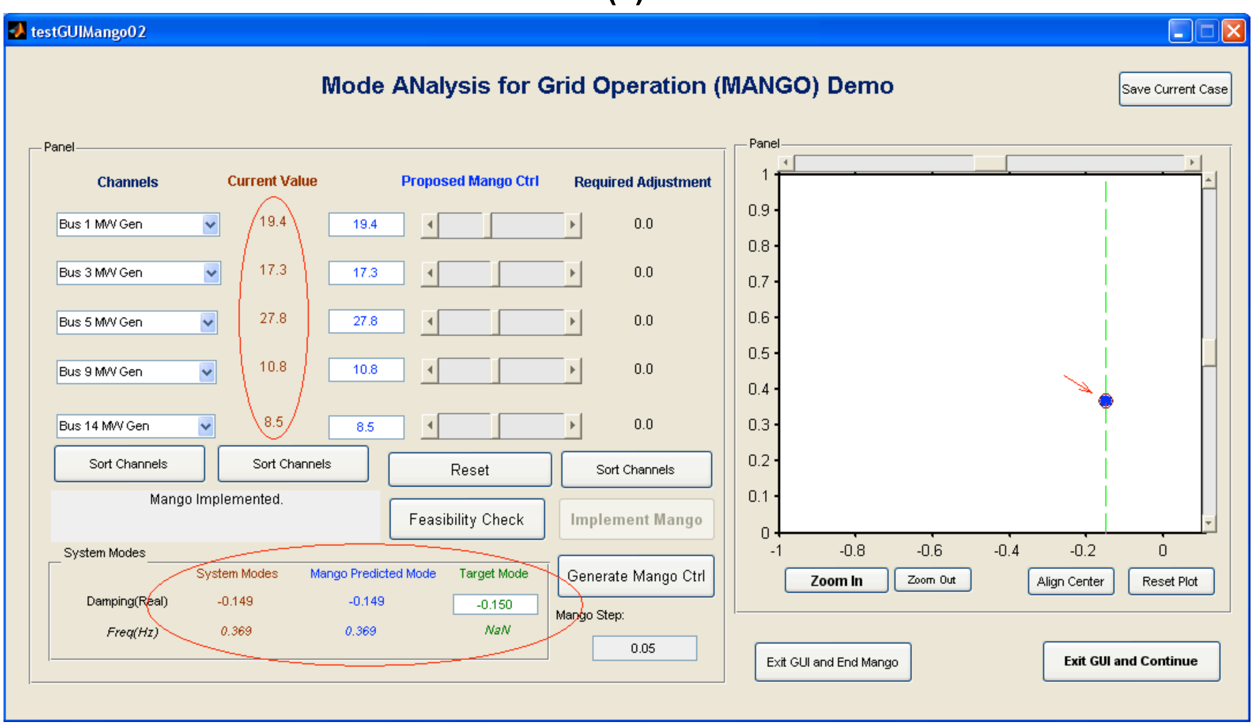

(b)

Figure 7-2. (a) Initial base case state. (b) MANGO representation of final base case solution.

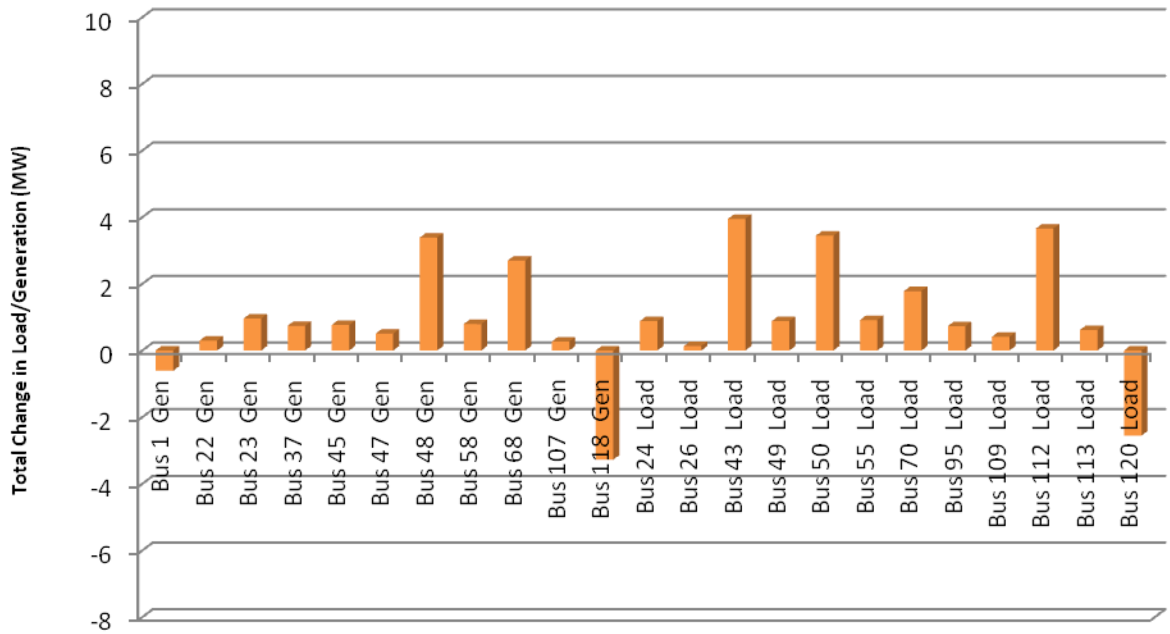

Figure 7-3. Total generation and load change implemented in base case.

7.4.2. A "less important" line status change (John Day-to-Grizzly 1).

This section and the next examine the applicability of the ANN trained with data sets from one topology to a different topology. First, a less important topology change (John Day-to-Grizzly 1) was studied. The ANN is trained with the base case data sets. Figure 7-4 shows the errors when the ANN is used to estimate modes for the case with the John Day-to-Grizzly 1 line being out-of-service. Figure 7-5 shows the errors with the ANN re-trained with data sets from both topologies and with the line status as an input.

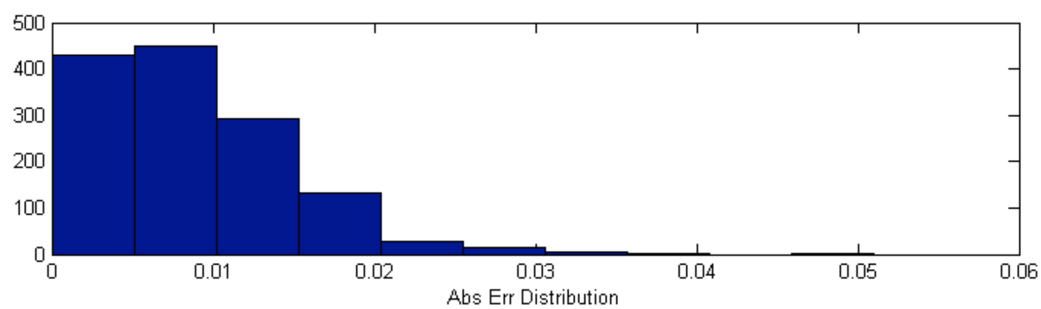

Figure 7-4. Error in ANN with single "less important" topology change (John Day to Grizzly 1), without line status at input.

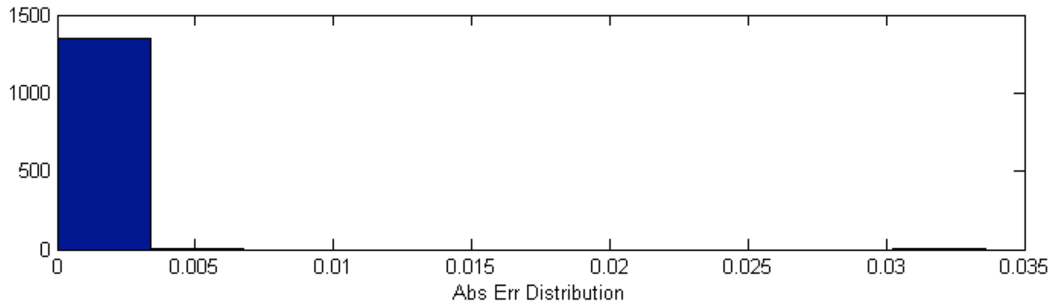

Figure 7-5. Error in ANN with single "less important" topology change (John Day to Grizzly 1), with line status as input.

Then the trained ANN was used to generate MANGO recommendations for the target damping of -0.150. After four to five iterations (depending on the system's initial damping and configuration), the desired results were obtained. Figure 7-6 shows the amount of generator and load change needed to achieve the desired damping.

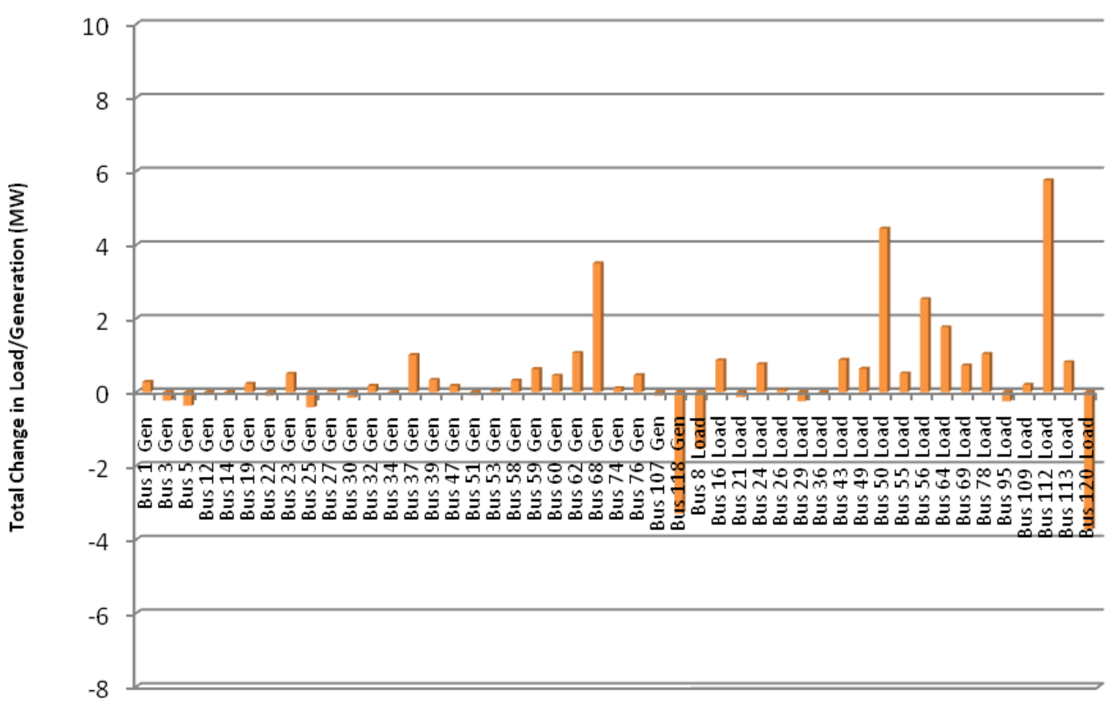

Figure 7-6. Load and generation changes recommended by MANGO for the John Day to Grizzly 1 topology case.

A number of observations can be made from these results. First, the ANN estimation error introduced by topology changes is larger than the base case. Second, it was noted that the addition of the line status as input to the ANN greatly improves the performance. While this creates an implementation difficulty within the existing MANGO procedure, it does indicate that knowledge of the topology during the training procedure can lead to better results when merging topologies. Since the MANGO procedure, as it stands now, is not able to directly use the line status vectors, all the MANGO recommendations used the results of the ANN without the line status. Despite this, when applying the ANN results to the MANGO procedure, in each case, it was able to find a solution through multiple iterations of MANGO adjustments. This was regardless of whether the test system used was either of the two topologies included in the ANN training (base topology and single line removed). This indicates that minor changes within the topology of the system can be handled by the MANGO procedure, but it is surmised that the additional line status vector will improve the performance.

7.4.3. A "more important" line status change (Malin-to-Round Mt. 2).

In order to observe the effect of an important line status change versus that of a less important line, a similar procedure to that used for the "less important" line was again used on a more important line case. Figure 7-7 shows the ANN training error for the Malin-to-Round Mt. 2 case without the line status, while Figure 7-8 shows the errors in the ANN with the line status included. Figure 7-9 shows the total generator and load adjustments needed to achieve the target damping In this case, a MANGO damping solution was found in four iterations.

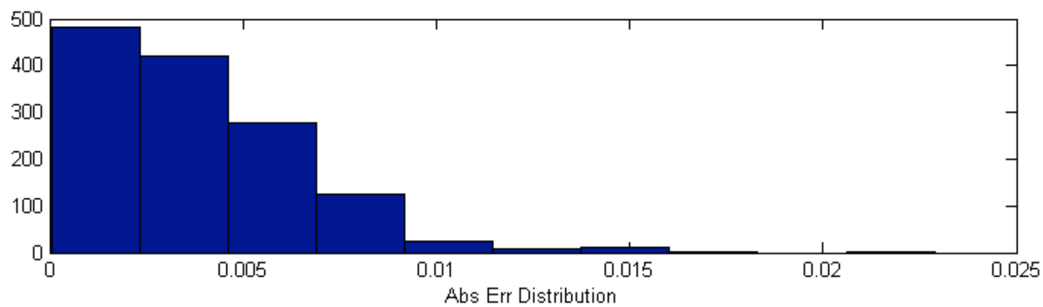

Figure 7-7. Error in ANN with single "more important" topology change (Malin-to_Round Mountain 2), without line status as input.

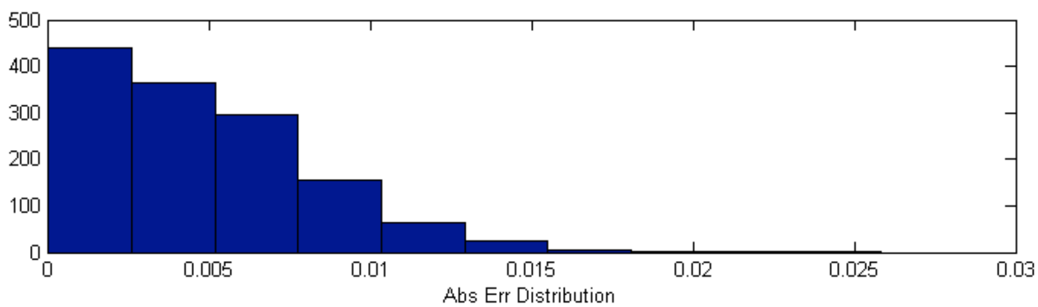

Figure 7-8. Error in ANN with single "more important" topology change (Malin-to-Round Mountain 2), with line status as input.

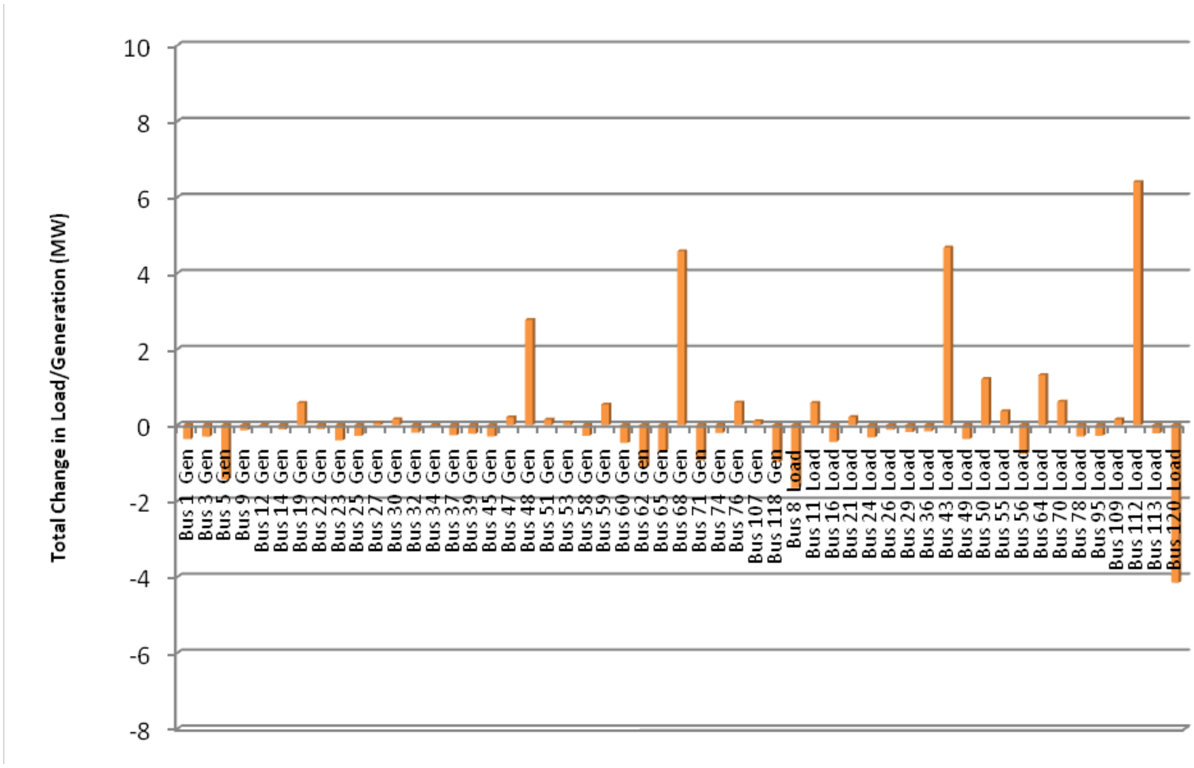

Figure 7-9. Load and generation changes implemented by MANGO procedure for Malin-to-Round Mountain 2 sample.

Like the less important line case, three observations can be made from these results. First, the error introduced by a more important topology change is similar to the less important case. Second, by including the line status to the ANN, a better fit to the non-linear solution can be found. Third, when applying an ANN, trained with multiple topology data, the MANGO procedure was able to determine the correct direction to move the system towards stability, regardless of whether the tested topology included the line status information or not. Exact target damping was achievable on multiple topologies with successive iterations of the MANGO procedure when merging two different topologies within the ANN. However, as compared to the base case and the less important topology change, both the number of generator and load changes and the magnitude of said changes increased with a more important topology change.

It is worth pointing out that the importance of the lines (as indicated in Table 7-1) is loosely defined by the impact on the British Columbia to Albert tie-line flow. This particular importance criterion was not selected based on any importance in terms of the damping values. As such, it is not surprising that the studies do not show significant difference in the application of the MANGO procedure.

7.4.4. Multiple topology changes.

The testing was expanded to include multiple topologies in the ANN solution. For this study, the number of training data set is increased along with the number of selected lines. Lines 83-84, 89-38, 113-75, and 79-7 (see Table 7-1) were removed individually, leading to five different topologies, when including the base case. The total number of training data set is 10,000. It should be noted that combinatorial topology changes were not used in training the ANN. Once again, including the line status as an ANN input decreased the training error, as can be seen in Figure 7-10 and Figure 7-11. It can also be seen that as more topologies were added to the ANN solver, validation error within the ANN increased only slightly. The MANGO procedure could similarly be applied in an iterative fashion using the ANN output, to solve any variation of the five topologies. As an example for the MANGO interface using this topology configuration, the initial test system started with a damping value of -0.024, and after eleven subsequent MANGO iterations and adjustments, the system approached the target damping of-0.150, with a final value of -0.148. The total specific amount of each bus adjustment needed is shown in Figure 7-12. It should be noted, that as the number of topologies included within the test increased, so did the number and magnitude of generator and load adjustments required to meet the target damping.

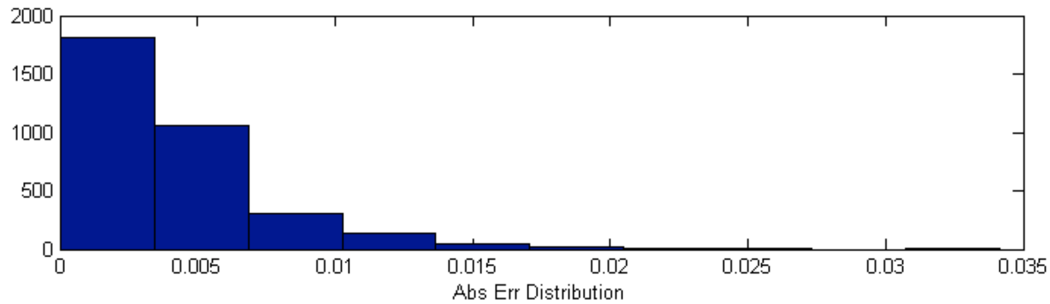

Figure 7-10. Error in ANN for multiple topologies without line status as input.

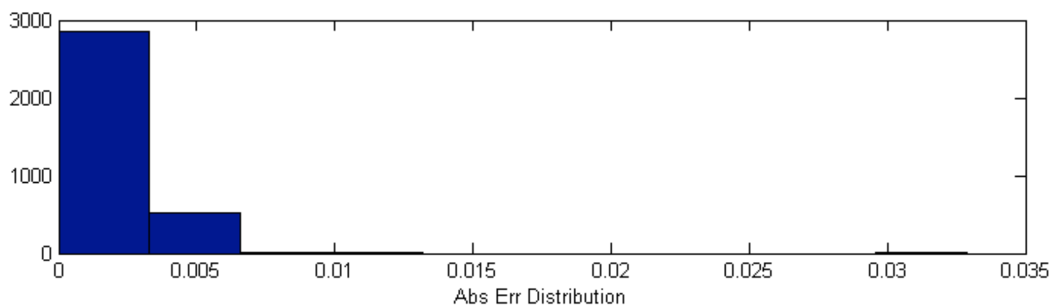

Figure 7-11. Error in ANN for multiple topologies with line status as input.

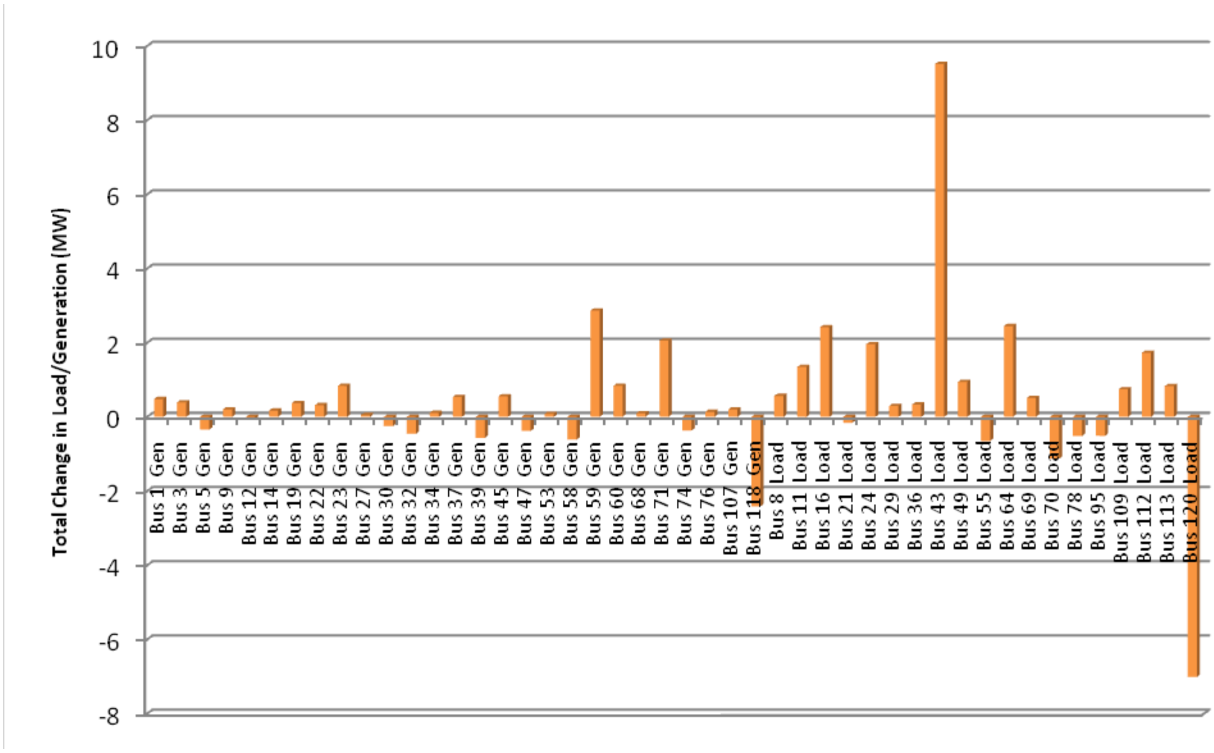

Figure 7-12. Total generator and load changes for the multiple merged topologies.

7.5. Preliminary Conclusions and Future Work on Topology Studies

From the current case studies, the following preliminary conclusions can be drawn:

1. The MANGO Framework can be applied to different topologies with the cost of generating additional training data sets and requiring an increased number of MANGO iterations.
2. Minor topological changes have an effect that can be understood and compensated for within the ANN-based MANGO procedure.
3. Including line status does decrease the variability of the ANN when merging multiple topologies, and may increase the effectiveness of the MANGO controller.
4. There is only a small difference between a "less important" line and "more important" line in terms of MANGO effectiveness, when applied to different power grid topologies.
5. When the number of topologies included in the process increases, it leads to increased recommended generator and load adjustments by the MANGO procedure.

Future work will include applying the current methodology to the full WECC system model to observe the performance of the ANN-MANGO framework. As the size of the WECC system and the number of possible topologies increases, further investigation on the selection of input data is needed. On-going work is being performed to find a suitable solution.

8.0 Initial Studies of the MANGO Framework for the WECC System

The size, complexity and time variation of WECC system brings in significant challenges in building a MANGO model. A typical WECC base case has over 3,000 generators and 14,000 buses. The dimensionality of the MANGO operator-actionable variables is extremely large. There are many special devices in the WECC system that require customized models. Only some specialized commercial software, such as PSLF, DSA tools (e.g., PSAT, SSAT), or PSS/E, can be used to perform dynamic study on a WECC-scale system. Also, the WECC system is continuously undergoing an autonomous evolution. Each year, there are some changes with load, generation, and transmission lines, as well as other devices. The WECC has to build updated base cases each year to keep up with the evolutionary steps of the WECC grid. In addition, based on the previous studies, the sensitivity relationship between operator actionable variables and damping ratios exists, but exhibits highly non-linear phenomena and varies with system stress levels and generation patterns. Thus, building a WECC MANGO model is very challenging task. In this section, some initial studies on the WECC MANGO model are described. Major challenges are identified and initial results are presented.

8.1. Description of the Methodology for Building a MANGO Model for WECC model

Due to the size, complexity, and time variations of the WECC system, some special considerations and procedures are identified in this section to deal with the major challenges. The procedures for building a WECC MANGO model are described as follows:

a) **Identify the model and simulation software to generate the reliable data sets for WECC system.** MANGO models are built from measurement data. It is easy to model a simple power system, which consists of standard components and hundreds of buses. Most simulation software can generate solid and consistent simulation results for simple systems. However, the WECC system is of large size, and consists of many non-standard components. These base cases are only available in PSLF format and PSS/E format. Yet, neither PSLF nor PSS/E provides a small signal stability analysis function, which is an essential function for generating mode information for MANGO studies. To the authors' best understanding, currently, the SSAT in DSA tools is the only software tool most commonly used in the WECC that provides small signal stability analysis function and can run a model of WECC size. To run the WECC model using SSAT, WECC models must be converted into SSAT compatible format. The conversion process is not straightforward for a complex system like WECC. Even though SSAT provides a model format conversion function, simply applying the function results in a model with inconsistent dynamic responses to the original. Supervised model conversion and simulation data verification are required to generate reliable simulation data for building a WECC MANGO model.

b) **Obtain the insight on the sensitivity of modes with respect to the operator actionable variables through massive simulation studies**. The dynamic features of a WECC system can be revealed through massive simulation studies. It is expected that a lot of decisions in building a WECC MANGO model will have to be based on engineering judgment. Complexity, large scale, high nonlinearity, and time variation of the WECC system makes it impractical to build a precise analytical model. Some approximation and simplification have to be used to reduce the complexity of the problem to a manageable level based on insight and experience. These insights and experiences can be accumulated through massive simulation studies. Some primitive MANGO recommendations can even be made through these engineering judgments. An example is the BPA's DSO 303, which requires reduction of tie line flows to damp inter-area oscillations. Insight built from massive simulations can help verify and improve this type of operating procedure and provide guidance in building MANGO models.

c) **Select a limited number of the operator actionable variables for building a MANGO model**. There are a large number of operator actionable variables in the WECC system. For example, there are more than 3000 generators in the WECC system, most of which are controllable. The amount of data required to identify the sensitivity for each individual operator actionable variable is prohibitively large and de facto impractical. To make the problem manageable, a limited number of operator actionable variables must be formed. Sensitivity of mode damping with respect to most individual components is usually not significant in a large power grid as the WECC system. Thus, a combination of similar components may help reduce the dimension of the problem, while increasing the sensitivity. Also, a subset of controllable variables may be obtained from engineering judgment. After initial efforts of reducing the problem dimension, a quantitative study can help calculate the sensitivity for building a MANGO model.

d) **Build linear and non-linear WECC MANGO models using measurement data**. Different model structures can be used to build MANGO models. Usually, initial selection of model structure is mainly based on "engineering judgment." Then, the MANGO models can be trained using an estimation data set. The parameters of the model are chosen to minimize the modeling residuals for the estimation data. The MANGO models should be checked for their performance using reserved validation data. Big modeling residuals from validation data indicate large modeling errors. With the size and complexity of the WECC system, an iterative procedure is expected to build a suitable WECC MANGO model with acceptable modeling errors.

e) **Generate and implement MANGO recommendation**. To achieve the goal of damping WECC inter-area oscillations, a MANGO recommendation needs to be generated by the WECC MANGO model and implemented by WECC operators. The MANGO recommendation should be verified with simulation models at different operational points and status. The validity of a MANGO recommendation shall be checked for all the security and stability considerations. For example, a valid MANGO recommendation should not only increase the damping of the mode of interest, but also keep all other modes at acceptable damping levels. In addition, it should not cause any voltage stability issues or thermal limit violations. To facilitate the implementation, MANGO recommendations should be compatible with current WECC operational procedures and can be implemented by operators with manageable effort levels. For example, simultaneously adjusting all generator outputs in WECC may not be practical considering the coordination efforts.

8.2. Model and Simulation Software Validation for the WECC model

The main objective of this task is to identify and validate a reliable simulation software package that can provide an accurate assessment of system damping ratios for a realistic power grid model. A good and robust tool helps to identify system health of the current operating condition, and provides insight on control schemes to enhance security and reliability. The authors' previous approach involved calculating system modal information from simulated system responses following a small disturbance using the DSI Toolbox's Prony analysis method. This method can provide an accurate result. However, the computational burden of time domain simulations and manually adjusting parameters for Prony analysis is impractical for massive simulation studies of a large range of operating conditions. Consequently, there was a need for finding a package to achieve the above goals. The sub-package in the DSA Tools, Small Signal Analysis Tool (SSAT), was a promising candidate. SSAT uses eigenanalysis techniques to estimate modal information from a system model, including items such as frequency, damping ratio, and mode shape. In this tool, no time domain simulations are required. This feature can significantly reduce computational burden, which is ideal for the massive number of simulations required for the MANGO project.

Before SSAT was used for detailed studies of the WECC system model, it was necessary to validate this package using realistic power network models; e.g., the operational model representing the whole WECC system. To validate this package, the main criterion was to compare the results (oscillation frequencies and damping ratios) obtained from SSAT and the ones from DSI Toolbox's Prony method, as discussed above.

Cross-validation of the DSA Tools was also made between the TSAT and SSAT programs. Using TSAT, a Chief Joseph dynamic brake insertion was simulated. This result was exported to MATLAB and analyzed using the DSI Toolbox's Prony feature. The same power flow situation was then examined using the SSAT program. If the programs are consistent, the results obtained from SSAT and TSAT are expected to be consistent. Another point was to compare system responses between different simulation packages for the purpose of checking the model compatibility. A good match assures the validity of various tools. Exhaustive simulations can be performed thereafter to reveal potential system problems. The following subsections provide detailed procedures to achieve this goal.

8.2.1. PSLF Data format

At this step, a system model representing the peak load condition in 2009 of the full WECC system is obtained from the WECC website [WECC 2009]. This model contains a power flow data file and a dynamic data file. The data is provided in two separate data formats: the PSLF format and PSS/E format. Initial validations began with the PSLF format data, due to its prominent use in the WECC area. The first study was conducted to compare system performance in time domain for model validation between PSLF and the DSA Tools. Figure 8-1and Figure 8-2 show a time-domain simulation using TSAT at the base case (no disturbance case). As they indicate, even for a no-disturbance simulation, there are some perturbations with the TSAT results. The transient near the beginning is not completely unexpected as the system needs to initialize itself, as well as the fact that there may be differences between the PSAT power flow solution and the TSAT power flow solution. However, the results near 35 seconds do not represent an acceptable no-disturbance simulation. Some adjustments are necessary to stabilize the system, even under this no-disturbance case.

Figure 8-2 shows the voltage magnitudes of selected buses for the same simulation. Just like the transmission line plot before it, there is a large transient at the beginning of the simulation. However, the disturbance around 35 seconds of the simulation is much more apparent in the voltage magnitudes. Furthermore, several low frequency oscillations are seen between the beginning and ending of this simulation interval. On the contrary, the simulation results performed using PSLF have shown quite flat responses, indicating no disturbance at all. Clearly some adjustments are needed to produce valid DSA Tools results before further study could proceed.

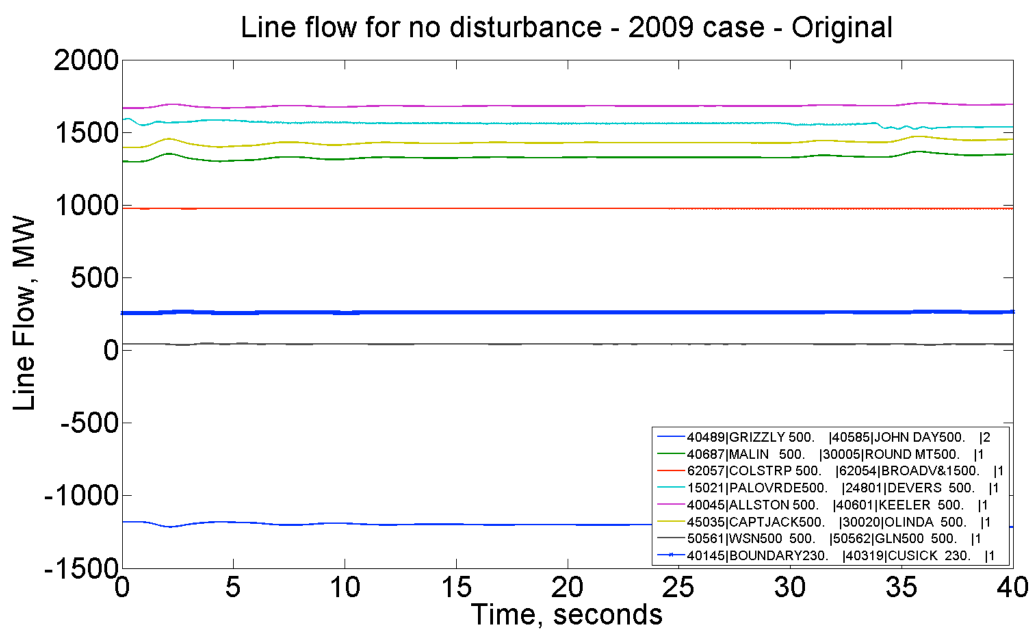

Figure 8-1. Original WECC Simulation - Real power of selected transmission lines.

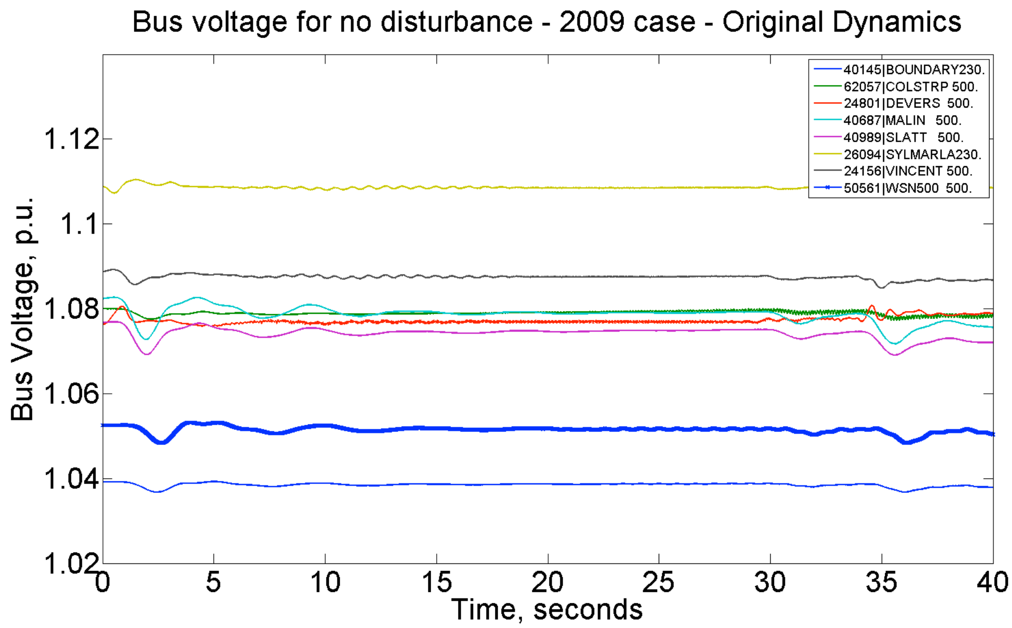

Figure 8-2. Original WECC Simulation - Voltage magnitude of selected buses.

Under the advice of Bill Mittelstadt of the Bonneville Power Administration and Xi Lin of PowerTech Labs, some adjustments were made to the simulation dynamics file. The dynamics file contains the parameters for different dynamic models in the simulation, such as the exciter gain values and time constants for a power system stabilizer (PSS) unit. Using speed deviations measured during the simulation, problematic models were tracked down and adjusted. Table 8-1 shows the changes made on the initial dynamic model parameter file to obtain a better no-disturbance simulation. Further changes could be made to increase the stability of the system, but the simulation results from the adjusted dynamic model file were deemed sufficient for these initial studies.

Table 8-1. PSLF Dynamic Model File Adjustments.

Bus	Name	Element	Change
15903	Agua Fria	Exciter	Turned off
15902	Agua Fria	Exciter	Turned off
34305	Chow II	Exciter	Turned off
34330	El Nido	Exciter	Turned off
14966	West Phoenix 5CT	Exciter	Turned off
14950	West Phoenix 4ST	Exciter	Turned off
14968	West Phoenix 5ST	Exciter	Turned off
14967	West Phoenix 5CT	Exciter	Turned off
26006	Castaic	Governor	Turned off
62049	Colstrip	Exciter Gain	K_A from 8.89 to 8.5
62050	Colstrip	Exciter Gain	K_A from 8.89 to 8.5
51054	Miller Creek	Exciter Gain	K_A from 100 to 90
51055	Miller Creek	Exciter Gain	K_A from 100 to 90
24005	Alamitos	Exciter Gain	K_A from 245 to 400
24123	Redondo	Exciter	Turned off
24124	Redondo	Exciter	Turned off

Using the adjusted model dynamics file, the no disturbance simulation was run again in TSAT. Figure 8-3 and Figure 8-4 show the same selected transmission lines and bus measurements of Figure 8-1 and Figure 8-2. As the figures indicate, most of the abnormal behavior from the original simulations has been eliminated. The voltage magnitudes of Figure 8-4 still show an initial transient, but at a much smaller magnitude than that of Figure 8-2. There are still some low-level oscillations present in the voltages near the end of the simulation, but again at a much lower level than the original simulation.

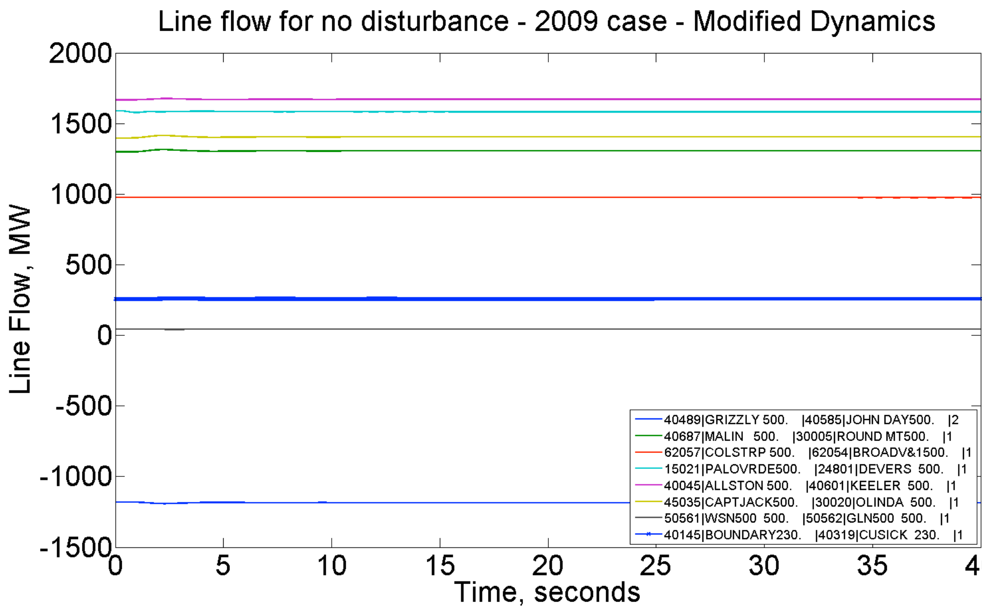

Figure 8-3. Modified WECC Simulation - Real power of selected transmission lines.

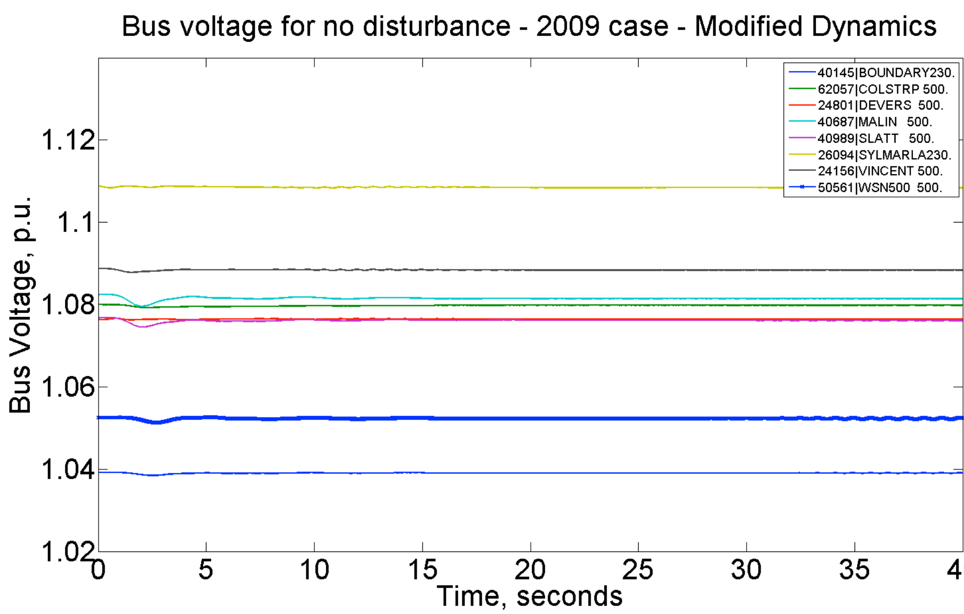

Figure 8-4. Modified WECC Simulation - Voltage magnitude of selected buses.

With the modified dynamic data, a 500 MW Chief Joseph dynamic brake insertion was simulated. This event occurs 16 seconds after initialization of the simulation to ensure all initial transients have subsided. After 0.5 seconds, this braking resistance was removed. This event was also simulated in PSLF using the original dynamic data. Figure 8-5 compares system performance using the two different simulation packages. A large difference in the active power flow for the line between Malin and Round Mountain is observed, but the transient pattern following the insertion of the dynamic brake is similar, as shown in Figure 8-6. There are some observable differences in the ringdown signals shown in Figure 8-6. In particular, the second swing is not as high in amplitude and there is a slight difference in modal response. However, these are acceptable differences.

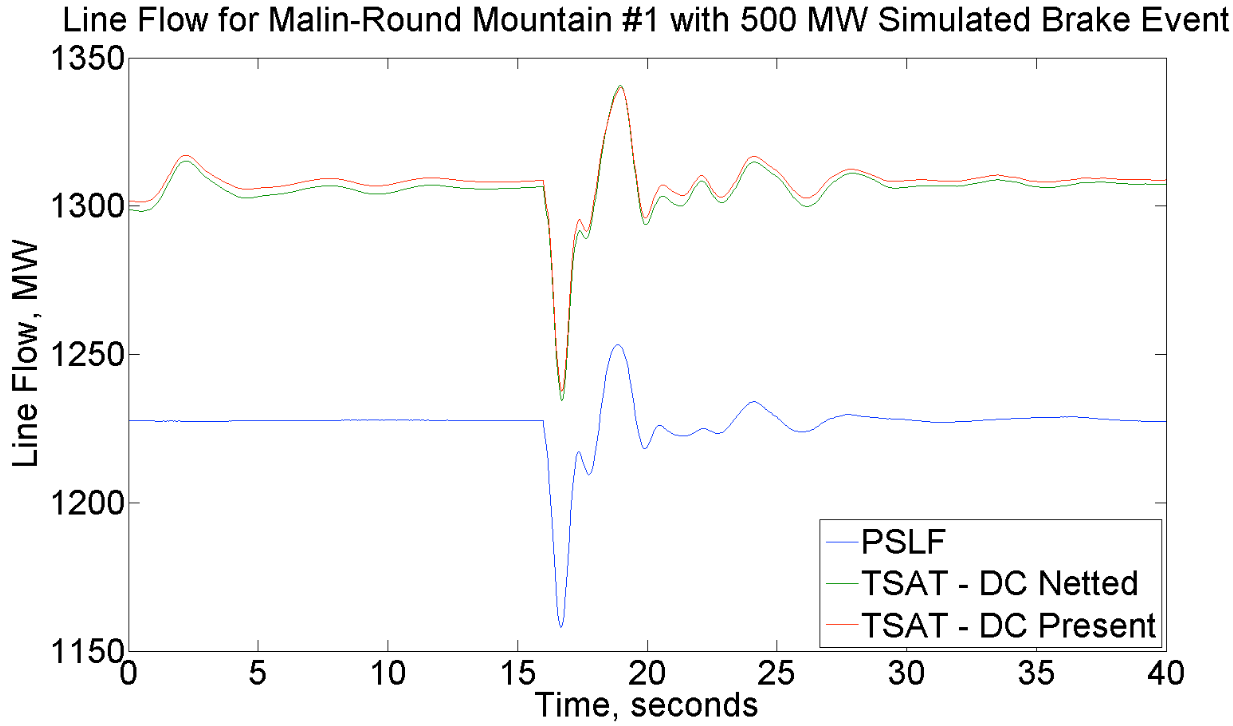

Figure 8-5. Comparison of line flows between PSLF and TSAT-PSLF.

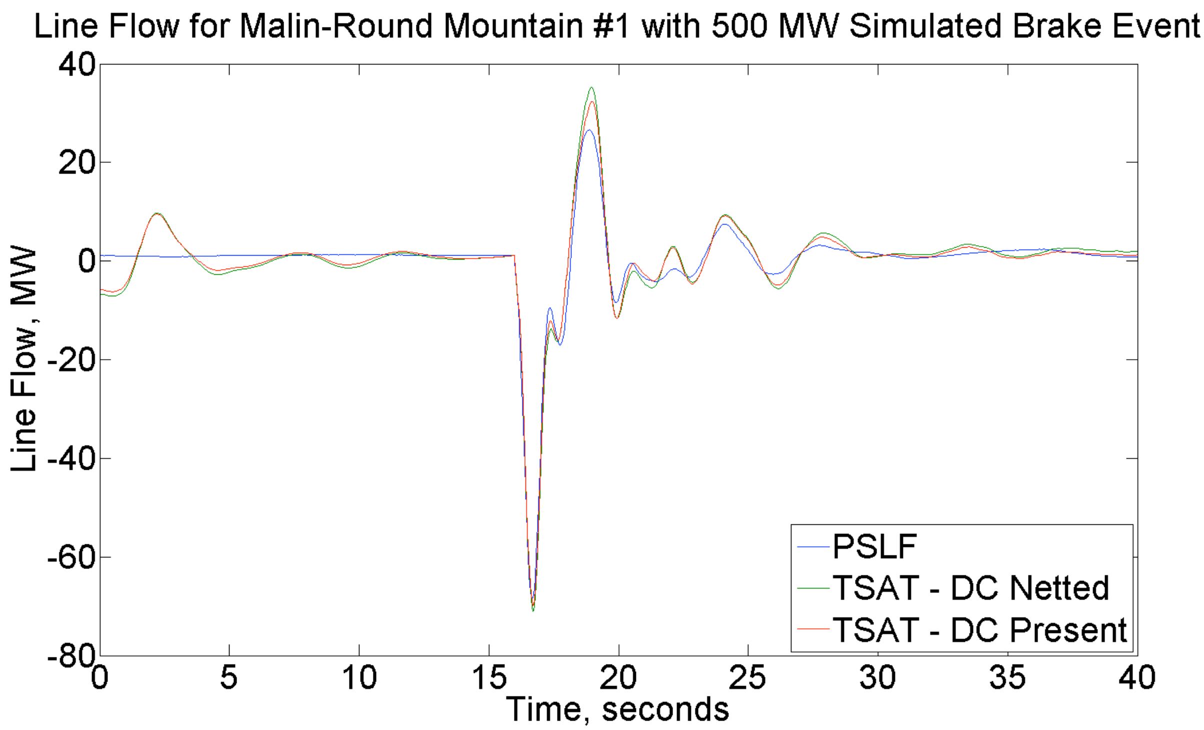

Figure 8-6. Comparison of line flow between PSLF and TSAT-PSLF with means removed.

The second comparison was made for small signal analysis. Small signal analysis of phasor measurement data on the WECC consistently points to two modes of interest. The mode examined (~0.2 Hz) is associated with the northern part of the system interacting with the southern part of the WECC (N-S). A secondary mode is associated with Alberta, Canada swinging against the WECC system. Both of these modes were detected with the comparison between different tools shown in Table 8-2. From Table 8-2, the results from SSAT and TSAT have shown to be a relatively good match. The PSLF results show a consistently higher damping ratio estimate, but are relatively similar as well. This is consistent with the results of Figure 8-6, where the PSLF results ringdown seemed to be damped faster than the TSAT simulation result.

Table 8-2. Comparison of two modes - PSLF based Data.

Base Power Flow	SSAT_new DYD		TSAT_new DYD		PSLF_new DYD		PSLF_orig DYD	
	Freq (Hz)	DR (%)	Freq (Hz)	DR (%)	Freq (Hz)	DR (%)	Freq (Hz)	DR (%)
N-S	0.2203	14.15	0.2176	15.56	0.2151	17.93	0.214	17.86
Alberta	0.3315	9.92	0.3275	11.73	0.3401	13.14	0.3401	13.15

From the above analyses, the transient responses in time domain have shown a noticeable difference between DSA Tools and PSLF. One explanation is the incompatibility of simulation tools. Some of the models provided in PSLF format cannot be recognized by TSAT. Other models in PSLF format can be converted to user defined models in TSAT, but quite a few warnings are encountered when running DSA Tools, showing improperly set parameters and other inconsistencies in the conversion. In order to obtain more consistent results, it would take a significant level of effort to change the system models one after another. To evaluate if a different data format yields better results or provides better compatibility, the validation procedure was reiterated using the data provided in PSS/E format.

8.2.2. PSS/E Data Format

The test procedure above was repeated, this time using PSS/E-formatted WECC dynamic data. After importing this set of data into TSAT, several errors were again found in the data models that needed to be corrected. Before continuing the validation, the modifications in Table 8-3 were performed.

Table 8-3. PSS/E Dynamic Model File Modifications.

Bus	Name	Element	Change
48275	Northeast	Governor	Removed
43905	PortWestward	Governor	Removed
35854	LECEFGT 1	Generator	Netted
35855	LECEFGT 2	Generator	Netted
35856	LECEFGT 3	Generator	Netted
35857	LECEFGT 4	Generator	Netted
48061	Cabinet Gorge	Exciter	Removed
48063	Cabinet Gorge	Exciter	Removed

With the problematic devices removed or modified, the no disturbance case was once again performed using the TSAT software package. Figure 8-7 and Figure 8-8 show the real power flow on selected transmission lines and selected bus voltages from the model. As the figure shows, the simulation output is mostly flat, as expected from a no disturbance case.

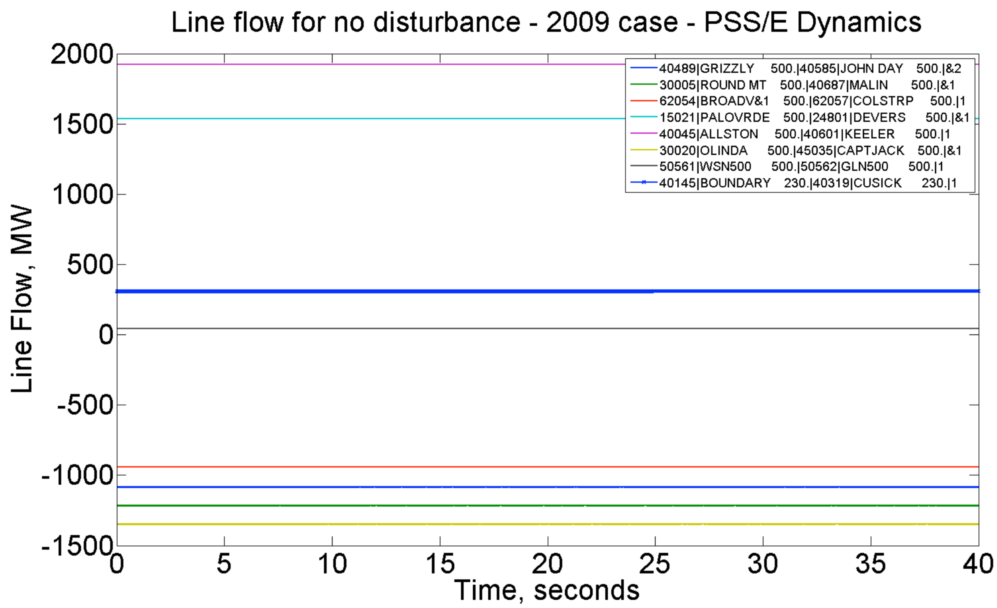

Figure 8-7. PSS/E Data Simulation - No Disturbance - Real power of selected transmission lines.

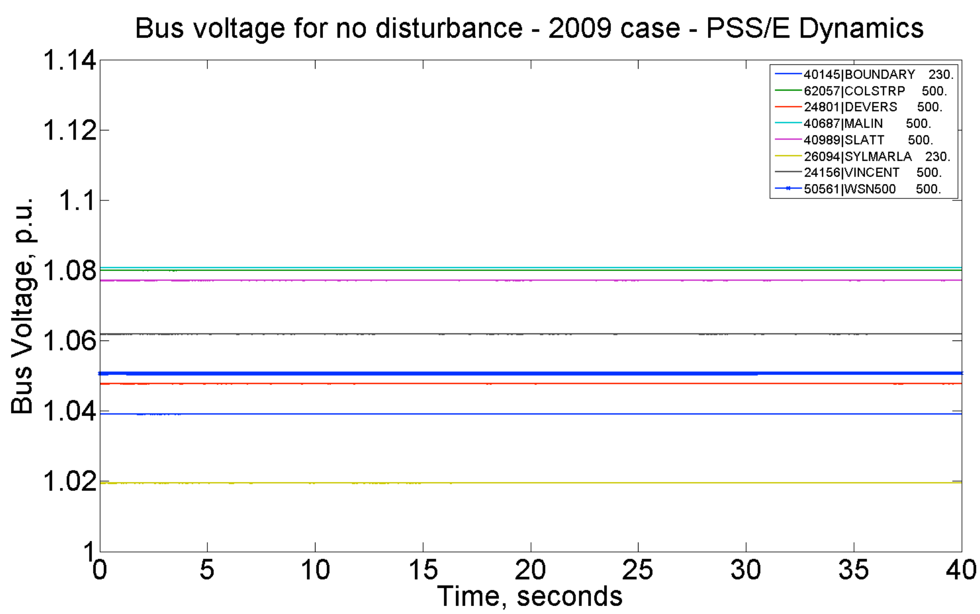

Figure 8-8. PSS/E Data Simulation - No Disturbance - Voltage magnitude of selected lines.

With a suitable no-disturbance simulation accomplished, the PSS/E-based TSAT simulation was further validated using a simulated Chief Joseph Brake insertion. As with the PSLF-based simulations, after 16.0 seconds, a 500 MW braking resistance was applied to the system. This braking resistance was removed 0.5 seconds later. Figure 8-9 shows the result overlaid with the PSLF generated cases.

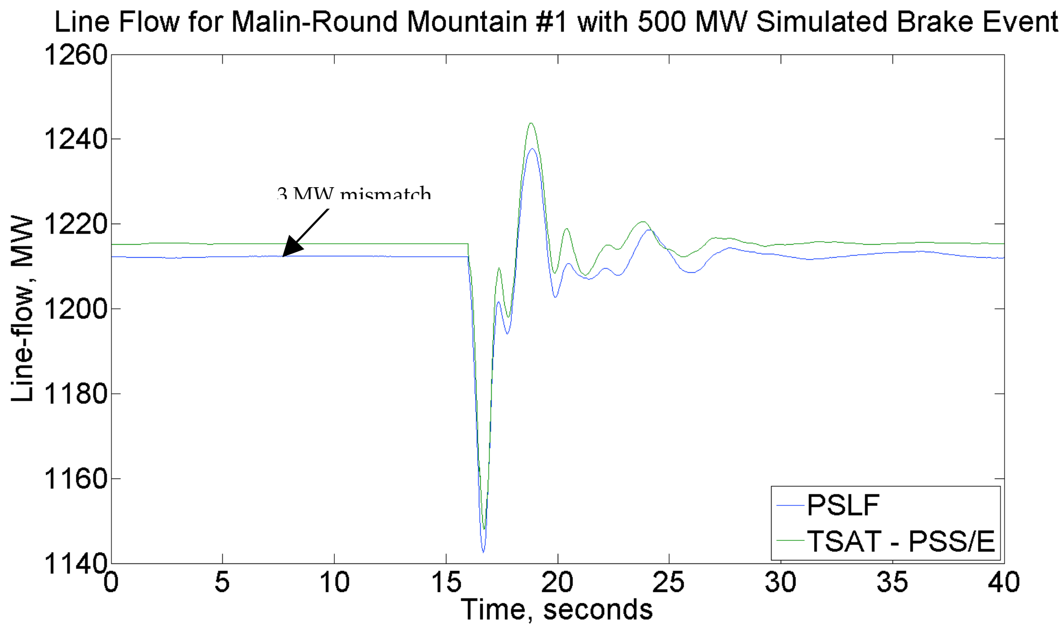

Figure 8-9. Comparison of line flow between PSLF and TSAT-PSS/E

As Figure 8-9 demonstrates, the responses from the PSLF software and the TSAT software (using PSS/E data) are very similar. There is a 3 MW offset between the two and some obvious differences in the ringdown after the brake insertion. Figure 8-10 is the same plot with the TSAT results offset by 3 MW to better overlay the PSLF results. As Figure 8-10 shows, the first couple swings of the brake response are nearly identical. However, there are clearly some different dynamics working on the subsequent swings, indicating some minor discrepancies between the PSLF and TSAT dynamic simulators.

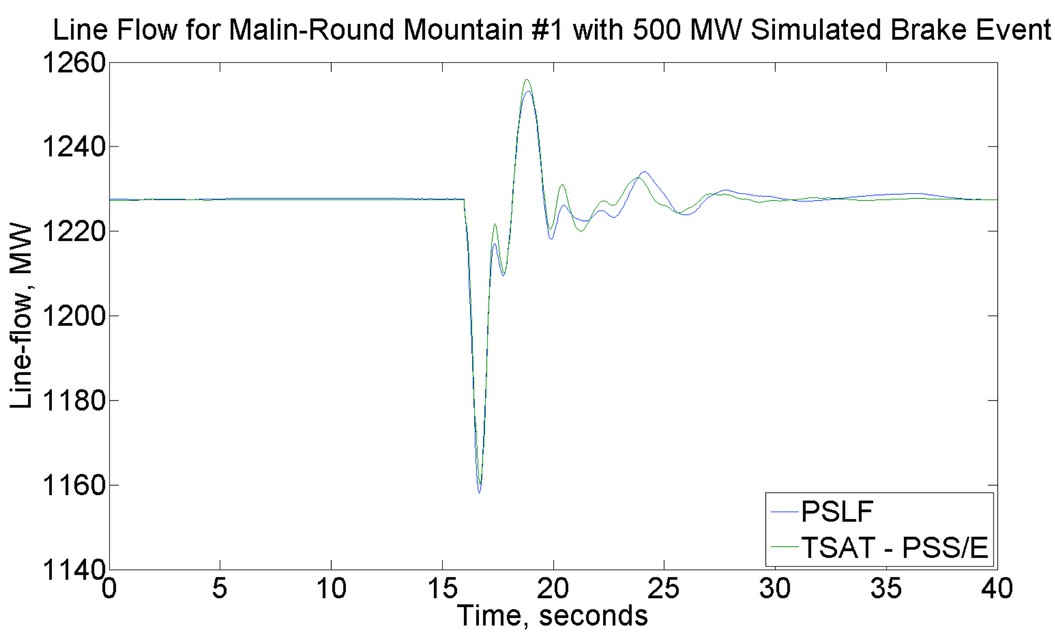

Figure 8-10. Comparison of line flow between PSLF and TSAT-PSS/E - Offset aligned

The modal results for the two simulations are compared in Table 8-4. Using the DSI Prony package, the ringdown from TSAT was analyzed. SSAT simulations were run for the new PSS/E-based data files as well. The results in Table 8-4 follow similar trends to those seen in Figure 8-9 and Figure 8-10. The North-South mode estimate is relatively the same for all three estimation methods. However, the Alberta mode shows some significant deviation between TSAT and the SSAT and PSLF results. Despite this TSAT difference, the SSAT results closely match the PSLF-ringdown results, especially for the North-South mode case. Since the simulation studies will be accomplished using primarily SSAT, this is a promising indicator that the results would be valid.

Table 8-4. Comparison of two modes - PSS/E-based Data.

2009 peak load case	SSAT		TSAT		PSLF	
	Freq(Hz)	Damping (%)	Freq(Hz)	Damping (%)	Freq(Hz)	Damping (%)
N-S	0.2474	19.13	0.231	19.20	0.214	17.86
Alb	0.3596	14.79	0.357	21.05	0.3401	13.15

As this section has shown, there are some obvious conversion and simulation differences between different software packages. Furthermore, different issues arise when importing different data formats into a third party tool; e.g., PSLF or PSS/E data into the DSA Tools. After some modifications to the imported data, reasonable results are obtained from the TSAT software. However, given the results of the various figures and tables, it appears the DSA Tools work better with PSS/E-imported data. The results for the PSS/E-data simulations were much more consistent with expectations, as well as requiring fewer alterations to get into a usable case. As such, all DSA Tools-based simulations for the MANGO procedure in the remainder of this report will utilize PSS/E based data.

8.3. Data Generation

To investigate the MANGO procedure on the full WECC model, some simulation data was generated and used to help verify the performance of the proposed MANGO framework. Initial studies focus on the adjustment of generators, and indirectly tie-line flow, to obtain sensitivity information about the relationship of specific generators and oscillatory modes of interest. This section will describe the process to generate the initial generator modification data sets for generation adjustment.

The process for data generation begins with selecting generators of interest. The full WECC system model contains 3217 generators that can be modified in one form or another. Such a high number of modification points can be very detrimental to sensitivity analysis (a.k.a. the "curse of dimensionality"). To help reduce the order of the sensitivity analysis, generator buses of interest were selected from modal eigenanalysis and expert knowledge. The 2009 Heavy Summer Full WECC simulation case was analyzed using the SSAT software package [PowerTech 2010]. Modal information was extracted for both the North-South mode (typically around 0.25 Hz) and the Alberta mode (typically around 0.40 Hz).

To determine generators of interest, the modal results need to be sorted. One method for sorting the modal results is to utilize participation factors. Participation factors provide a unitless quantity for determining how influential a particular state is in an eigenvalue of interest. Utilizing equation (6-1), the participation factor is given by

$$\text{Participation Factor} = \Phi_{ij}\Psi_{ji} \tag{8-1}$$

where Φ and Ψ are the left and right eigenvalues from (6-1), and i and j the indexing of associating the ith state on the jth eigenvalue [Kundur 1994; Rogers 2000]. Once normalized by the largest participation value, a participation factor near 1.0 indicates a significant contribution to the eigenvalue of interest.

Utilizing participation factors, the top 200 participants of both the North-South and Alberta modes were selected. Since the North-South and Alberta modes share contributing generators, the separate lists were then combined into a list of 141 distinct generation buses. These results were then correlated to the original WECC system. During this step, a simultaneous expansion and contraction of the modification list occurred. As the generator bus values were expanded into individual generation units, generators below 40 MVA nameplate capacity were eliminated. This resulted in 123 distinct generators to modify for data generation. Figure 8-11 shows the modeshape, by areas, associated with the North-South mode for these selected generators. As expected by the modeshape, there are primarily generators in the north of the system (NorthWest, B.C. Hydro, and Alberta) interacting with generators in the south of the system (Arizona, Mexico, and Southern California).

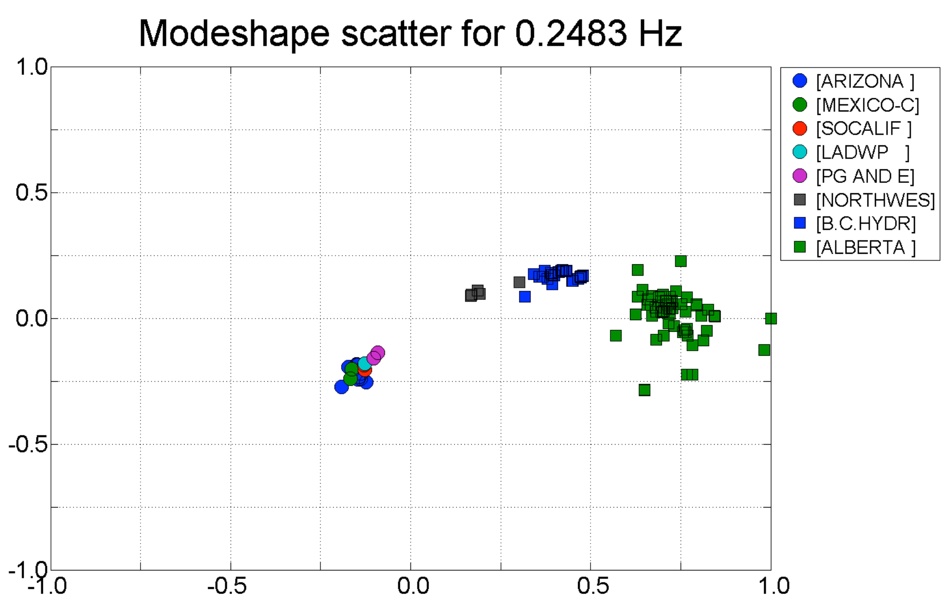

Figure 8-11. Mode shape area scatter for generators of interest of the North-South mode.

Once the modification points were selected, it was necessary to randomly vary the output of each generator slightly. Each variation application creates a slightly different operating point of the WECC system, useful for the application of sensitivity analysis. The real power output of the generators of interest was varied over a uniform distribution of ±5.0%. Real power limits were taken into consideration during the adjustment, so generators were unable to generate more than 100% of their rated output. VAr control and nameplate limitations were not explicitly handled in the variations, but rather by the PSAT powerflow software [PowerTech 2010]. PSAT's powerflow solver was utilized to ensure the new, unique operating point was a valid powerflow case.

With a new powerflow operation point of the WECC system obtained, several quantities of the system were of interest. The obvious first quantity is the final output of all of the generators of interest. Once properly limited and adjusted into a convergent powerflow solution, the final values of the generators were not necessarily the same as the initial ±5.0% variation adjustment. Figure 8-12 shows the histogram for all 123 generators modified in the ±5.0% variation case. Individual generators are represented by color. Most of the adjustments follow a uniform distribution over the ±5.0% range. Some large peaks in the histogram are due to limits in the generator output power. If a generator was operating at or near its maximum output in the base case, any adjustments to increase its output were stopped at the maximum output threshold. To ensure a proper representation of the new operating point in the sensitivity studies, especially considering these limiting conditions, the final values of the generators of interest were extracted and saved.

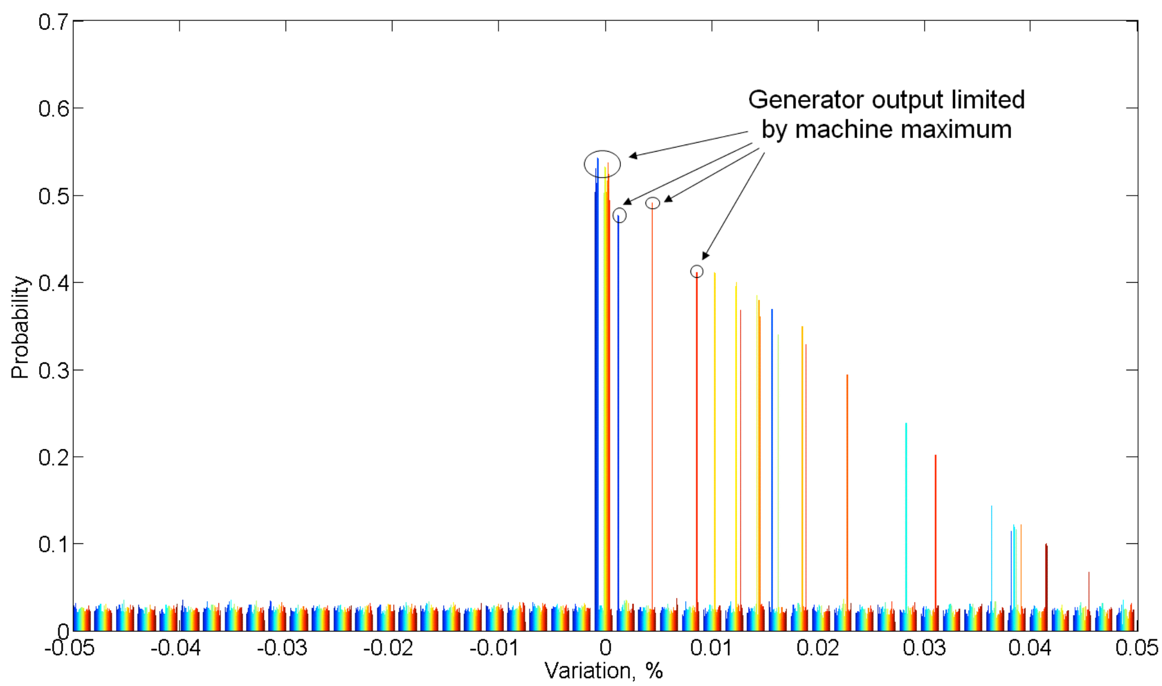

Figure 8-12. Histogram for modified generators in ±5.0 variation case of WECC model.

Closely related to generator output values, power flow on tie lines of interest is also a candidate for the MANGO procedure. To help investigate and evaluate this relationship between tie-line flow and modal parameters, the power flow through selected lines was also obtained. For the initial pass, all tie lines operating at 500 kV or 345 kV were included. Selected 230 kV lines, such as those connecting British Columbia and eastern Washington, were also included. Some of these lines may be redundant or provide no benefit to the analysis, but that determination will be made during the analysis stage of the MANGO procedure.

With a new, stable powerflow solution and new operating point for the full WECC model, SSAT was once again invoked. SSAT performed eigenanalysis on the system. In particular, the new frequency and damping ratio values for the North-South and Alberta modes of interest were obtained.

Once the simulation data was created, a particular oddity was encountered in the modal information extracted. The two inter-area modes of interest (North-South and Alberta) were split into two distinct clusters. Figure 8-13 shows the clustering of the North-South mode. As the figure shows, this mode is divided into two distinct frequency sets. Further analysis revealed a limiting case for one of the generators on the Genesee bus in Alberta, Canada caused the mode splitting. One set of the clustered modes was associated with the generator in a limited condition (maximum output), and the other set was associated with a "normal" operation range. Since many other generators reach their output limit and do not cause mode splitting, it is suspected that a poorly chosen model or poorly modeled limiting device is present on this bus. Before proceeding with the analysis of the 2009 Heavy Summer WECC model data, all results associated with the "limited output" case were removed. The result was a scatter plot for both modes that matches Figure 8-14.

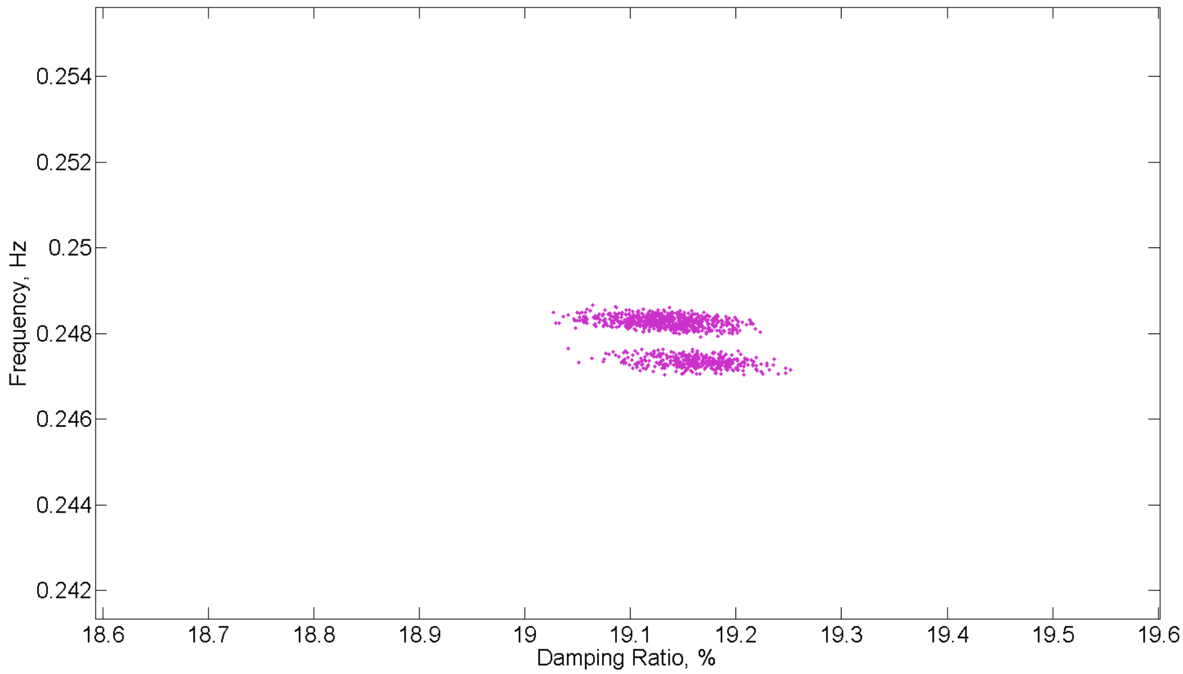

Figure 8-13. Scatter plot of 0.248 Hz mode over 1000 2009 Heavy Summer WECC Simulations.

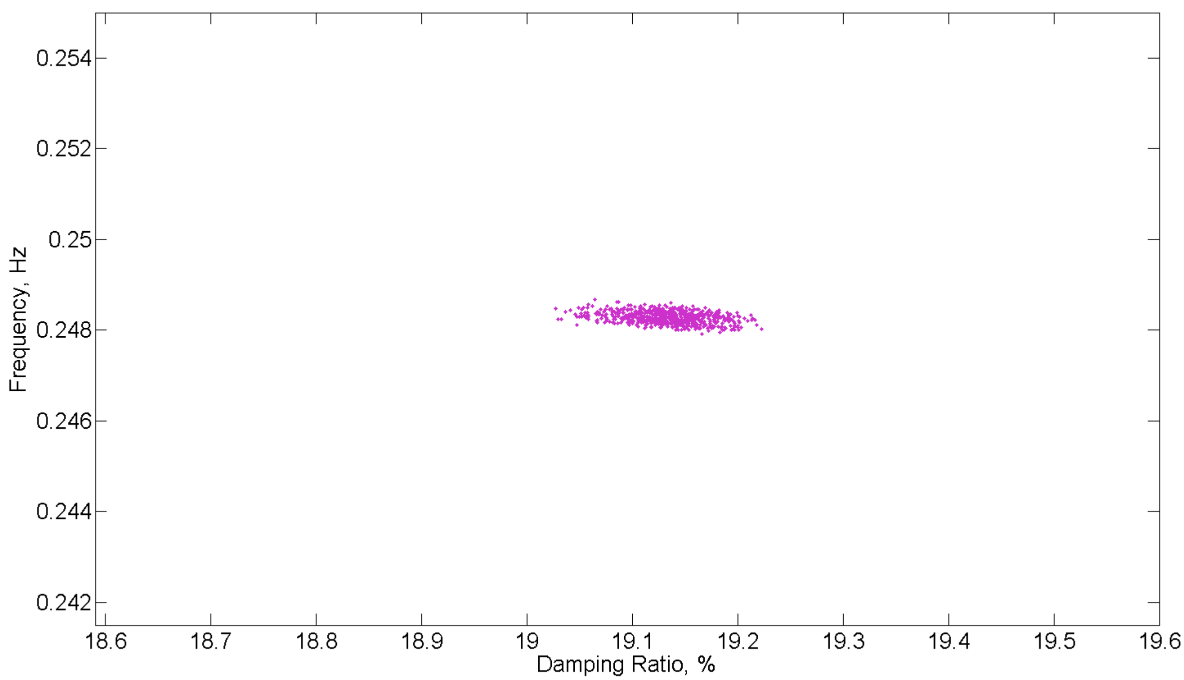

Figure 8-14. Scatter plot of 0.248 Hz mode after removing cases associated with Geneseee limiter condition.

Once the information of a new operation point of the WECC model was obtained, the procedure restarted. Using the original 2009 Heavy Summer WECC model, a new set of generator variations was created and applied to the model. This procedure was repeated approximately 1000 times to generate 1000 new, slightly different operating points of the 2009 Heavy Summer WECC model. Once aggregated into a single repository, the generator of interest output values, tie-line of interest output values, and modal estimates for this Monte-Carlo simulation set represent a data set to perform sensitivity analysis. Utilizing the MANGO framework, these sensitivity studies allow a reduce subset of the generators and tie-lines of interest to be constructed for future simulations.

8.4. Technical Approach of Applying the MANGO Framework for the WECC System

To apply MANGO frame work for the WECC system, the first step is to build an empirical relationship between mode changes and power flow pattern. Due to the complexity of the WECC system, it is hard to build an accurate mathematical model for describing the sensitivity of the modes with respect to power flow patterns at the initial stage. But, some initial recommendation may come from engineering judgment based on operational experience. The first step of the study includes collecting the experience from experts, and determining an empirical based MANGO recommendation. Then, perform a large number of simulations using the WECC base case to verify and improve the empirical MANGO model. BPA's DSO 303, which recommends reducing tie line flows to damp inter-area oscillations, can serve as a starting point. Extensive simulation will be carried out to verify and improve the operational standards.

The second step is to conduct mode sensitivity analysis using the simulation data from the WECC base case. Simulation can provide a large amount of typical operational data. Furthermore, true mode sensitivity can be obtained with proper mode analysis software. With large amount simulation data, the sensitivity analysis discussed in Chapter 6.0 and Chapter 7.0 can be applied to build MANGO models for the WECC system. Initial efforts of applying the sensitivity analysis on the WECC simulation data have been carried out, but direct application of mode sensitivity analysis has encountered some difficulties due to the size and complexity of the WECC system. It is expected that some adaptation, preprocessing, and parameter-fine-tuning are needed before an acceptable WECC MANGO model can be built.

After a WECC MANGO model is built based on simulation data, the model is going to be validated, and the performance evaluated. Additional WECC base-cases will be introduced into MANGO studies to test the generalization and robustness of the proposed method.

8.5. E-tag and Implementation

To facilitate implementation of MANGO recommendations in a real system, the MANGO recommendations should be compatible with current operational procedures. As discussed in the previous chapters, MANGO recommendations involve adjustment of generation, load, and tie-line flow. These adjustments can be made through the E-tag system in the WECC system. WECC has a WECC Interchange Tool (WIT) to provide the E-tag service.

The E-tag system is also known as NERC tag [Wikipedia 2010]. The E-tag tool provides a service to track and manage power transactions. In 1997, the North American power system started deregulation efforts and market operations were introduced into power grids. The power transactions increased and have become more and more complex as a result. To operate a power grid in a reliable way, it is very important for an operator to know how each power transaction influences transmission line power flow. The E-tag system was first introduced by NERC to track the power transaction and manage the transmission line power flow. For each power transaction, an E-tag is created. The E-tag records the information about the source and sink of each transaction. When an E-tag is approved and implemented, its influence on power flow pattern can be derived from power flow calculations.

MANGO recommendations can be implemented through E-tag adjustment and curtailment. Each E-tag can be considered as an operator actionable variable in a MANGO model. An E-tag can be adjusted/curtailed by a security coordinator for reliability consideration [NERC March 2010]. The adjustment/curtailment can be carried out during the planning stage, as well as during operation. During power system operation, once a lightly damped oscillation is observed, a MANGO model shall generate a recommendation for E-tag adjustment/curtailment to improve damping. An operator can review and choose to implement a MANGO recommendation to adjust/curtail some E-tags.

9.0 MANGO Prototype Testing and Evaluation Specifications

As the MANGO process proceeds towards system-level viability and implementation, specific testing criteria and evaluation must occur. The evaluation of the MANGO procedure is split into four different modeling levels: a small, representative model; a full scale model; a realistic constrained and metered model; and finally actual system-level tests. A brief description of these tasks is outlined in the follow sections.

9.1. Small Representative Model

For successful validation and progression to more complicated systems, the MANGO procedure must first show expected results on a smaller, representative model of the full system. For WECC-based evaluations, the minniWECC model is chosen for this study [Trudnowski and Undrill 2008]. The minniWECC model provides a relatively low order analog to the full WECC system. Many of the real system interaction paths and modal properties are represented in the minniWECC model. A successful test of the minniWECC system promotes confidence that larger, more complicated models will benefit from the MANGO procedure as well.

The minniWECC-level tests can utilize all lines and generators in the system, or a reduced subset of interest. Some modifications are necessary to accommodate the reduced nature of the model, such as the line duplications mentioned in Section 7.0. With a suitable model available, the pure line status and generator information will be fed into the MANGO prototype. With the inclusion of a desired damping, the MANGO prototype can act on the particular configuration being tested. The MANGO prototype will generate a list of generation adjustments, as well as an expected damping.

With the MANGO output obtained for the smaller model, validation will consist of applying the recommended changes and examining how close the final system damping matches the MANGO predicted value. Different permutations of line and system configurations will be evaluated to determine the robustness of the MANGO prototype.

9.2. Full Scale Model

With a successful validation series conducted on the minniWECC model, testing of the MANGO prototype will proceed to larger, more complicated systems. These larger models will be full WECC planning cases [WECC 2008, 2009]. Unlike the minniWECC model, this WECC planning cases are much more representative of the actual WECC system. Some equivalence modeling and complexity reduction does occur, but on the whole, the model represents individual physical lines and generators in the WECC.

As with the minniWECC validation, the full WECC models will import generator output and line status information into the MANGO prototype. Unfortunately, the sheer number of these quantities means a reduced subset must be examined. Using modeshape analysis and expert knowledge, a subset of "interesting" generators and lines will be selected. This subset will then be passed into the MANGO prototype with a desired damping value. The MANGO procedure should generate a list of recommended generator output changes, as well as the expected damping value.

Initial tests utilizing the full WECC planning cases will allows changes to all generators of interest. This will be evaluated in a manner similar to that for the minniWECC system. The expected improvement in damping will be compared to the final damping value. As with the minniWECC system, different outages and system configurations will be evaluated using the MANGO procedure as well.

Unlike the previous validation, another constraint will be introduced into the MANGO prototype at this time. To prepare for operator-level advisement, the list of suggested generator changes will need to be prioritized and reduced. Methods to reduce the subset of interesting generators from a large number (e.g., 150) to a much smaller number (e.g., 15) will be investigated and evaluated. To effectively advise system operators on methods for improving grid stability, MANGO will need to provide concise results that can quickly and easily be evaluated. A system operator could quickly be overwhelmed if MANGO mandated 150 generation output changes to improve the damping of a mode of interest. Reducing this quantity to a more manageable number, or simply presenting the MANGO recommendation in terms of areas or tie-lines instead of actual generators, will make the recommendations more manageable and realistic for implementation.

9.3. Constrained and Metered Model

With the successful reduction or prioritization of MANGO recommendations, validation of the MANGO prototype will continue by implementing further constraints on the information passed to the prototype, as well as changes that can occur. In the previous modifications, the subset of generators would likely limit their output values inside the power simulation software. For example, MANGO may recommend increasing a generator output by 210 MW, but the generator may reach a limit at 205 MW. The nature of the MANGO process should prevent this from being an issue, but it provides a simple illustration of an "unexpected" change between the recommended and actual changes of the system. This type of constraints will be extended to include other constraining factors, such as economic or other operational limits. The best example is nuclear generation plants. Operational constraints may exclude nuclear generation modifications. The exact nature of these economic and operational restrictions still need to be evaluated and determined, but use of the WECC E-Tag system for such constraints may be a reasonable starting point.

With the constraints and other limiting factors included, the available changes and desired damping can again be fed into the MANGO prototype. As with previous cases, the recommended changes and expected damping value will be produced. The expected and actual damping value can quickly be compared. A relatively small difference will indicate the successful inclusion of real system operating constraints into the MANGO procedure.

The second extension of the full WECC planning cases will be full time-domain simulated data. Up to this point, it is expected that the MANGO procedure will be running offline on static power flow conditions. The next step is to produce a time series of power flow conditions similar to the natural variations of operating conditions over time in a real system. This simulation can build on the earlier, static power flow case's constrained generator and line-status list. However, measurements will be incorporated in a real world manner. For example, the MANGO prototype may receive Supervisory Control and Data Acquisition (SCADA)-type information about the generators on a minute level basis, but supplement this information with realistically located Phasor Measurement Unit (PMU) data at a much higher data rate.

Related to MANGO, but possibly under different restrictions, some form of real-time modal estimation will need to run on this time-series measurement data. A proper representation of these time-varying modal estimates, as well as the time-varying generator output, will need to be integrated into the MANGO prototype. Such a simulated measurement system will start introducing measurement and estimation errors into the data provided to the MANGO prototype. The successful improvement of modal damping under these more realistic operating conditions will be a key to proceeding with the MANGO testing.

9.4. System Tests

Once sufficient time-domain, reality-based simulations using the MANGO prototype have been completed, the next logical step will be providing the prototype tool to grid operators for evaluation. Initial evaluations will be open-loop and occur under very constrained and closely monitored conditions. One such example would be during WECC-coordinated system tests. These tests would not only provide a very specific interval for evaluating the MANGO prototype, but methods for improving the system identification (such as mid-level probing or braking resistance insertions) will likely be present to help evaluate MANGO's effectiveness.

Further testing will likely proceed in "safe" operating conditions. During times of low demand and relatively high system stability, the MANGO prototype may be consulted to perform normal grid operations. With a relatively large margin of stability, the effectiveness of MANGO could be evaluated with smaller risk to the power grid as a whole. As confidence in the validity of the MANGO prototype increases, the use of the tool could extend into more demanding hours of grid operation. Eventually, confidence in the MANGO procedure is hoped to reach a point where it is in operation full time, and consulted by grid operators on a regular basis.

Such a fully integrated, grid operations center implementation is the ultimate goal of the MANGO prototype. At this stage of implementation, the MANGO procedure could begin transitioning to autonomous control of the grid. However, such a transition would require its own set of evaluation protocols and criteria.

10.0 Conclusions and Future Work

Continued from the previous report, the work reported herein is focused on the following four aspects:

1. Established a MANGO procedure and discussed practical implementation issues;
2. Developed methods for modal sensitivity estimation with case studies to show the effectiveness of using sensitivity information for MANGO control;
3. Studied the impact of topology change on damping; and
4. Conducted WECC simulation studies for further work on developing MANGO control for the full-WECC scale system.

Based on the effect of operating points on modal damping, a MANGO procedure was proposed for improving small signal stability through operating point adjustment. Extensive simulation studies show that damping ratios can be controlled by operators through adjustment of operating parameters such as generation re-dispatch, or load reduction as a last resort. Damping ratios decrease consistently with the increase of overall system stress levels. At the same stress level (total system load), inter-area oscillation modes can be controlled by adjusting generation patterns to reduce flow on the interconnecting tie-line(s). The effectiveness of the MANGO control is dependent on specific locations where the adjustment is applied. The MANGO procedure consists of three major steps:

1. Recognition – operator recognizes the need for operating point adjustment through on-line ModeMeter monitoring,
2. Implementation – operator implements the adjustment per recommendations by the MANGO approach, and
3. Evaluation – operator evaluates the effectiveness of the adjustment using ModeMeter and repeats the procedure of necessary.

As the first stage, the MANGO procedure is a measurement-based and operator-in-the-loop procedure. Practical implementation is envisioned to be achieved by integrating MANGO recommendations into existing operating procedures per NERC and WECC standards. The E-tag system can be used an implementation mechanism, which has been addressed in this report. The MANGO model can be updated according to the current measurement and mode estimation results. Operators are included into the loop to bring in expert knowledge. In the future, after the confidence and accuracy of MANGO model is built up, it is expected that the automatic, closed loop control will be introduced to speed up the implementation and avoid human errors. The automatic process can be integrated into a remedial action scheme (RAS) system or a special protection system (SPS).

Both Steps 1 and 3 rely on a good ModeMeter to estimate the current modes, while Step 2 builds on modal sensitivity, i.e., the relationship of oscillation modes and operating parameters. The relationship is generally non-linear, and thus it is impractical to derive a closed-form analytical solution for this relationship. Calculating sensitivity from the system model is not applicable, as the model is usually not able to reflect real-time operating conditions. Therefore, our work has been primarily centered on estimating modal sensitivity from real-time measurement. Eigenvalue-theory-based sensitivity has been studied and concluded to be not applicable for real-time estimation. Many items in the eigensensitivity equations cannot be estimated with regular phasor measurements. Several approaches for estimating modal sensitivities are proposed to approximate the relationship. These approaches include ANN-based non-linear mapping, relative sensitivity estimation, and relative participation, energy, and mode shapes. ANN-based non-linear mapping has been studied, and it can successfully approximate the modal sensitivity from testing results with medium size systems. The relative sensitivity is formulated using least square principles in the form which can be estimated directly from measurement. The testing has been carried out with a medium-sized system. The results indicate how strong generation output relates to the damping, giving clear guidance which generator needs to be adjusted in order to improve damping. The same modal sensitivity estimation approach has also been successfully applied to key tie-line flow with a medium size system. The last three ideas will be further developed in future work.

In the modal sensitivity analysis, continuously changing parameters can be well considered. However, it cannot consider discrete changes because the function relationship is not differentiable in mathematical terms. Therefore, extensive topology analysis is conducted to characterize the impact of topology change in oscillation modes. ANN-based non-linear mapping is used in these studies. It was found that for some topology changes, the same ANN can generate reasonable estimate of modal sensitivity, but for some other topology changes, each topology condition would require a newly trained ANN, which is not practical in on-line application. The ANN-based non-linear mapping is improved to consider line status. Test results with a medium size system show the same ANN can then cover multiple topology conditions.

To pave the way to full-WECC MANGO application, extensive simulation studies of the full-WECC model have been conducted. A number of problems with WECC models and simulation tools have been solved during this process. More than 1000 cases with randomly adjusted generation outputs were created using an eigenvalue analysis tool. The data sets from these cases will be used to test the modal sensitivity estimation methods in the full-WECC system application. These data will also be further analyzed to derive empirical relationship between damping and operating parameters. This empirical relationship can be used to validate the modal sensitivity estimation approach ,and also as an interim approach for damping control.

In summary, significant progress has been made since last report. A MANGO procedure has been established with practical considerations. The key step in the procedure is the modal sensitivity. Two approaches – ANN-based non-linear mapping and direct modal sensitivity estimation – have been formulated and heavily studied with promising results from a medium-size system. Impact of topology change on damping has been identified using the ANN-based non-linear mapping. The full-WECC simulation studies were conducted, and the resulting data pave the road for full-WECC MANGO application. Further work will continue the development of modal sensitivity estimation and application to the full-WECC system, specifically including work on:

1. Testing the modal sensitivity estimation method with the full-WECC system;
2. Topology analysis for the full-WECC system;
3. Analysis of WECC simulation data to derive empirical relationship between damping and operating parameters.

Bibliography

Chow J.H. and K. W. Cheurg, "A Toolbox for Power System Dynamics and Control Engineering Education and Research," *IEEE Transactions on Power Systems*, vol. 7, no. 4, pp. 1559-1564, November 1992.

Chow, J. and G. Rogers, Power System Toolbox, Cherry Tree Scientific Software, [Online] Available: http://www.eagle.ca/~cherry/pst.htm, 2000.

CIGRE Technical Brochure, "Analysis and Control of Power System Oscillations," CIGRE Task Force 38.01.07, December 1996 (contains extensive materials from BPA and PNNL).

Demuth, H., M. Beale, and M. Hagan, *MATLAB Neural Network Toolbox 6 User's Guide*, The MathWorks 2009.

Farmer, R.G. and E. H. Allen, "Power System Dynamic Performance Advancement From History of North American Blackouts," *in Proceedings of Power Systems Conference and Exposition 2006*, Atlanta, GA, pp. 293-300, November 2006.

Hauer, J.F. "Interim Report on the Model Validation Tests of June 7, 2000 – Part I: Oscillatory Dynamics," WSCC Performance Validation Task Force (PVTF) of Modeling and Validation Work Group, October 26, 2000.

Hauer, J.F. "Preliminary Examination of the Alberta Trip on August 4, 2000," Working Note for the WECC Modeling and Validation Work Group, June 20, 2002.

Hauer, J.F., M.J. Beshir, and W. A. Mittelstadt in association with WSCC work groups, "Dynamic Performance Validation in the Western Power System," *in Proceedings of APEx 2000 Conference*, Kananaskis, Alberta, Canada, October 2000.

Hauer, J.F. and J.E. Dagle, "Review of Recent Reliability Issues and System Events," PNNL technical report PNNL-13150, prepared for the U.S. Department of Energy Transmission Reliability Program by the Consortium for Electric Reliability Solutions (CERTS), December 1999.

Hauer, J.F., C.J. Demeure, and L. L. Scharf, "Initial Results in Prony Analysis of Power System Response Signals," *in IEEE Transactions on Power Systems*, vol. 5, no. 1, pp. 80-89, February 1990.

Hauer, J.F. and J. R. Hunt in association with the WSCC System Oscillations Work Groups, *V Symposium of Specialists in Electric Operational and Expansion Planning (SEPOPE)*, Recife (PE), Brazil, May 19-24, 1996.

Hauer, J.F., H. Lee, J. Burns, and R. Baker, "Preliminary Analysis of Western System Oscillation Event on June 4, 2003: BPA and Canada," Working Note for the WECC Disturbance Monitoring Work Group, July 7, 2003.

Hauer, J.F., W.A. Mittelstadt, K.E. Martin, J.W. Burns, and H. Lee in association with the Disturbance Monitoring Work Group of the Western Electricity Coordinating Council, "Integrated Dynamic Information for the Western power System: WAMS Analysis in 2005," *The Electric Power Engineering Handbook*,, Chapter 14 of volume *Power System Stability and Control*, 2nd edition, L. L. Grigsby ed., CRC Press, Boca Raton, FL, 2007.

Hauer, J.F., D. J. Trudnowski, and J.D. DeSteese, "WAMS Analysis Tool for Tracking of Oscillatory Dynamics," *in Proceedings of the IEEE Power Engineering Society General Meeting 2007*, Tampa, FL, June 24-28, 2007.

Huang, Z., N. Zhou, F. Tuffner, Y. Chen, D. Trudnowski, J. Dagle, and J. Hauer, "MANGO Framework and Its Applicability for the Western Interconnection," Technical Report to the CEC, PNNL-18680, August 2009.

IEEE Task Force, *Blackout Experiences and Lessons, Best Practices for System Dynamic Performance, and the Role of New Technologies*, IEEE Special Publication 07TP190, July 2007.

Kamwa, I., G. Trudel, and L. Gerin-Lajoie, "Low-order Black-box Models for Control System Design in Large Power Systems," *IEEE Transactions on Power Systems*, vol. 11, no. 1, pp. 303-311, February 1996.

Kosterev, D. N., C. W. Taylor, and W. A. Mittelstadt, "Model Validation for the August 10, 1996 WSCC System Outage,´ *IEEE Transactions on Power Systems*, vol. 14, no. 3, pp. 967-979, August 1999.

Kundur, P. *Power System Stability and Control*, McGraw-Hill Inc., New York, NY, 1994.

MathWorks, *MATLAB User's Manual*, The MathWorks, 2010.

Messina, A.R. and V. Vittal, "Nonlinear, Non-stationary Analysis of Interarea Oscillations via Hilbert Spectral Analysis," *IEEE Transactions on Power Systems*, vol. 21, no. 3, pp. 1234-1241, August 2006.

North American Electric Reliability Corporation (NERC), "Standard TOP-007-0 — Reporting SOL and IROL Violations", April 1, 2005.

North American Electric Reliability Corporation (NERC), "Standard TOP-008-0 — Response to Transmission Limit Violations", April 1, 2005.

North American Electric Reliability Corporation (NERC), "Standard TOP-008-1 — Response to Transmission Limit Violations", January 1, 2007.

North American Electric Reliability Corporation (NERC), "Standard TOP-004-1 — Transmission Operations", October 1, 2007.

North American Electric Reliability Corporation (NERC), "Standard IRO-006-4 — Reliability Coordination — Transmission Loading Relief", October 23, 2007.

North American Electric Reliability Corporation (NERC), "Standard TOP-004-3 — Real-time Transmission Operations" (Draft), March 26, 2009.

North American Electric Reliability Corporation (NERC), "Electronic Tagging Version 1.8," [Online] Available: http://reg.tsin.com/Tagging/e-tag/, Accessed March 1, 2010.

Pai, M.A., D.P. Sen-Gupta, and K.R.Padiyar, *Small Signal Analysis of Power Systems*, Alpha Science International, Ltd., Harrow, Middlesex, UK, 2004.

Pierre, J.W., D. J. Trudnowski, M. K. Donnelly, "Initial Results in Electromechanical Mode Identification from Ambient Data," *IEEE Transactions on Power Systems*, vol. 12, no. 3, pp. 1245-1251, August 1997.

PowerTech Labs, Dynamic Security Assessment Tools, PowerTech Labs, [Online] Available: http://www.dsatools.com, 2010.

Rogers, G., *Power System Oscillations*, Kluwer Academic Publishers, Norwell, MA, 2000.

Sanchez-Gasca, J.J. and J.H. Chow, "Performance Comparison of Three Identification Methods for the Analysis of Electromechanical Oscillations," *IEEE Transactions on Power Systems*, vol. 14, no. 3, pp. 995-1001, August 1999.

Stoica, P. and R.L. Moses, *Introduction to Spectral Analysis*, Prentice-Hall, Upper Saddle River, NJ, 1997.

Trudnowski, D.J., "Estimating Electromechanical Mode Shape From Synchrophasor Measurements," *IEEE Transactions on Power Systems*, vol. 23, no. 3, pp. 1188-1195, August 2008.

Trudnowski, D.J., J.M. Johnson, and J.F. Hauer, "Making Prony Analysis More Accurate Using Multiple Signals," *IEEE Transactions on Power Systems,* vol. 14, no. 1, pp. 226-231, February 1999.

Trudnowski, D.J., J.W. Pierre, Z. Zhou, J. Hauer, and M. Parashar, "Performance of Three Mode-Meter Block-Processing Algorithms for Automated Dynamic Stability Assessment," *IEEE Transactions on Power Systems*, vol. 23, no. 2, pp. 680-690, May 2008.

Trudnowski, D.J. and J. Undrill, *The minniWECC System Model*, technical report, September 2008.

U.S.-Canada Outage Task Force, "Final Report on the August 14, 2003 Blackout in the United States and Canada: Causes and Recommendations," technical report, April 5, 2004.

Western Electricity Coordinating Council (WECC), "WECC Standard TOP-007-WECC-1 – System Operating Limits", March 12, 2008.

Western Electricity Coordinating Council (WECC), "Associated Material For 2008 HS4A Operating Case," February 2008.

Western Electricity Coordinating Council (WECC), "WECC Standard IRO-STD-006-0 – Qualified Path Unscheduled Flow Relief".

Western Electricity Coordinating Council (WECC), "2008 Heavy Summer Operating Case," February 8, 2008.

Western Electricity Coordinating Council (WECC), "2009 Heavy Summer Operating Case," February 4, 2009.

Wies, R. W., A. Balasubramanian, and J. W. Pierre, "Combining Least Mean Squares Adaptive Filter and Auto-Regressive Block Processing Techniques for Estimating the Low-Frequency Electromechanical Modes in Power Systems," in *Proceedings of the IEEE Power Engineering Society General Meeting 2006*, Montreal, Quebec, Canada, June 2006.

Wikipedia Contributors, "NERC Tag," *Wikipedia, the free encyclopedia*, [Online] Available: http://en.wikipedia.org/wiki/NERC_Tag, Accessed March 1, 2010.

Zhou, N., J. Pierre, and J. Hauer, "Initial Results in Power System Identification from Injected Probing Signals Using a Subspace Method," *IEEE Transactions on Power Systems*, vol. 21, no. 3, pp. 1296-1302, August 2006.

Zhou, N., J. Pierre, D. Trudnowski, and R. Guttromson, "Robust RLS Methods for On-line Estimation of Power System Electromechanical Modes," *IEEE Transactions on Power Systems*, vol. 22, no. 3, pp. 1240-1249, August 2007.

Zhou, N., D. Trudnowski, J. Pierre, and W. Mittelstadt, "Electromechanical Mode On-Line Estimation using Regularized Robust RLS Methods," accepted *IEEE Transactions on Power Systems*, 2008.

Zhou, N., D. Trudnowski, and J. Pierre, "Mode Initialization for On-Line Estimation of Power System Electromechanical Modes," in *Proceedings of the 2009 Power Systems Conference and Exposition (PSCE)*, Seattle, WA, March 15-19, 2009.

Zhou, N., Z. Huang, L. Dosiek, D. Trudnowski, and J. W. Pierre, "Electromechanical Mode Shape Estimation based on Transfer Function Identification using PMU Measurements," in *Proceedings of the IEEE Power Engineering Society General Meeting 2009*, Calgary, Canada, July 26-30, 2009.

Appendix

1. System Models

Throughout the report, several model systems have been referenced. This appendix will provide further information about the system models.

a) Two-Area-Four-Machine System

Initial studies for the MANGO procedure began with a simple model from [Kundur 1994]. This model has four generators separated into two areas. The basic topology of the system is shown in Figure A-1. The system is balanced in such a way that power predominately flows from the left area of the system to the right area. Loads at bus 7 and bus 9 consume the power produced by the four generators.

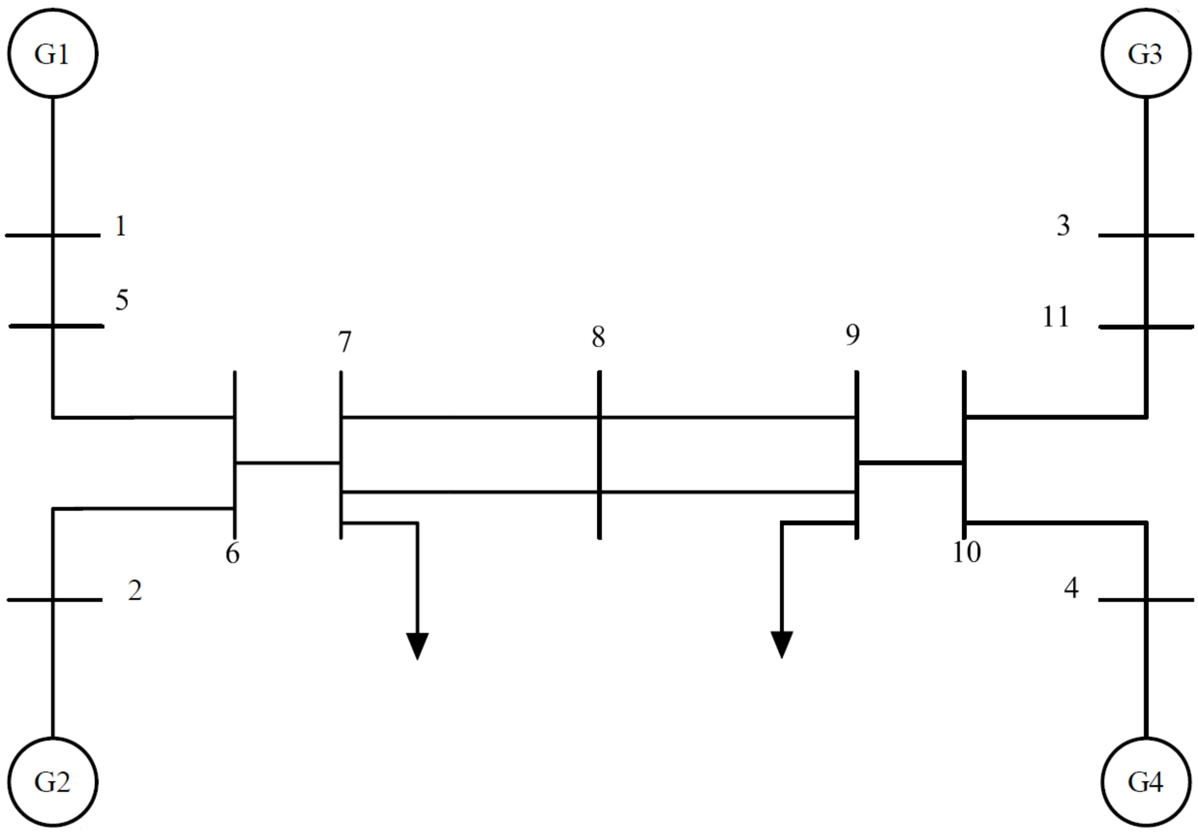

Figure A-1. Topology of two-area system from [Kundur 1994]

The four generators of the system are modeled nearly identically. Each generator is a 900-MVA unit on a 20-kV basis. Each of the generators is modeled as a "voltage behind the transient reactance". The block diagram of the direct and quadrature axes of these generators is shown in Figure A-2 and Figure A-3, respectively. In the block diagrams, E_{fd} represents the stator field voltage, E'_q represents the quadrature axis voltage, and E'_d represents the direct axis voltage. F_{sat} represents the magnetic field saturation. The direct axis model has an open circuit time constant of $T'_{d0} = 8.0$ seconds, a d-axis synchronous reactance of $X_d = 1.8$ p.u., and a d-axis transient reactance of $X'_d = 0.3$ p.u.. The quadrature axis model has an open circuit time constant of $T'_{q0} = 0.4$ seconds, a q-axis synchronous reactance of $X_q = 1.7$ p.u., and a q-axis transient reactance of $X'_q = 0.55$ p.u. The only parameter different between the two models is the inertia constant. The left generators (G1 and G2) were assigned an inertia constant of $H = 6.5$ seconds, while the right generators (G3 and G4) were assigned a slightly smaller inertia constant of $H = 6.175$ seconds [Chow and Rogers 2000; Kundur 1994]. All p.u. values are based on the machine's own MVA base.

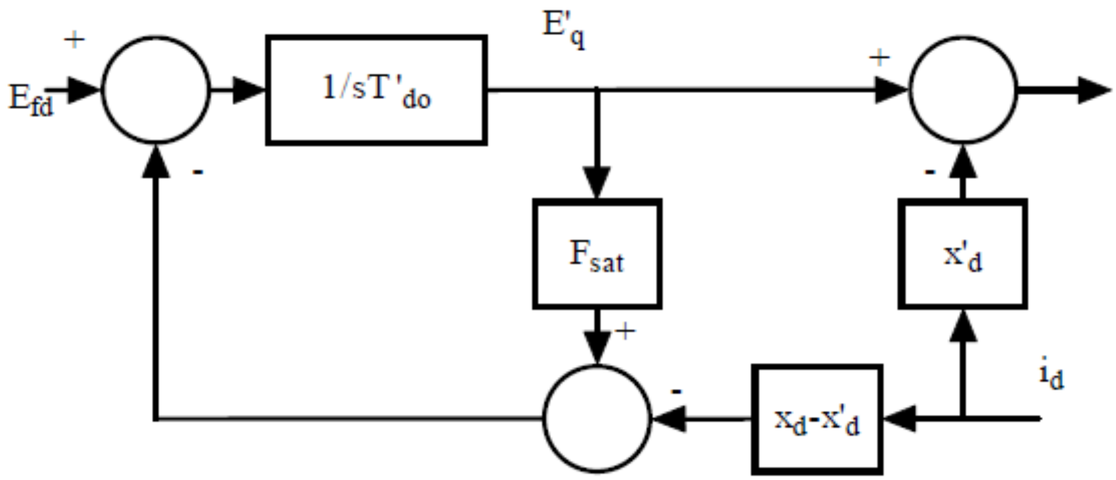

Figure A-2. Transient generator direct axis model [Chow and Rogers 2000].

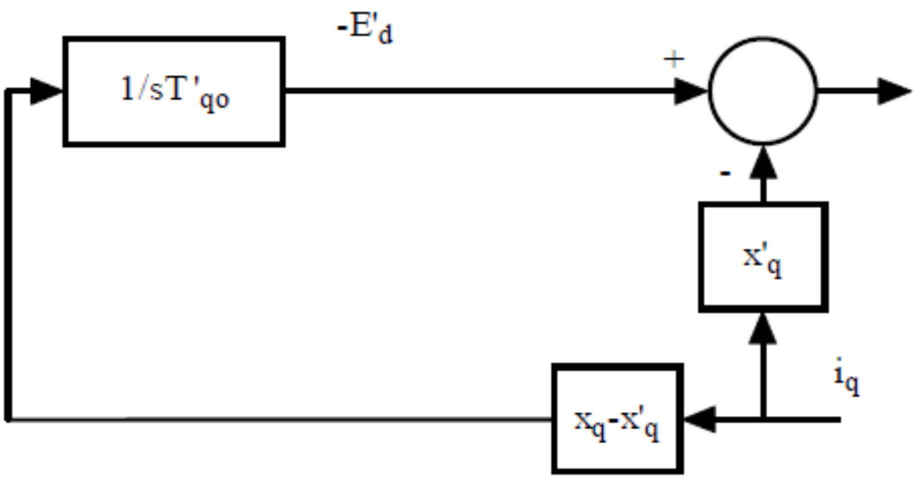

Figure A-3. Transient generator quadrature axis model [Chow and Rogers 2000].

In addition to the same generator model, each of the generators was equipped with an identical exciter. All exciters are modeled as thyristor exciters with a high transient gain and follow the block diagram shown in Figure A-4. The simple exciters contain no transient gain reduction. Each exciter has the transducer filter time constant as $T_R = 0.01$ seconds and the exciter voltage regulator gain set as $K_A = 200$. Not shown in Figure A-4 is the limiter on the output of the exciter. For the purposes of this study, the exciter regulator was set to a minimum and maximum output of ±5.0 p.u. to effectively remove any effects it would have on the transient analysis.

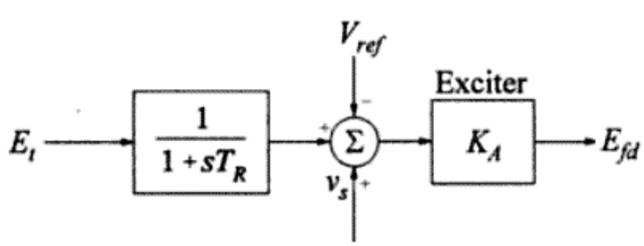

Figure A-4. Simple exciter model [Chow and Rogers 2000; Kundur 1994].

To stabilize the simple two-area system, power system stabilizer (PSS) units are also included on each of the four generators. As with the exciters, all of the PSS units are identical and are tuned to the same parameters. The simple block diagram of Figure A-5 represents the shaft speed-based power system stabilizers used in the two-area system. For each of the PSS units, the PSS gain was set as $K_{STAB} = 300$, and the washout time constant was set to $T_W = 20.0$ seconds. The lead lag networks of the PSS units were set using $T_1 = 0.05$, $T_2 = 0.02$, $T_3 = 3.0$, and $T_4 = 5.4$ seconds each [Kundur 1994].

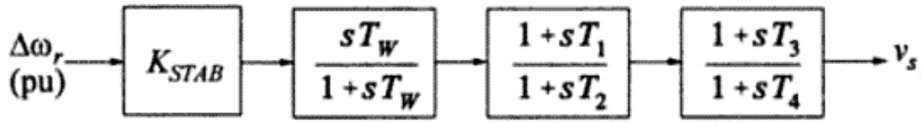

Figure A-5. Simplified PSS model [Chow and Rogers 2000; Kundur 1994].

b) 17-Machine System

To provide a more complex, realistic system for evaluating various operator actionable control methods, a 17-machine system was also investigated. This system is a very rough analog to the Western Electricity Coordinating Council (WECC). The one-line diagram for this system is shown in Figure A-6. It is useful to note that the high-voltage direct current (HVDC) intertie is modeled as loads on the system. That is, bus 42 is a load on the system of 10 p.u. and bus 43 provides -10 p.u. power back into the system. No dynamics of the DC controls are modeled, nor are the rectifier and inverter. Despite the indications on the one-line diagram, the physical interconnection between bus 42 and bus 43 does not exist in the system model. While some rough comparisons could be made between various geographic generator sets and their positioning in the one-line diagram, only a very weak correlation exists. As such, modes are not expected to follow identical interaction paths or inhabit the same frequency bands as the full WECC system.

All generators within the 17-machine system are modeled as synchronous machines with the voltage behind subtransient reactance from the Power Systems Toolbox [Chow and Rogers 2000]. These models are slightly more complex than the transient reactance models used in the two-area model. Similarly, the machines can be split into a direct-axis model and a quadrature-axis model. The block diagrams of these two representations are shown in Figure A-7 and Figure A-8, respectively. The details of the numerous parameters and their substitutions are available in [Chow and Rogers 2000].

Along with the different generator model, the implementation of the generators in the 17-machine system is different. With the exception of generator 17, all of the machines occur in pairs. Each "true" generator is effectively split into two separately modeled generators, so the system could almost be thought of as a 9-machine system. In each of these pairs, one generator is set up as a base generation unit and one is set up as a load-following generator.

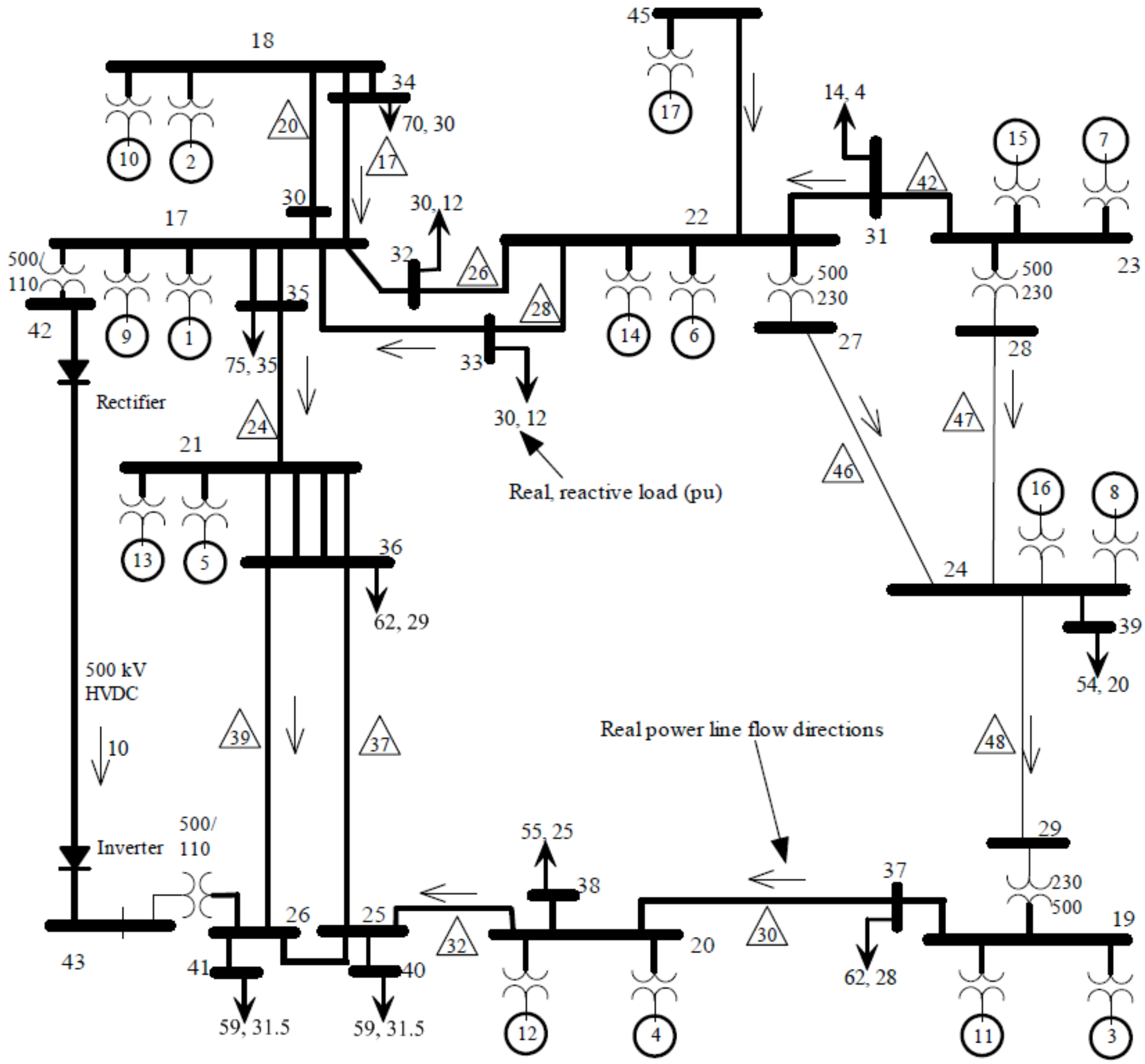

Figure A-6. Topology of 17-machine system [Trudnowski 2008].

All of the load-following generators include a speed governor model. All governors are modeled as steam-turbine governors following the block diagram of Figure A-9. All of the load-following generators contain identical settings for the first two parameters. The steady state gain is set to $\frac{1}{r} = 20.0$ p.u. and the maximum power order is set as $T_{\max} = 1.00$ p.u. For other parameters, the load-following generators are split into two groups, with generators 9, 10, 14, and 16 being in one group with one set of governor parameters and generators 11, 12, 13, and 15 with a second set of parameters.

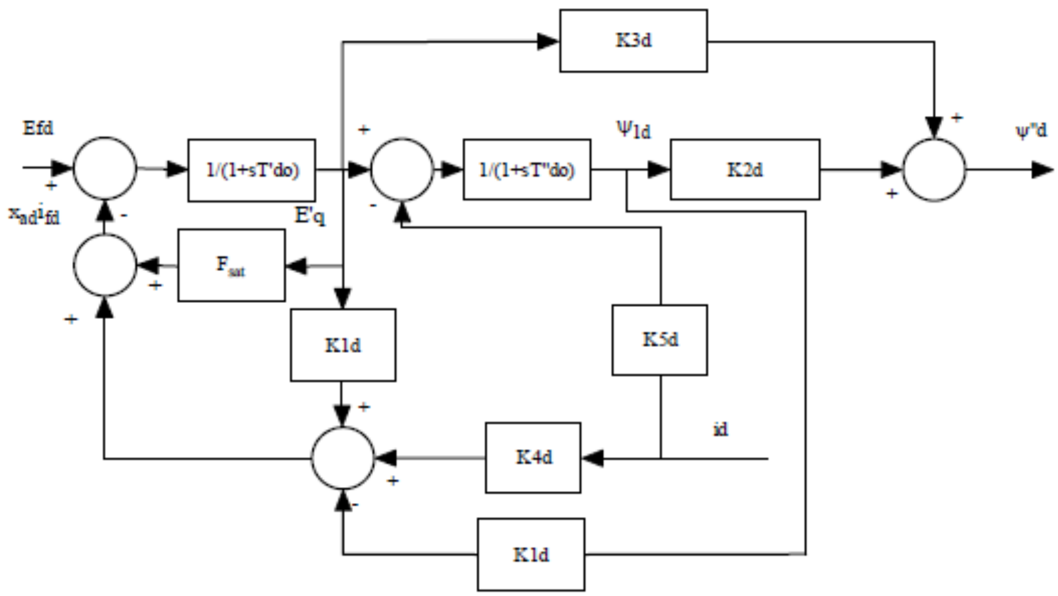

Figure A-7. Subtransient generator direct axis model [Chow and Rogers 2000].

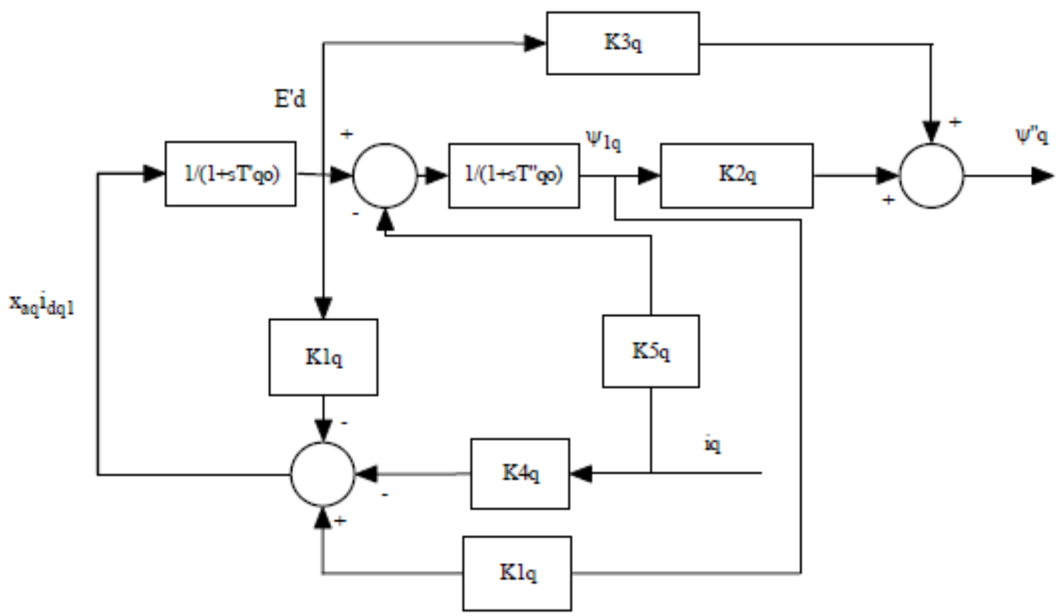

Figure A-8. Subtransient generator quadrature axis model [Chow and Rogers 2000].

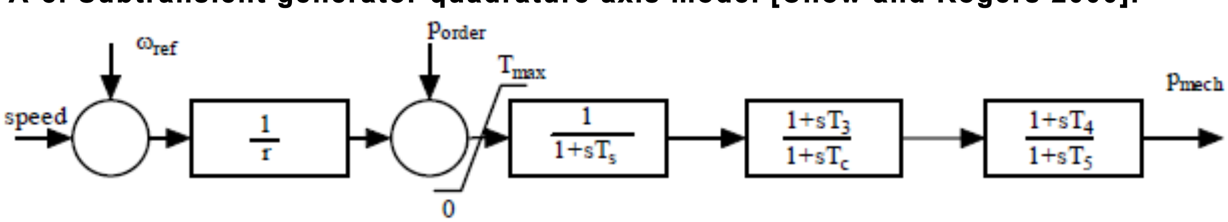

Figure A-9. Generator governor block diagram [Chow and Rogers 2000].

The first set of generators set the servo time constant to $T_s = 0.40$ seconds, the governor time constant as $T_c = 75.0$ seconds, the transient gain time constant at $T_3 = 10.0$ seconds, the high pressure (HP) section time constant as $T_4 = -2.4$ seconds, and finally the reheater time constant as $T_5 = 1.2$ seconds. This model is indicated as hydro-generation units.

The second set of generators has a servo time constant of $T_s = 0.04$ seconds, a governor time constant of $T_c = 0.2$ seconds, no transient gain time constant ($T_3 = 0$), a HP section time constant of $T_4 = 1.5$ seconds, and finally a reheater time constant of $T_5 = 5.0$ seconds. The smaller time constants give the governor a larger bandwidth and responds to speed changes more quickly than the "hydro" governors modeled on the first set of generators.

Much like the two-area system, all of the generators in the 17-machine system utilize a simple exciter. Unlike the two-area system, each of the 17-machine system generators include transient gain reduction as part of the functionality. However, they also eliminate the transducer filter time constant. As such, the 17-machine exciters follow the form of Figure A-10. Similar to the governor models, two parameter sets exist for the exciters. All of the generators except 3, 5, 11, and 13 use an exciter gain of $K_A = 200$ and a voltage regulator time constant of $T_A = 0.04$ seconds. However, generators 3, 5, 11, and 13 use a gain of $K_A = 250$ and a voltage regulator time constant set to $T_A = 0.03$ seconds. All generators have the transient gain reduction portion set using $T_B = 12.0$ seconds and $T_C = 1.0$ seconds. The limiters of all of the exciters are again scaled to significantly larger values to prevent saturation of the output.

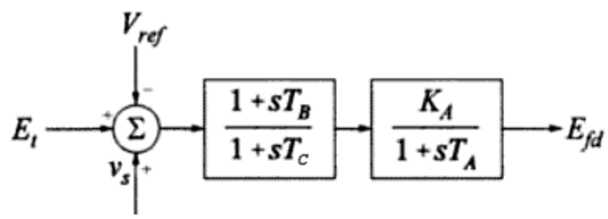

Figure A-10. Exciter model of 17-machine system [Chow and Rogers 2000].

The 17-machine system includes PSS units as well. All of these PSS units follow the same model shown in Figure A-5 in the section of the two-area system. Each PSS unit is reported to have been tuned using the procedure outlined in [Rogers 2000].

Through the combination of more complex models and an increase in the number of generators, the 17-machine system provides a more realistic system to analyze. Several inter-area modes of oscillation exist in the model. In addition, more complex control devices provide a better approximation of how various operator actionable control schemes may affect the stability of a mode of interest.

c) minniWECC Model

Further validation and testing of the MANGO procedure occurred using the minniWECC model. The minniWECC model is a reduced order model of the WECC system. Unlike the 17-machine, which is only a rough analog, the minniWECC model provides a highly detailed model of the WECC power grid. This includes geographical correlations as the diagram of Figure A-11 demonstrates

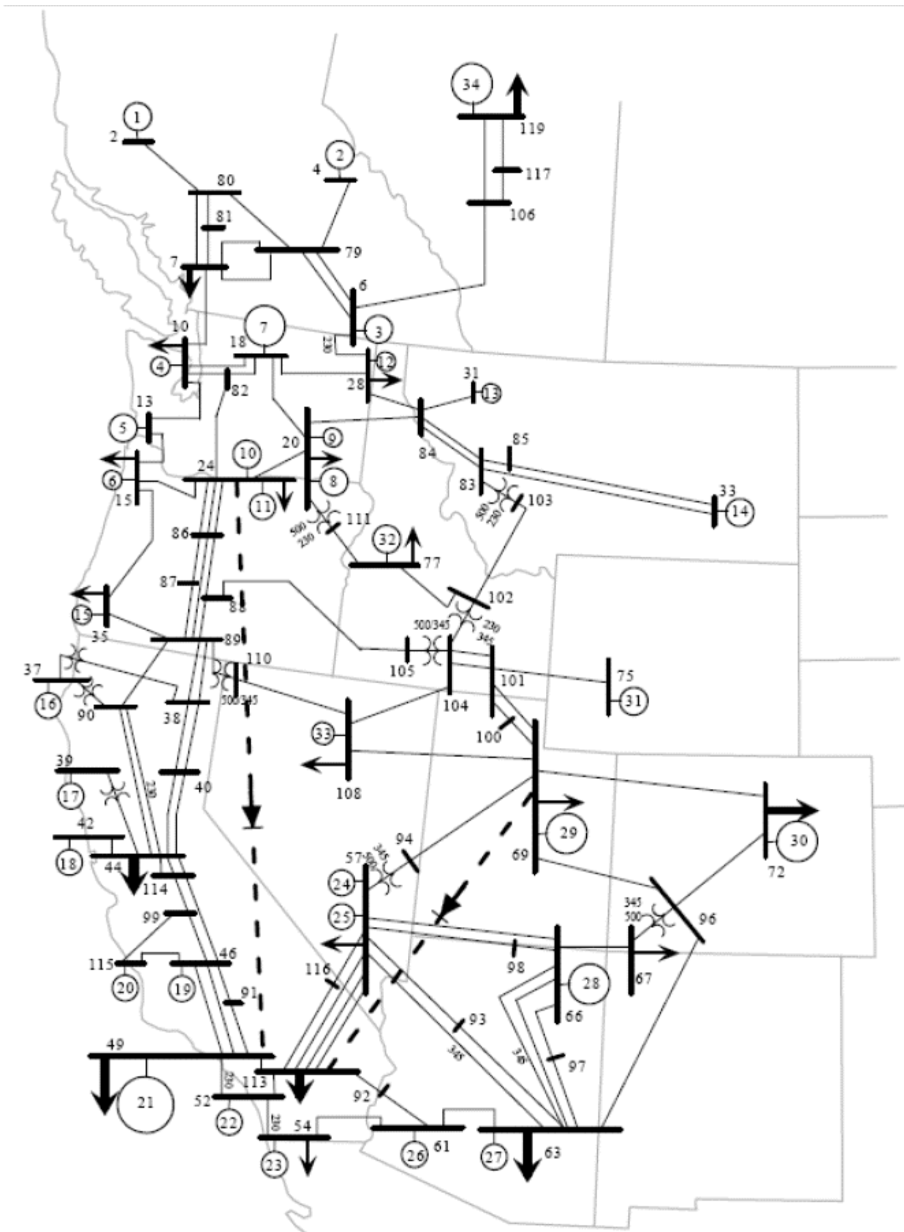

Figure A-11. Topology of minniWECC System [Trudnowski and Undrill 2008].

The minniWECC model shares many underlying model characteristics with the 17-machine model. As with the 17-machine model, the minniWECC model utilizes generators modeled as synchronous machines with the voltage behind subtransient reactance from the Power Systems Toolbox [Chow and Rogers 2000]. This generator model provides a high level of detail for machine responses. Coupled with the appropriate governor and control schemes, the interactions of different generator sizes and types are better modeled in the system. Furthermore, the minniWECC model continues to model the DC interties as constant power loads and injections at either end. This prevents any ambiguous or uncertified results from the inverter models or even the model of the line itself from causing unexpected influences in the system. Unlike the 17-machine model, all of the limits to the generators and exciters have been left in place. This helps create a more realistic simulation of the actual WECC power grid for study.

d) WECC 2008 and 2009 Heavy Summer Cases

The final models under examination and testing as part of the MANGO procedure were the 2008 and 2009 WECC Heavy Summer Cases. No one line diagram is available for these models, but the comprehensive models encompasses most of the WECC. The interchange diagram for the 2008 Heavy Summer case is shown in Figure A-12. The interchange diagram for the 2009 Heavy Summer case is shown in Figure A-13. The models are composed of 15680 different busses with 3116 generators and 7777 loads. The powerflow and modal analysis are all performed using the PSAT and SSAT software packages, with appropriate governor and generator models selected by the software.

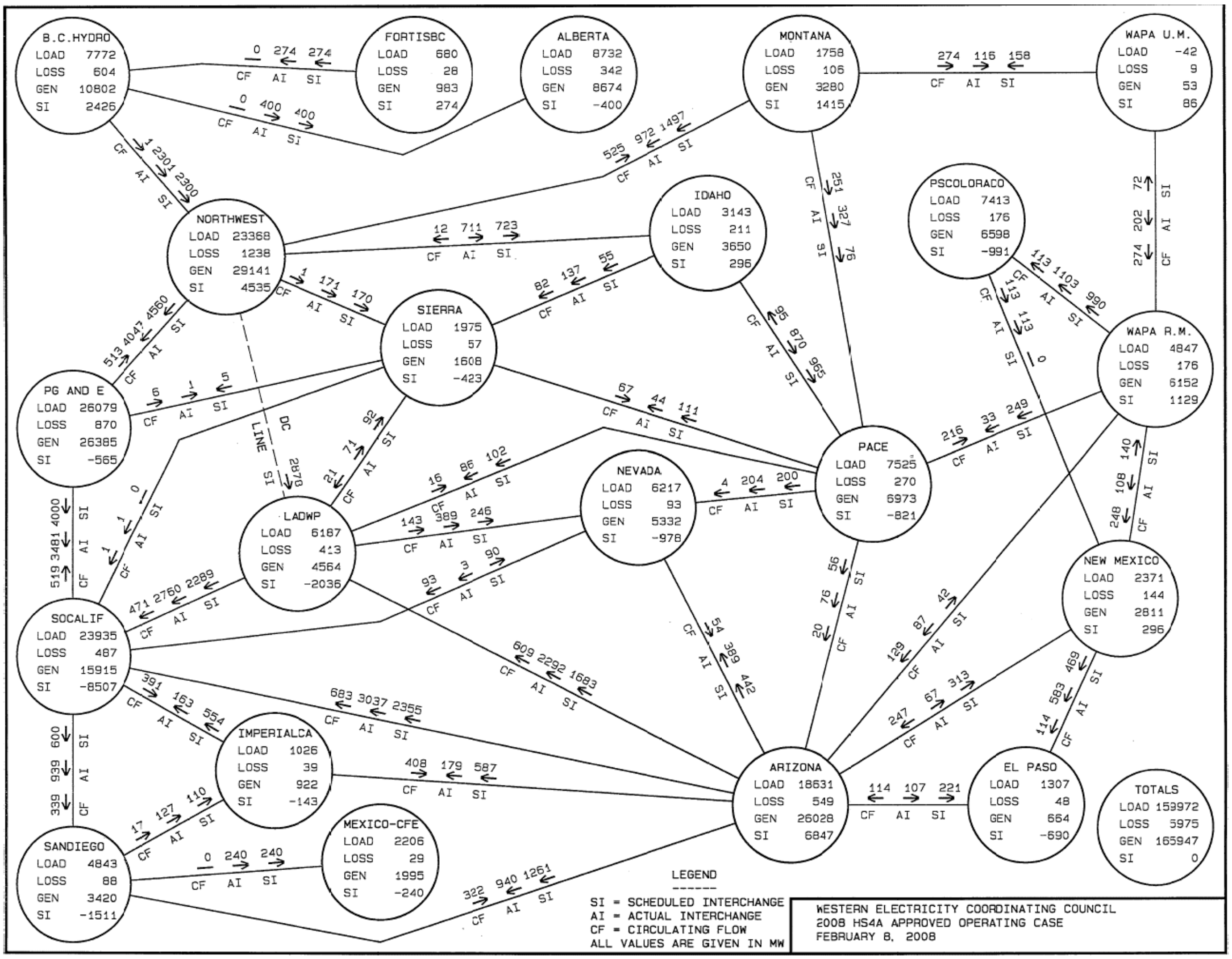

Figure A-12. WECC 2008 Heavy Summer Model Interchange Diagram [WECC 2008].

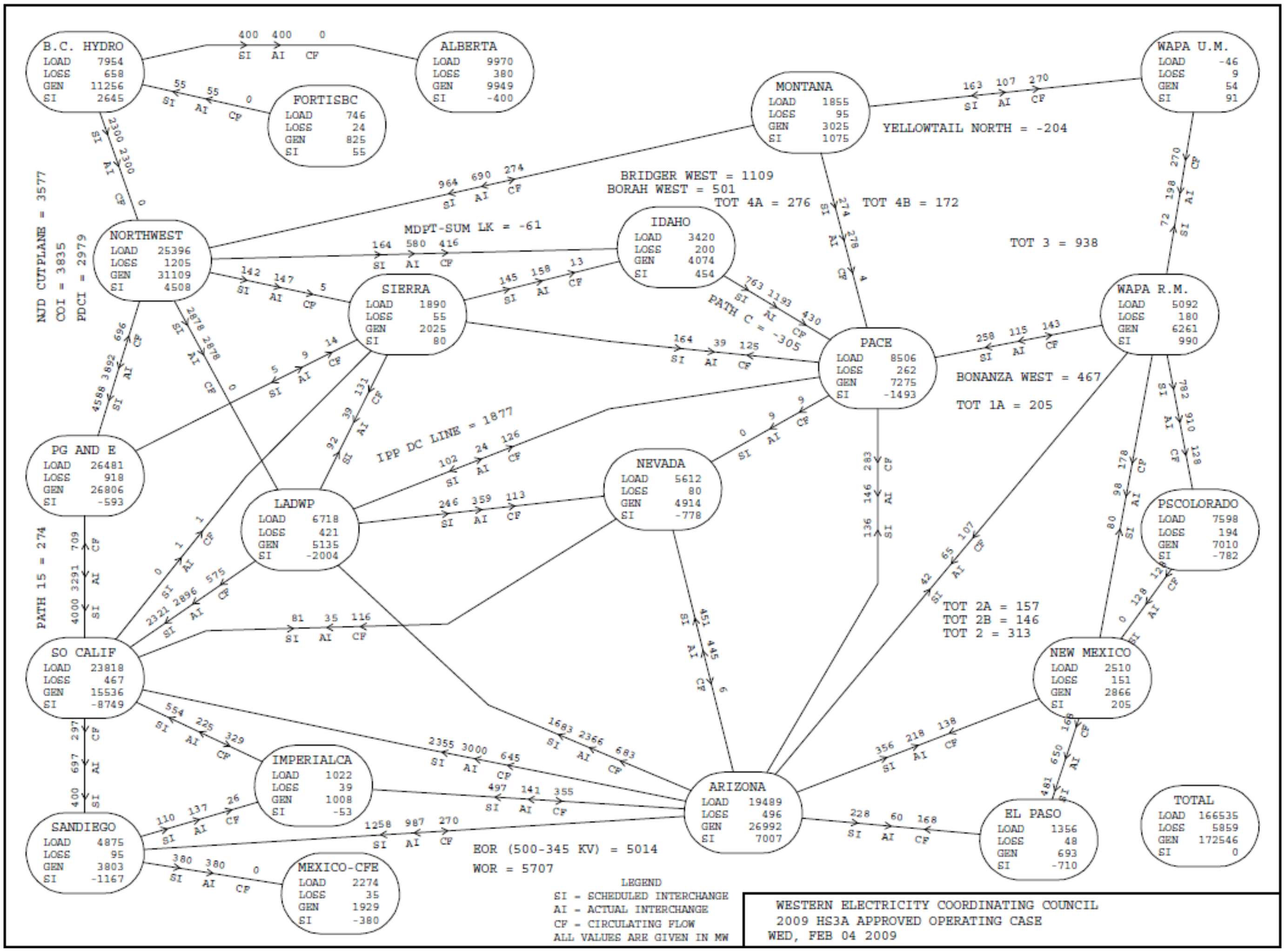

Figure A-13. WECC 2009 Heavy Summer Model Interchange Diagram [WECC 2009].

2) Baseline Parameters

This section presents baseline properties for modes of interest in each model.

4-Machine Model

Frequency (Hz)	Damping Ratio (%)
0.6085	13.60
1.2463	21.61
1.2941	21.62

17-Machine Model

Frequency (Hz)	Damping Ratio (%)
0.2988	12.66
0.4010	1.94
0.6097	3.59
0.6513	7.86
0.7970	4.20
0.8944	7.91
1.2005	7.29

minniWECC Model – COI_P = 0

Frequency (Hz)	Damping Ratio (%)
0.1681	27.88
0.3219	-1.03
0.5071	9.21
0.5486	6.25
0.6219	0.70
0.6858	5.73
0.7086	4.54
0.7963	20.85

minniWECC Model – COI_P = 10

Frequency (Hz)	Damping Ratio (%)
0.1691	28.22
0.3390	1.73
0.5098	9.05
0.5551	6.47
0.6208	0.77
0.6885	5.63
0.7190	4.88
0.7964	20.87

minniWECC Model – COI_P = 20

Frequency (Hz)	Damping Ratio (%)
0.1698	28.31
0.3507	3.71
0.5115	8.90
0.5588	6.67
0.6184	0.92
0.6904	5.58
0.7243	5.52
0.7965	20.88

WECC 2008 Heavy Summer Model

Frequency (Hz)	Damping Ratio (%)
0.2269	8.84
0.3546	10.10